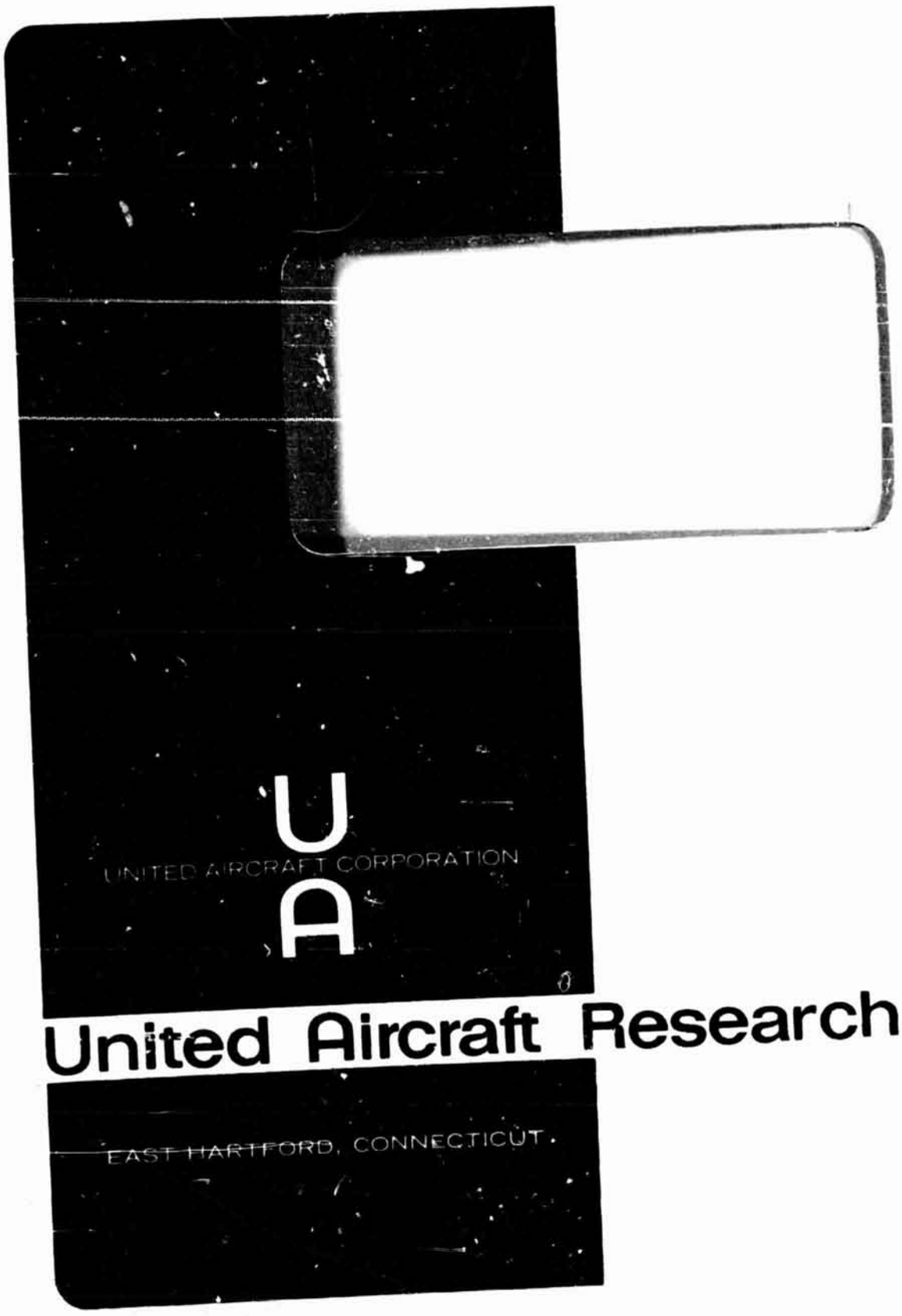

United Aircraft Research Laboratories

EAST HARTFORD, CONNECTICUT

United Aircraft Research Laboratories

UNITED AIRCRAFT CORPORATION

EAST HARTFORD, CONNECTICUT 06108

Report K-910900-8

Experiments to Simulate Heating of the Propellant in a Nuclear Light Bulb Engine Using Thermal Radiation From a D-C Arc Radiant Energy Source

Contract No. SNPC-70

REPORTED BY John F. Klein
John F. Klein

APPROVED BY James W. Clark
James W. Clark, Chief
Fluid and Systems Dynamics

DATE September 1971

NO. OF PAGES 71

COPY NO. 26

FOREWORD

An exploratory experimental and theoretical investigation of gaseous nuclear rocket technology is being conducted by the United Aircraft Research Laboratories under Contract SNPC-70 with the joint AEC-NASA Space Nuclear Systems Office. The Technical Supervisor of the Contract for NASA was Captain C. E. Franklin (USAF) for the first portion of the contract performance period and was Dr. Karlheinz Thom for the last portion of the contract performance period. Results obtained during the period September 16, 1970 and September 15, 1971 are described in the following seven reports (including the present report) which comprise the required second Interim Summary Technical Report under the Contract:

1. Roman, W. C. and J. F. Jaminet: Experimental Investigations to Simulate the Thermal Environment and Fuel Region in Nuclear Light Bulb Reactors Using an R-F Radiant Energy Source. United Aircraft Research Laboratories Report K-910900-7, September 1971.

2. Klein, J. F.: Experiments to Simulate Heating of the Propellant in a Nuclear Light Bulb Engine Using Thermal Radiation from a D-C Arc Radiant Energy Source. United Aircraft Research Laboratories Report K-910900-8, September 1971. (present report)

3. Bauer, H. E.: Initial Experiments to Investigate Condensation of Flowing Metal-Vapor/Heated-Gas Mixtures in a Duct. United Aircraft Research Laboratories Report K-910900-9, September 1971.

4. Rodgers, R. J., T. S. Latham and H. E. Bauer: Analytical Studies of Nuclear Light Bulb Engine Radiant Heat Transfer and Performance Characteristics. United Aircraft Research Laboratories Report K-910900-10, September 1971.

5. Latham, T. S. and H. E. Bauer: Analytical Design Studies of In-Reactor Tests of a Nuclear Light Bulb Unit Cell. United Aircraft Research Laboratories Report K-910900-11, September 1971.

6. Krascella, N. L.: Spectral Absorption Coefficients of Helium and Neon Buffer Gases and Nitric Oxide-Oxygen Seed Gas Mixture. United Aircraft Research Laboratories Report K-910904-2, September 1971.

7. Palma, G. E. and R. M. Gagosz: Effect of 1.5 Mev Electron Irradiation on the Transmission of Optical Materials. United Aircraft Research Laboratories Report K-990929-2, September 1971.

Report K-910900-8

Experiments to Simulate Heating of the Propellant in a Nuclear Light Bulb Engine Using Thermal Radiation From a D-C Arc Radiant Energy Source

TABLE OF CONTENTS

TABLE OF CONTENTS (Continued)

Report K-910900-8

Experiments to Simulate Heating of the Propellant in a Nuclear Light Bulb Engine Using Thermal Radiation From a D-C Arc Radiant Energy Source

SUMMARY

Experiments were conducted to simulate radiant heating of the propellant stream of a nuclear light bulb engine. The primary objective was to obtain high exit temperatures in the simulated propellant stream due to the absorption of large percentages of the incident thermal radiation. A 500-kw d-c arc was used as the radiant energy source and argon seeded with carbon particles was used to simulate the propellant. Unseeded buffer layers were used to prevent coating of the transparent duct walls. Methods were developed for introducing micron-sized carbon seeds into the central region of a three-stream flow in a rectangular duct to simulate a portion of the propellant stream.

The bulk exit temperature in the exhaust of the reference nuclear light bulb engine design is 6660 K (12,000 R). A long-range goal of the propellant heating experiments conducted in the laboratory is to obtain as high a value as possible of this bulk exit temperature in a configuration closely simulating that of the engine.

In the tests reported herein, simulated propellant bulk exit temperatures up to 3860 K (6950 R) were achieved. The bulk exit temperatures were determined by a calorimetric technique developed during this program. The maximum bulk exit temperatures were limited primarily by vaporization of the carbon seeds and the amount of radiation incident on the test section.

It is estimated that substantially higher propellant bulk exit temperatures can be obtained. This can be achieved by further improvements to the d-c arc radiant energy source (in particular, improvement of the reflectivity of the mirrors used) and by the use of tungsten seeds which will remain in particle form to higher temperatures than carbon seeds.

RESULTS AND CONCLUSIONS

1. Simulated propellant bulk exit temperatures up to 3860 K (6950 R) were obtained by absorption of thermal radiation from a d-c arc source. The simulated propellant was argon seeded with carbon particles. The maximum temperature was limited primarily by vaporization of the particles and the amount of radiation incident on the test section. In some tests, up to 99 percent of the radiation reaching the simulated propellant through the transparent duct wall was absorbed by the simulated propellant; less than 2 percent of the arc radiation incident on the transparent wall was absorbed by seeds deposited on the wall.

2. In preparation for these tests, a two-dimensional propellant duct inlet configuration was developed. The results of cold-flow tests indicated that two 1.5-cm (0.59-in.)-wide buffer layers and a 0.3-cm (0.12-in.)-wide central seeded stream (dimensions at the inlet) would provide the desired seed flow while maintaining relatively clean walls. The average velocities of the three streams were matched at 0.8 m/sec (2.6 ft/sec). Cold-flow tests were conducted in which the simulated propellant transmitted less than 3 percent of the incident radiation for periods up to 13 min. After these tests, the transparent wall transmission was still 98 percent of its original value. These tests were conducted using a sonic orifice to deagglomerate the seeds.

3. Also in preparation for these tests, the d-c arc simulated propellant heating configuration was modified to operate at up to 500 kw. This argon, vortex-stabilized, arc provides up to 240 kw of radiation over the 12.7-cm (5.0-in.) length adjacent to the test section; of this, about 35 kw is directed at the test section. Thus, the maximum radiation incident on the simulated propellant was increased by a factor of fifteen relative to the levels available in previous tests. A calorimetric technique for determining simulated propellant bulk exit temperature was also developed.

4. Continued research in the laboratory on simulated propellant heating is required to reach bulk exit temperatures approaching those expected in the nuclear light bulb engine. By improving the mirrors used with the d-c arc radiant energy source and by using tungsten seed, which has higher melting and boiling points than carbon, it should be possible to obtain substantially higher bulk exit temperatures.

INTRODUCTION

An experimental and theoretical investigation of gaseous nuclear rocket technology is being conducted by the United Aircraft Research Laboratories (UARL) under Contract SNPC-70 administered by the joint AEC-NASA Space Nuclear Systems Office. The overall research program is presently directed toward investigating the feasibility of the nuclear light bulb engine. This report discusses the portion of the research program in which a seeded simulated propellant was heated to high bulk temperatures (greater than 3330 K (6000 R)) by absorption of thermal radiation from a d-c arc radiant energy source. Simulated propellant bulk temperatures between 1660 K (3000 R) and 2220 K (4000 R) have been obtained in previous tests.

Nuclear Light Bulb Concept and Reference Engine Configuration

The nuclear light bulb concept described in Refs. 1 and 2 is based on the principle of transfer of energy by thermal radiation from a fissioning gaseous nuclear fuel to seeded hydrogen propellant flowing through an annulus surrounding the nuclear fuel. Radiant energy is transferred through an internally cooled transparent wall which separates the nuclear fuel from the propellant stream. Figure 1(a) illustrates this principle of operation with a cross section of one unit cavity. The reference engine (Ref. 3) is formed by a cluster of seven such cavities to increase the effective radiating surface area of the nuclear fuel cloud. Figure 1(b) is a schematic of the d-c arc radiant energy source used in the propellant heating simulation tests. The significant dimensions of both the unit cavity and the propellant heating configuration are indicated. Figure 2 is a sketch showing additional detailed dimensions of one unit cavity of the reference engine. One-half of the rotationally symmetric cavity is shown. The propellant region is a divergent annulus 1.8-m long with a 0.49-m inside diameter. The annulus width increases uniformly from 0.013 m at the inlet to 0.161 m at the exhaust.

In the reference engine, approximately 98 percent of the total thermal radiation incident on the propellant stream is calculated to be absorbed by the hydrogen propellant (Ref. 3). Hydrogen is essentially transparent to thermal radiation at the engine operating pressure of 500 atm and below a temperature of approximately 7780 K (14,000 R). Therefore, a seed material must be added to the propellant stream to provide the required opacity. The ideal seed material would consist of nonreactive, high-melting-point, high-boiling-point, submicron-sized metal particles that exhibit good absorption characteristics in both the particle and vapor forms. Submicron-sized particles, low-ionization-potential metal vapors, and various polyatomic gases have been examined theoretically and experimentally as possible seed materials for the propellant stream (Refs. 4 through 12). Submicron-sized solid or liquid particles exhibit essentially continuous spectral absorption characteristics as contrasted with

discrete spectral absorption characteristics exhibited by low-ionization-potential metal vapors and polyatomic gases. Theoretical studies (Refs. 4 through 8) of the absorption properties of small solid particles have been based on the Mie theory (Ref. 13). This theory describes the spectral extinction, absorption, and scattering of radiation by spherical particles as functions of particle size, material properties, and the wavelength of the incident radiation. The results of these studies indicate that tungsten is attractive as a seed material because of its high melting point, high boiling point, and low reactivity with hydrogen. In the reference engine, nominal 0.05-micron-dia tungsten particles are assumed to be used as a propellant seed material.

In each unit cavity the inner wall of the propellant annulus is highly transparent. The outer wall is highly reflective to reduce the heat load to the moderator and to increase the effective radiant energy path length in the propellant region. A thin layer of unseeded gas flows adjacent to both the inner and the outer walls of the propellant region. These thin unseeded layers serve as buffer regions which prevent the degradation of the optical properties of the walls due to coating by the propellant seed. They also aid in keeping hot gases away from the walls, thus reducing the heat transfer to the duct walls.

Principal Objectives

The principal objectives of this portion of the nuclear light bulb engine research are:

(1) to experimentally demonstrate the heating of a simulated propellant to bulk exit temperatures greater than 3330 K (6000 R) by the absorption of thermal radiation,

(2) to use a flow configuration similar to that of the nuclear light bulb engine in the sense of providing simulated propellant opacity with micron-sized solid particle seeds, which are separated from the propellant duct walls by buffer layers of unseeded gas, and

(3) to develop methods of dispersing, deagglomerating and introducing the particle seed into the central portion of the simulated propellant flow.

Experimental Approach

Two basic changes were made in the experimental approach over the approach used in the first phase of this program (Refs. 14 and 15) to provide a simulated propellant heating configuration with which the principal objectives can be achieved. First, the annular propellant duct was replaced by a rectangular duct, simulating a portion

of the engine propellant duct. Cold-flow tests were conducted to find an inlet configuration suitable for propellant heating. The inlet used for these tests was designed to be compatable with the d-c arc radiant energy source. The carbon seed supply system was modified to allow operation with the use of an orifice for seed deagglomeration.

Second, the d-c arc radiant energy source was modified for high-power, short test time operation. The objective of the d-c arc modifications was to increase the radiant flux incident on the simulated propellant stream. The major modifications were (1) removal of the locator, (2) shortening of the arc length, (3) removal of the water cooling from the fused silica tube surrounding the arc, (4) modification of the vortex inlet, and (5) surrounding the arc with a water-cooled mirror. Based on the tests discussed in Ref. 14, new diagnostic methods were required. As a result, a new calorimetric method for determining the simulated propellant bulk exit temperature was developed.

The results of the cold-flow tests, d-c arc modification, and calorimeter development were combined in the propellant heating tests.

This report is divided into separate sections discussing the d-c arc radiant energy source, the cold-flow tests, and the simulated-propellant heating tests. Also included are two appendixes describing the d-c arc system and discussing the calorimeter radiation corrections.

D-C ARC RADIANT ENERGY SOURCE

Objective

The objective of the d-c arc modification and test series was to provide enough radiation incident on the simulated propellant flow to heat it to a bulk exit temperature greater than 3330 K (6000 R) by absorption of thermal radiation. To satisfy this objective, the UARL d-c arc heater was modified to a 500-kw, short-test-time (0.5-sec) configuration. The results of the d-c arc tests and the techniques used to measure arc radiation are discussed in this portion of the report. Descriptions are given in Appendix A of the d-c arc electrical components, configuration, electrodes, vortex system, gas and water-cooling systems, starting and control systems, and a summary of modifications to the d-c configuration.

Radiation Measurements

Configuration

Figure 3 shows a sketch of the basic d-c arc and radiometer optical system. The 1-atm argon arc was vortex stabilized and was enclosed within a 4.0-cm (1.57-in.)-ID, uncooled, fused silica tube. The arc was struck between a thoriated tungsten cathode and a magnetically augmented, water-cooled, copper anode which were 17.78 cm (7.0 in.) apart.

As shown in Fig. 3, total radiation measurements were made of the power radiated from the d-c arc column using a radiometer which incorporated a barium fluoride (BaF_2) thermopile detector. This arrangement of the thermopile and aperture allowed the radiometer to view a section of the d-c arc column which was 2.54-cm (1.0-in.)-high and wider than the diameter of the fused silica tube enclosing the d-c arc column. Therefore, the radiometer viewed a section of the column that always included the entire arc diameter. As shown in Fig. 3, the section of the arc column viewed was halfway between the anode and cathode. Total radiation measurements were obtained in the wavelength range from 0.22 to 2.3 microns (the range of high transmittance for the fused silica tube).

Calibration

The radiometer was calibrated using a standard lamp (a General Electric DXW quartz-iodine tungsten filament having lamp known spectral characteristics). The 2.54-cm (1.0-in.)-long filament of the lamp was positioned in a location equivalent to the position of d-c arc centerline in Fig. 3, within the viewing field of the radiometer. The known intensity of radiation from the standard lamp at the location

of the thermopile element was used to calibrate the radiometer. Two alternate methods for measuring the arc radiation were used in previous tests (Ref. 14) --- one employed a blackened sleeve around the arc, and the other employed an annulus of water containing dye. Radiation measurements made by these two alternate methods were consistent with the calibrated radiometer measurements made at that time. In addition, another method was used in the present study --- absorption of radiation in a blackened copper slug (discussed in the section entitled SIMULATED PROPELLANT HEATING TESTS). The results also showed good agreement with the calibrated radiometer measurements.

Results

The results of measurements of the power radiated from the d-c arc plasma in the modified configuration are summarized in Fig. 4. The results are expressed as the power radiated from a 12.7-cm (5.0-in.) test section --- the length of the test section used subsequently in propellant heating tests --- as a function of total arc power. Total power radiated in the test section length was obtained by multiplying the power radiated from a 2.54-cm (1.0-in.) arc length, as measured by the radiometer, by a factor of five. As shown on Fig. 4, the power radiated from the test section length ranged from 15 kw to 238 kw while the corresponding total arc powers ranged from 50 kw to 500 kw. In terms of the maximum total power radiated in the test section length, this configuration represents a factor of 8.3 increase above that of the d-c arc propellant heating configuration used in Ref. 14. For these tests it is estimated that the radiation efficiency, defined as the power radiated from the arc column per unit length divided by the power deposited in the arc column per unit length, ranged from 50 to 80 percent.

Figure 5 shows the voltage-current relationship. The arc voltage ranged from about 80 v to 160 v while the current ranged from about 600 to 3000 a. For all tests, the d-c arc configuration, argon flow rate, inlet geometry, cathode position, and vortex flow injection angle were held constant. Test time for all tests was about 0.5 sec. The ballast resistance was varied to permit arc operation over the power range shown. The maximum electrical power deposited in the arc column was about 22.5 kw/cm (57 kw/in.) which approaches the state of the art in d-c arc technology. Success with this high power d-c arc radiant energy source was a major step towards the achievement of high simulated propellant bulk exit temperatures due to the absorption of thermal radiation.

COLD-FLOW TESTS

Objectives

The major objective of the cold-flow tests was to develop a simulated propellant flow configuration which could subsequently be heated to high temperatures by the absorption of thermal radiation. The desired flow configuration consisted of a central seeded gas stream separated from transparent duct walls by buffer layers of unseeded gas to prevent transparent wall coating by the seed material.

Unlike the annular duct used in Refs. 14 and 15, the duct used in the present tests was rectangular in cross section. The change from annular to rectangular was made for several reasons: (1) most of the d-c arc radiant energy source could be enclosed within a mirror to increase the radiant flux incident on the simulated propellant (see Fig. 1(b)); (2) construction of the calorimeter to be used for the measurement of simulated propellant bulk exit temperature was simpler and less expensive; (3) the weight flow rate of the simulated propellant was less, thereby reducing the amount of energy required to raise its temperature to a given value; and (4) less carbon seed was required and, hence, the existing seeder could be used for longer periods without refilling.

A second objective of the cold-flow tests was to obtain higher values of the seed mass attenuation coefficient within the simulated propellant heating test section. This was to be accomplished using the sonic orifice techniques discussed in Ref. 14. This technique is based on previous experiments discussed in Refs. 9 through 12.

Seed Dispersal System

The use of the sonic orifices for the simulated propellant flow required modification of the seed dispersal system used previously in this program. Figure 6 is a schematic diagram of the simulated propellant flow system and high-pressure seed dispersal system. This system provides the required flows of seeds, carrier gas, and buffer gas. Carbon seed material having a nominal diameter of 0.012 microns was used in these tests instead of tungsten as considered for the reference nuclear light bulb engine because it is readily available, inexpensive, and easier to handle than tungsten. Also, carbon has good optical absorption characteristics over the size range of interest. Argon was used as the seed carrier and buffer gas in all tests.

The seed dispersal system consists of a 12.7-cm (5.0-in.)-ID by 29.8-cm (11.75-in.)-deep, high-pressure (3000 psig), stainless steel canister. However, for the tests reported herein, the maximum canister pressure used was 300 psig. This maximum operating pressure was used in tests in which sonic orifices were used for seed deagglomeration as shown in Fig. 6. High-pressure operation of the seed supply canister required a new method for seed aggitation. The rotating agitator blades in the upper portion of the seed supply canister (see Fig. 15 of Ref. 14) were replaced by a dust-sealed, tube-axial fan located in the lower portion of the canister. The motor for the fan was self-contained in the fan shaft with the electrical leads entering the canister through a high-pressure electrical feed-through. Sometimes clogging of the fan shaft with carbon seed was noted. In most cases, the carbon could be removed and the fan restored to normal operation. However, the fan was replaced three times during the course of the program due to clogging by the carbon.

Argon was passed through the canister, entraining dispersed carbon particles with it. Argon entering the canister also helped to agitate the carbon powder through aerodynamic forces. The ratio of total argon weight flow rate to carbon weight flow rate was varied by allowing some of the total argon carrier flow to bypass the canister (see Fig. 6). The seeded argon flow line was connected to the plenum of the seeded gas inlet in the simulated propellant flow chamber. For the typical carbon seed weight flow rates used, the capacity of the canister was sufficient to permit total test times of approximately 10 min before the carbon supply was depleted. At the beginning of each test series the canister was filled approximately 2/3 full with carbon particles.

Two argon flow lines for the buffer layers were also connected to their respective inlets in the simulated propellant flow chamber (see Fig. 6). Individual pressure regulators, pressure gauges, control valves, and flow metering equipment were used for each system. Argon flow rates were measured using rotameters.

Configuration

A sketch of a cross section of the rectangular propellant duct mock-up is shown in Fig. 7. The simulated propellant duct was mocked-up by an assembly which could be attached to the inlet housing (Fig. 7). Construction was such that the spacing between the two transparent fused silica walls protected by unseeded buffer layers was adjustable. These transparent walls extended beyond the 12.7-cm (5.0-in.)-long test section. The remaining two side walls of the simulated propellant duct were aluminum in the 12.7-cm (5.0-in.) test section; beyond the test section they were glass to allow photographs to be taken from the side as the simulated propellant leaves the test section. Photographs from the side indicate the relative widths of the unseeded buffer layers and central seeded gas stream. The aluminum side walls and their glass extensions were allowed to contact the seeded gas flow. These side walls became coated by the carbon seed.

A radiometer viewed a tungsten filament lamp through the test section. As shown, the radiometer line of sight (Fig. 7) was located near the test section exit and passed through the transparent fused silica walls protected by unseeded buffer layers, and through the seeded gas flow. In this way, radiometer measurements could be made of the transmission of the transparent walls protected by unseeded buffer layers or the transmission of the seeded gas flow.

Figure 8 is a photograph of the two-dimensional propellant duct mock-up. It serves to further illustrate the relationship between the transparent fused silica walls protected by unseeded buffer layers, the line of sight of the radiometer, and the direction in which photographs were taken.

The gas inlet shape shown in Fig. 7 is based on the understanding of inlet configurations developed in the cold-flow tests discussed in Ref. 14. The general nature of the inlets was the same. However, the inlet in Fig. 7 was rectangular, while that described in Ref. 14 was annular. This required that a suitable relationship between the widths of the seed gas inlet and buffer inlets be redetermined for the rectangular (two-dimensional) inlet. Several width relationships were investigated and the most promising one, described in the following subsection, was used for the simulated propellant heating tests. The inlet used for the cold-flow tests was designed so that the same parts could be used for the simulated propellant heating tests. For this reason the inlet housing contains, in one integral piece, the inlets for the simulated propellant flow and the d-c arc vortex.

Results

Final Duct and Inlet Geometry

Cold-flow tests were performed to determine inlet buffer flow passage dimensions for use in the simulated propellant heating tests. Figure 7 shows the configuration that was determined to be the most suitable. The final width of the propellant duct was 3.3 cm (1.3 in.); the depth was 2.3 cm (0.9 in.); and the length was 12.7 cm (5.0 in.) measured from the downstream face of the porous foam to the end of the test section.

Porous foam was located in the inlets of the two unseeded buffer layers and at the entrance to the test section as shown in Fig. 7. The foam material was the same porosity (45 ppi) as the foam used in the propellant heating tests described in Ref. 15.

The 0.3-cm (0.12-in.) wide seed inlet duct was formed by two stainless steel plates which tapered to knife edges at the inlet plane. Each buffer layer was 1.5-cm (0.59-in.) wide at the inlet to the test section. The average velocities of the three streams were matched at about 0.8 m/sec (2.6 ft/sec).

As depicted in Fig. 7, the seed flow spread considerably as it passed through the foam at the entrance to the test section. The amount of seed spreading through the foam was greater than that obtained in the tests described in Ref. 14, although the foam material used in the two test series was nominally the same. However, the foam used in the present tests seemed to accumulate carbon more rapidly, and this is a possible cause of the observed increased spreading. This problem was overcome by increasing the buffer layer width at the inlet to 1.5 cm (0.54 in.) (compared with 1.0 cm (0.39 in.) in previous tests). It has also been found that careful cutting and positioning of the foam material is required for reliable, repeatable buffer layer performance. As represented in Fig. 7, the seeded flow occupied a large fraction of the propellant duct (as much as 75 percent of the duct volume in some tests). The actual buffer layer thickness in the test section --- the distance between the transparent wall and the seeded stream --- appeared to be about 0.4 cm (0.16 in.) for these tests.

Photographs During Test Series

Figure 9 presents a series of photographs taken during the cold-flow tests from the side of the variable-width propellant duct, as indicated in Fig. 8. The results of transmission measurements for these conditions are shown in Fig. 10.

The photograph in Fig. 9(a) shows the test configuration as viewed from the side. The radiometer viewed a tungsten filament lamp through the transparent walls at a point about 1.27 cm (0.5 in.) downstream of the end of the section (see Figs. 7 and 8). Photographs (b), (d), and (f) in Fig. 9 show side views of the seeded gas flow for various levels of seed transmission. The unseeded buffer layers separating front and rear transparent walls are clearly shown in all the photographs (see Fig. 9(b), for example). Side views of the test section without seeds flowing are shown in Figs. 9(c), (e), and (g). The central portion of the left and right side walls, which were unprotected by buffer layers, became coated with carbon seed. Shown below each of the photographs is the time in minutes from the beginning of the test series at which the photograph was taken and the value of either seed or wall transmission at the time the photograph was taken.

Transmission Measurements During Test Series

In Fig. 10, the dashed line shows the variation with time of the average value of the precent of radiation incident on the seeds that was transmitted through the seeds. The levels shown correspond to average values of the transmission over various time periods. The value of transmission was corrected for any decrease in transmission that might be due to seed coating on the front and rear transparent walls. The level of seed transmission was adjusted to that shown by varying the amount of bypass through the seed supply system (see Fig. 6).

For the tests shown in Figs. 9 and 10, an orifice (0.016-in. dia) was used to deagglomerate the carbon seed (also shown in Fig. 6). Estimates of the carbon seed mass attenuation coefficient at the exit of the test section indicate a value well in excess of 5000 cm^2/g averaged over the wavelength interval from 0.22 to 2.3 microns.

Also shown in Fig. 10 (solid line) is the level of transmission of the transparent duct walls compared with their initially clean condition. These measurements were obtained by turning the seed flow off periodically as the test series progressed. The points at which these measurements were made are marked on the figure. The resulting values are connected by straight lines to represent average values of wall transmission between measurements. Average values of seed transmission of about 1 percent were obtained over a period of about 13 min. After this 13-min period, the duct wall transmission was still about 99 percent of its starting value. As shown below in Fig. 9(d), which was taken at t = 6.6 min, for some portions of the test period the seed attenuation was so great that zero seed transmission was indicated.

Shortly after 13 min, the wall transmission began to decrease (Fig. 10). After 30 min, the wall transmission decreased to 85 percent of its starting value. This decrease in buffer layer effectiveness with time corresponds to an observed accumulation of carbon in the foam material at the inlet plane, and increased turbulence in the flow as evidenced by the seed flow. The coating on the unprotected side wall shown in Fig. 9(g) indicates that by the end of the test the seeded gas occupied most of the duct volume. By the end of the test period, when wall coating has been measured, visible carbon deposits were observed on the transparent walls that had been protected by buffer layers, similar to those on the unprotected side walls. The wall coating therefore appears to be caused by the deterioration of the fluid mechanics at the inlet. This wall coating, caused by inlet foam clogging, was not a cause for concern in the propellant heating tests because the foam can be replaced easily. Also, as shown by the test results, each piece of foam was usable for several minutes.

Cold-flow tests were also performed in which no orifice was used for seed deagglomeration. The test results were similar to those obtained when orifices were used in terms of total absorption and buffer layer effectiveness (see preceding paragraph).

The results of the cold-flow tests showed, therefore, that the carbon seed could be effectively confined to the central portion of the simulated propellant flow to prevent coating of the transparent duct walls and that high values of the carbon seed mass attenuation coefficient (greater than 5000 cm^2/g averaged over the wavelength interval from 0.22 to 2.3 microns) could be obtained within the simulated propellant heating test section. The simulated propellant flow configuration determined from these cold-flow tests described in this section was then used in the simulated propellant heating tests.

SIMULATED PROPELLANT HEATING TESTS

Objectives

The main objective of this portion of the program was to obtain simulated propellant bulk temperatures in excess of 3330 K (6000 R). The long-term objective is to obtain bulk exit temperatures approaching 6660 K (12,000 R) with tungsten seeds as required for the reference nuclear light bulb engine (Ref. 3). The simulated propellant flow was similar to that of the nuclear light bulb engine in the sense that the thermal radiation is absorbed by micron-sized solid particle seeds, and that buffer layers of unseeded gas prevent coating of the propellant duct walls by the seeds.

The results of the simulated propellant heating tests discussed in Ref. 14 pointed to the need for an improved method of determining the simulated propellant bulk exit temperature. As a result, an objective of this program was to develop a calorimetric technique for determining the simulated propellant bulk exit temperature.

Three test configurations were tested during this program. Most of the tests were performed using one basic simulated propellant heating configuration. This configuration is described in detail together with the diagnostic equipment used for all the tests. The results of the tests with the basic configuration are then discussed. Following this discussion, tests of a configuration with reflecting walls in the simulated propellant duct and a configuration with divergent walls in the simulated propellant duct are described. The results of the tests with each of these configurations are discussed following the description of their respective test configurations.

Basic Test Configuration

The basic simulated propellant heating configuration combines the results of the tests discussed in the preceding sections. A mirror is used around the d-c arc radiant energy source to increase the radiation from the d-c arc that is incident in the simulated propellant flow.

Figure 11 is a photograph of the d-c arc configuration showing the general relationship between the mirror housing, calorimeter assembly, seeded gas inlet, buffer gas inlet, and arc vortex inlet. The locations of the simulated propellant heating test section, exhaust hood, d-c arc anode and fused silica tube are also shown.

Figures 12 and 13 show cross sections of the propellant heating configuration. Figure 12 is a cross section of the lower portion of the configuration. Section A-A shows the 4.0-cm (1.57-in.)-ID uncooled fused silica tube that encloses the d-c arc radiant energy source (see Fig. 3) surrounded by a water-cooled mirror. The fused silica tube was separated from the reflecting surface by a space about 0.073-cm (0.030-in.) wide. Reflecting surfaces were copper coated with kanigen which was then polished and vapor coated with aluminum. The function of the mirror was to increase the amount of radiation from d-c arc, in the direction of the simulated propellant flow, above the radiation from the d-c arc alone.

The front wall of the simulated propellant duct was a 0.25-cm (0.10-in.)-thick uncooled, fused silica plate (Fig. 12) and the rear wall was a similar uncooled, fused silica plate. Both side walls of the duct were made of 0.64-cm (0.25-in.)-thick steel plates. The dimensions of the simulated propellant duct and inlet geometry were the same as those of the duct used in the cold-flow tests. As shown in Fig. 12, the spacing between the transparent walls was 3.3 cm (1.3 in.); it was 2.3 cm (0.9 in.) between the steel walls.

As illustrated in Fig. 12, the seeded gas was introduced into the central portion of the simulated propellant flow, and was separated from the front and rear transparent walls by unseeded buffer layers. The seeded gas was allowed to contact the steel side walls. For all the tests, argon seeded with carbon was used as the simulated propellant.

The simulated propellant entered the lower end of the 12.7-cm (5.0-in.)-long test section and flowed upward, parallel to the axis of the d-c arc, into the calorimeter. Seeded gas is introduced through a 0.3-cm (0.12-in.)-wide slot. The buffer gas inlets were 1.5-cm (0.59-in.) wide. As illustrated in Fig. 12, the seed flow spread as it passed through the porous foam at the beginning of the test section.

The average velocities of the seed and buffer flows are matched at 0.8 m/sec (2.6 ft/sec). Porous foam was used at the beginning of the test section to smooth the velocity profiles at the junction of the three parallel flows. This minimized the spreading of the seed flow in the simulated propellant duct.

The porous foam at the beginning of the test section is exposed to radiation from the d-c arc. In the tests discussed in Ref. 14, melting of the porous foam was a limitation on the power level at which the d-c arc could be operated. Two steps were taken to overcome this difficulty. The first step was to place a water-cooled shield between the foam and the d-c arc (Fig. 12). This blocked the radiation from the portion of the arc near the cathode; however, the foam was still exposed to radiation from the upper portion of the d-c arc column. For most tests, this radiation caused significant damage to the foam only after the cumulative effects of several runs. At the highest arc power levels used, the foam needed to be replaced

after two or three tests. In anticipation of this, the second step taken was to design the assembly for easy replacement of the porous foam. An additional factor in prolonging the useful life of a given piece of porous foam is the short test time used for these tests. The test time was about 0.5 sec for all the simulated propellant heating tests discussed in this report. Test times of several seconds were used in most of the tests described in Ref. 14.

Figure 13 is a sketch of the upper portion of the propellant heating configuration. The simulated propellant flowed into the calorimeter at the end of the test section (the calorimeter is discussed in detail subsequently). Cold-flow tests with the calorimeter indicated that the presence of the calorimeter at the exit of the test section did not adversely effect the simulated propellant flow in the test section.

As shown in Fig. 13, the anode for the d-c arc was located about 3.8 cm (1.5 in.) above the mirror assembly. This positioning was used to minimize possible arc shorting through the copper mirror assembly. The fused silica tube enclosing the arc also extended beyond the mirror assembly. The d-c arc anode, cathode, and vortex inlet are described in Appendix A.

Diagnostics

Calorimeter Measurements

The position of the water-cooled calorimeter assembly relative to the test section is shown in Fig. 13. Its purpose was to measure, based on the water-cooling temperature change, the energy contained in the hot simulated propellant flow.

Because of the 0.5-sec test time, the calorimeter did not come to thermal equilibrium with the simulated propellant flow. As a result, the simulated propellant bulk temperature was determined using a transient method. Simulated propellant was allowed to flow through the system while the difference between the calorimeter inlet and outlet water-cooling temperatures was monitored using a thermopile and a strip-chart recorder. Then the d-c arc was turned on for about 0.5 sec. Energy was removed from the hot simulated propellant and stored in the metal parts of the calorimeter which were, in turn, cooled by the calorimeter water. The water-cooling temperature rise was monitored until the temperature difference between the inlet and outlet returned to its value before the d-c arc was turned on.

Figure 14 is an example of a calorimeter water-cooling temperature rise trace. The response of the calorimeter is long compared to the simulated propellant heating test time of 0.5 sec. The water-cooling temperature rise was integrated and related through the water-cooling flow rate to the total energy deposited in the calorimeter. This total energy divided by the test time gives the average rate at which energy was

deposited into the calorimeter during the test. The average rate of energy deposited was then related, through the simulated propellant mass flow rate and specific heat, to the simulated propellant bulk temperature. The bulk temperature determined in this way is a time-averaged temperature over the propellant heating test time. As shown in Fig. 13, a chromel/alumel thermocouple recorded the temperature of the simulated propellant as it left the calorimeter after being cooled down. This thermocouple temperature returned to its initial value in about 1.5 sec. The temperature rise as determined by the thermocouple was added directly to the time-averaged bulk exit temperature determined above. The exit thermocouple temperature rise was generally less than 3 percent of the time-averaged bulk exit temperature rise determined by the calorimeter.

As shown in Fig. 13, the calorimeter had water-cooled walls and water-cooled coils in the upper section. The lower portion, which served as an adaptor to the test section, did not have coils. The water-cooled walls of the adaptor section extended down into the mirror housing to the end of the test section. Water from the adaptor passed upward and cooled the walls of the upper section containing the coils. Each of the two coils was separately water-cooled. The water-cooling for the entire calorimeter originated from one inlet in which water temperature was measured. Water-cooling to each element could be varied separately. Water-cooling flows from all the elements was collected in a plenum at the top of the calorimeter and removed through one main exhaust. The plenum was designed to promote mixing between the flows. Water temperature was measured in the exhaust after leaving the plenum.

The calorimeter was prevented from contacting the mirror housing by insulating pieces of super-mica (Fig. 13). A super-mica heat shield prevented direct radiation from the arc to the calorimeter in the region between the top of the mirror housing and the anode. The entire calorimeter assembly was enclosed in fiberglass insulation and wrapped with asbestos tape. All the water-cooling inlet and exhaust hoses were also wrapped in insulation. An asbestos heat shield was positioned as shown in Fig. 13 to prevent the hot exhaust gases from the d-c arc contacting the calorimeter. Tests were conducted to determine the thermal insulation effectiveness by blocking the test section off from the d-c arc and initiating the arc (see later discussion of Fig. 17). During these tests, the calorimeter absorbed a negligible amount of heat, demonstrating that it was effectively insulated from its surroundings. Radiation from the d-c arc, which passed through the test section, was absorbed by the calorimeter when the test section was not blocked off. Most of this radiation can be blocked from direct entry into the calorimeter if the simulated propellant transmission is low. This effect is discussed later.

Radiation Measurements

Measurements were made of the radiation transmitted through the simulated propellant as it flowed through the test section with the d-c arc on. These measurements were compared with the radiation passing through the test section at the same d-c arc conditions without seeds flowing. This comparison gives a measure of the fraction of the incident radiation that was transmitted through the simulated propellant. These measurements were made at a position halfway between the beginning and end of the test section (i.e., 6.3 cm (2.5 in.) downstream of the beginning of the test section). They were made using the same radiometer and aperture system described in the D-C ARC RADIANT ENERGY SOURCE section. All the relative dimensions and positions of the radiometer and aperture are the same as shown in Fig. 3 with the exception of the axial position of the portion of the d-c arc that was viewed.

Measurements were made of the effect of the mirror assembly on increasing the arc radiation in the direction of the test section. It is important at this point to differentiate between the original plan of achieving high radiant heat fluxes incident on the simulated propellant and the actual method used. The original plan called for a reflecting surface with about an 80 percent reflectivity and a d-c arc providing about 100 kw of radiation in the 12.7-cm (5.0-in.) test length. The actual mirror reflectivity was less than about 40 percent. The low reflectivity resulted mainly from accidental wetting of the mirror with water during early tests. This would not normally have caused a problem if the vendor had been able to coat the mirror with silicon monoxide, or another protective coating, in accordance with the design. However, as discussed in an earlier section, the arc was modified to provide up to 238 kw of radiation in the test length. This increased radiation was enough to compensate for the low reflectivity of the mirror.

The mirror assembly did in fact increase the radiation directed toward the test section from the arc, but not to the degree anticipated for a highly reflective mirror. Measurements were made of the effect of the mirror assembly using the test configuration illustrated in Figs. 15 and 16. The configuration in Fig. 15 was also used to check the radiometer measurements of the d-c arc. The opening between arc and test section was mocked up using a 12.7-cm (5.0-in.)-long by 2.3-cm (0.9-in.)-wide rectangular hole in an aluminum plate. The aluminum shield was positioned close to the fused silica tube to simulate the view factor from the arc, through the mirror, to the simulated propellant test section. A copper slug with blackened front surface was used to absorb the radiation from the d-c arc. The copper slug was 12.7-cm (5.0-in.) long, 2.37-cm (0.9-in.) wide, and 0.64-cm (0.25-in.) thick. The blackened face of the copper slug is positioned 3.5 cm (1.38 in.) from the arc centerline. This position corresponds to the propellant side of the front transparent wall of the simulated propellant duct. A thermocouple was placed in a hole drilled from the back side of the copper slug to within 0.16 cm (0.06 in.) of the blackened front face. The thermocouple was located in the center of the front face of the copper slug.

The temperature rise of the copper slug was monitored when the d-c arc was turned on. It was observed to increase rapidly when the arc was on, level off shortly after the arc was turned off, and then decrease slowly after remaining at a constant value for about 2 sec. The constant value of copper slug temperature was used, together with the slug density and specific heat, to calculate the heat flux from the arc. Thermocouples were also located at the top and bottom of the copper slug. These thermocouples generally read between 93 and 97 percent of the value of the thermocouple in the center. Lower values at the ends are to be expected because the view factor from the arc to an element of the slug on the end is lower than that view factor to an element in the center.

At the same time that the copper slug measurements were made, radiometer measurements were made of the arc radiation. The radiant flux determined by the copper slug is plotted against that determined by the radiometer, using open square symbols, in Fig. 16. The data show good agreement between the two methods for determining the flux.

Since the agreement was good between the copper slug and radiometer measurements, the copper slug technique was then used to measure the radiant flux incident on the test section with the mirror assembly in place. This test configuration is sketched in Fig. 17. The copper slug was positioned just behind the front transparent wall. Total arc power was measured and, from this, the radiant flux without the mirror for that power was determined. The radiant flux based on the copper slug is compared in Fig. 16 with the radiant flux at the same position based on the d-c arc radiation measurements shown in Fig. 4. The data are plotted as open circle symbols. For comparison, a dashed line representing a 44 percent increase due to the mirror assembly is shown. Thus, it appears that the mirror assembly increased the radiation incident on the simulated propellant by about 44 percent.

Thermocouple Measurements

The high temperature thermocouple measurements discussed in Ref. 14 were performed using thermocouples that had slow response times (about 15 sec). For this test program, some fast response thermocouples were obtained. They were bare wire, exposed junction, tungsten-5-percent-rhenium/tungsten-26-percent-rhenium thermocouples made from 0.76-mm (0.003-in.)-dia wire. Fine wire thermocouples are very fragile. The thermocouple leads were enclosed in a double bore alumina tube. The thermocouple element and about 0.32 cm (0.125 in.) of lead wire were exposed to the stream. The thermocouple response time was about 0.15 sec. The results and limitations of these measurements are discussed later.

Results

Tests with the basic configuration were conducted with and without the use of orifices for seed deagglomeration. These tests are discussed first. Then, tests using a propellant duct with reflecting walls and tests using a propellant duct with divergent transparent walls are discussed.

Tests with Basic Configuration

Simulated propellant heating tests were conducted using the basic configuration shown in Figs. 12 and 13. This configuration has transparent front and rear walls in the simulated propellant heating test section.

Tests Without Orifices

If the simulated propellant is sufficiently opaque, then it can block the radiation from the d-c arc passing obliquely through the test section to the calorimeter (see geometry in adaptor region in Fig. 13). However, the initial seed density must also be high enough to compensate for the expansion of the simulated propellant as it is heated. Tests were conducted without orifices because it was possible to provide sufficient seed opacity to reduce, to acceptably low levels, the possible errors in the calorimeter measurements due to direct radiation from the d-c arc. When an orifice was not used with the seeder system (Fig. 6), enough seed flow could be provided to obtain fractional transmission values for the simulated propellant as low as 0.0005 in the propellant heating tests. When orifices were used, thermal expansion of the simulated propellant limited the fraction transmitted to values greater than 0.3. These fractional transmissions were determined from radiometer measurements made halfway between the beginning and end of the test section. The radiation path length through the seeded gas flow from the arc to the calorimeter adaptor was longer than from the d-c arc to the radiometer. Therefore, radiation directed toward the calorimeter adaptor had a smaller fraction transmitted than the fraction transmitted as measured by the radiometer.

An estimate was made of the correction needed to the calorimeter energy measurement to account for radiation to the calorimeter inlet directly from the d-c arc and for reradiation from the simulated propellant. The method for estimating this correction, which was applied to all the calorimeter data, is discussed in Appendix B. The correction reduced the amount of energy measured by the calorimeter that was attributed to heat content of the simulated propellant. It resulted in reductions of the calorimeter measurements which ranged from 7 percent for data with low seed transmission to 40 percent for data with high seed transmission.

The seed weight flow rate for low transmission levels was estimated by weighing the carbon and dividing by the time period over which it was used. It was determined that an average carbon seed weight flow rate of about 0.44 g/sec (0.00096 lb/sec) was associated with tests whose fraction of radiation transmitted, measured at the mid-station of the test section using the radiometer, ranged from 0.05 to 0.0005. The total argon weight flow rate (seeded and unseeded streams) was 1.09 g/sec (0.0024 lb/sec) for all tests. These values of carbon seed and argon weight flow rates were used for all tests to determine the simulated propellant bulk exit temperature.

Simulated propellant heating tests were conducted without orifices using d-c arc powers up to 500 kw with about 240 kw radiated from the arc in the 12.7-cm (5.0-in.) test length. Up to about 35 kw of radiation was incident on the simulated propellant heating test section. This represents an increase by a factor of about fifteen in the radiant flux incident on the simulated propellant over the radiant flux available in the simulated propellant heating tests discussed in Ref. 14.

The results of the tests are summarized on Fig. 18, which is a plot of the simulated propellant bulk exit temperature versus the radiation incident on the simulated propellant heating test section. The radiation incident on the test section was based on the results of the copper slug tests with the mirror (Fig. 16) and the d-c arc tests (Fig. 4); bulk exit temperatures were determined from the calorimeter measurements, taking into account the aforementioned corrections and using a specific heat for carbon which was a function of temperature (discussed later).

Figure 18 shows the highest simulated-propellant time-averaged bulk exit temperature obtained to be 3860 K (6950 R). Twelve of the fifty-three data points obtained are above the 3330 K (6000 R) minimum temperature objective. Many of these bulk exit temperatures are higher than the bulk exit temperature for the solid core nuclear rocket (about 2200 K, or 4000 R) and are in the range of interest for low-power nuclear light bulb engines.

The data in Fig. 18 have been plotted in three groups, one group with low fractional seed transmission (between about 0.0005 and 0.1 --- solid circles), a second group with intermediate fractional transmission levels (between 0.1 and 0.2 --- half shaded squares), and the third group with high fractional transmission (between 0.2 and 0.6 --- open diamonds). The data generally fall into three groups with those points corresponding to higher fractional transmission having lower bulk exit temperatures for the same incident radiation.

The same data are plotted on Fig. 19 as the simulated propellant bulk exit temperature versus radiation absorbed by the propellant. The radiation absorbed by the simulated propellant was determined from radiation measurements using the radiometer at the midstation of the test section. This measurement gives an indication of the opacity of the simulated propellant. However, the local transmission is

expected to vary somewhat along the length of the test section. The radiation absorbed was obtained by multiplying the fraction absorbed (1 - fraction transmitted) by the incident radiation. As shown in Fig. 19, the data fall together in a single group, as would be expected when the effect of varying transmission is taken into account.

Table I lists the values of incident radiation, seed transmission, absorbed radiation, calorimeter measurement, calorimeter correction factor, heat in the gas, time-averaged bulk exit temperature, and local thermocouple temperature for each data point in Figs. 18 and 19.

Figure 20 is a parametric plot of calculated bulk exit temperature versus the power deposited in gas, for the same argon weight flow rate as in Figs. 18 and 19, with several different ratios of seed flow rate to argon flow rate. The average carbon weight flow rate used to reduce the aforementioned data corresponds to a seed fraction of 0.4 on Fig. 20.

The calculations in Fig. 20 include the effect of carbon vaporization based on JANAF vapor pressure data for carbon (Ref. 15). As the temperature of the carbon and argon mixture approaches the 4200 K (7560 R) sublimation temperature, a substantial amount of the absorbed power causes carbon vaporization rather than increases in the mixture bulk temperature.

Figure 20 also illustrates the effect of seed weight flow fraction on bulk exit temperature. For tests with high seed transmission the carbon weight flow rate was probably lower than the average value used to calculate the bulk exit temperatures in Figs. 18 and 19. Estimates of this effect indicate that a higher bulk exit temperature than 3860 K (6950 R) may have been obtained in tests with fractional transmissions in the 0.1 and 0.2 range. The maximum temperature for these tests may have been as high as 4000 K (7200 R).

For some tests, attempts were made to obtain thermocouple measurements of local simulated propellant temperature. The thermocouple was located in the center of the flow 1.91-cm (0.75-in.) beyond the end of the test section (Fig. 13). Figure 21 compares local temperatures measured by the thermocouple with bulk exit temperatures determined from calorimeter measurements. The local temperatures indicated by the thermocouple were lower than the bulk temperatures for all tests. It is difficult to understand how the local temperatures at this point in the duct could be as low, relative to the bulk exit temperatures, as shown in Fig. 21. It was recognized in the tests reported in Ref. 14 that local temperature measurements are difficult in a high temperature, low velocity, seeded gas stream. These difficulties were further aggravated in Ref. 14 by the long response time of the thermocouple (greater than 15 sec). A considerable improvement in the thermocouple response time --- a reduction to about 0.15 sec --- was obtained by using exposed junction thermocouples made with

0.76-mm (0.003-in.)-dia wire. However, the sources of error in the thermocouple measurements from carbon coating and radiation were still present. The sketch in Fig. 21 summarizes the factors that affect the thermocouple measurements. The low-velocity gas stream results in a thermal boundary layer which causes the temperature at the thermocouple junction to differ from that of the free-stream gas temperature due to conduction to the main thermocouple support. Coating of the thermocouple by solid seed particles changes the heat transfer to the thermocouple. Carbon coating of the thermocouple would probably cause the temperature indicated by the thermocouple to be lower than it would be without the coating. Heavy coatings of the thermocouple were observed for all the tests. The immersion length of the thermocouple stem into the gas stream also affects the accuracy of the thermocouple measurement. For a gas as hot as the simulated propellantstream, heat conduction along the stem can cause large errors in the local temperature measurement by thermocouples. This type of error would cause a low thermocouple reading. Stem heat conduction errors can be reduced by having a long stem immersion length ($L/D \approx 40$). The immersion length of the thermocouple leads based on their diameter was about 40. It is difficult to evaluate the effect of the alumina stem, which was about 0.32-cm (0.125-in.) in diameter, on the flow near the thermocouple and the heat transfer to the thermocouple element. Radiation effects are also a source of error. The error caused by radiation heat transfer is complicated by reradiation from the thermocouple to its surroundings and by the effect that seed coating would have on the absorption and emission characteristics of the thermocouple.

Although the thermocouple measurement techniques have been improved over those used in the past, the measurements are still questionable. It may be possible to further improve the thermocouple techniques for temperature measurement when lower seed rates are used and when the thermocouple can be positioned to minimize radiation effects.

Tests with Orifices

Simulated propellant heating tests were also conducted with the basic configuration using sonic orifices for seed deagglomeration. With orifices, the carbon seed weight flow rate was estimated to be only 0.055 g/sec (0.00012 lb/sec); hence, the average seed density at the inlet was reduced by a factor of eight relative to the tests without orifices. This corresponds to a fractional seed flow rate of 0.05 on Fig. 20. In the cold-flow tests, this seed weight flow rate was sufficient to provide very low values of seed transmission (see Figs. 9(b), (d), and (f)).

For the simulated propellant heating tests, the maximum seed flow with an orifice was not sufficient to compensate for the reduction in seed density caused by expansion due to heating. The expansion limited the fractional transmission to values above 0.3. The expansion effect is counteracted in the reference engine (Fig. 2) by a substantial area increase in the propellant duct flow area.

Temperatures were calculated for these tests by applying the correction to the calorimeter measurements discussed in Appendix B. These corrections are at best estimates for low seed transmission ($\eta_t > 0.1$) and may in fact allow errors for high seed transmission.

The simulated propellant temperatures obtained are summarized in Fig. 22 and Table II. Bulk exit temperatures up to about 2500 K (4500 R) were obtained. A comparison between Fig. 22 and Fig. 19 indicates that substantially less absorbed power was required to obtain a given temperature with an orifice, due to the much lower carbon seed density (and, therefore, the much lower average mixture specific heat). These tests were not continued to higher temperatures because it was recognized that too much radiation from the arc was getting directly into the calorimeter due to the low seed opacity; this problem was discussed previously.

As illustrated in Fig. 20, vaporization of the carbon seeds would eventually limit the benefits obtained from the lighter carbon seed flow rates. The use of tungsten seeds in future simulated propellant heating tests is expected to overcome the vaporization limitations caused by the carbon seeds in the present tests.

Tests with Reflecting Propellant Duct Walls

Simulated propellant heating tests were also conducted using a configuration having reflecting, water-cooled, propellant duct walls (Figs. 23 and 24). The front wall facing the d-c arc was transparent and the other three walls were reflecting. As in previous tests, the rear reflecting wall and front transparent wall were protected by unseeded buffer layers and the reflecting walls on both sides were allowed to contact the seeded gas. The rear reflecting wall had a 0.16-cm (0.063-in.)-dia hole in the center of the duct, 1.5-in. downstream of the beginning of the test section (Fig. 23), through which the seed transmission was measured. The remainder of the configuration was the same as that shown in Figs. 12 and 13.

The results are shown in Figs. 26 and 27 which correspond to Figs. 18 and 19 for the configuration with nonreflecting walls. Comparison of the two sets of figures shows that the results of the tests with reflecting walls are not significantly different from the results with nonreflecting walls.

The reflecting walls would change the results significantly only if they returned radiation transmitted or reradiated from the simulated propellant to the test section. The data points with fractional transmissions greater than 0.2 do, in fact, have bulk temperatures somewhat higher for the test with reflecting walls than with transparent walls. This might be because transmitted radiation was reflected back to the simulated propellant. More data are required to establish this effect. The bulk temperatures obtained with seed transmission less than 0.2 are about the same with reflecting walls and transparent walls. This could be explained if the reradiation only escaped inward toward the d-c arc, while the reradiation directed away from the arc toward the reflecting wall was re-absorbed by the simulated propellant.

The rear wall reflecting surface, which was protected by an unseeded buffer layer, was not adversely affected by the testing; it retained its high reflectivity (about 80 percent) for all tests. The side walls were coated with carbon and completely blackened during the tests. This carbon could be cleaned off, but the surface was reduced to a dull finish. The results of these tests indicate that reflecting rear walls can be fabricated and used in high-temperature simulated propellant heating tests, and may help in reducing radiation losses.

Tests with Divergent Propellant Duct

Exploratory tests were conducted at low powers to investigate the effects of divergent propellant duct walls on heating of the simulated propellant. Divergent walls are expected to help overcome the effect of decreasing seed density due to expansion of the simulated propellant as it is heated.

The rear transparent wall of the test section was slanted at an angle of about 5 deg as shown in Fig. 27, thereby providing about a 30-percent increase in flow area through the test section. The calorimeter was not used for these tests. Tests were conducted with incident radiation levels up to about 10 kw without an orifice for seed deagglomeration.

Qualitative observations of the buffer layer performance were made. The inner buffer layer was observed to perform well while the outer buffer layer allowed some light wall coating. The inlet and flow configurations were the same as in all other simulated propellant tests (inlet average velocities were matched at about 0.8 m/sec (2.6 ft/sec)). For some tests, the injection velocity of the buffer flow adjacent to the rear divergent wall was increased to about 1.22 m/sec (4 ft/sec) with the result that there appeared to be less coating by the seed on the rear divergent wall.

These preliminary tests indicate that it may be advantageous to use divergent walls in future simulated propellant heating tests.

Summary of Key Simulated Propellant Heating Test Results

Bulk exit temperatures up to 3860 K (6950 R) were obtained using argon seed with sub-micron carbon particles as simulated propellant. These bulk exit temperatures are in the range of interest for low-power nuclear light bulb engines and exceed those of the solid-core nuclear rocket. They were obtained in a simulated propellant duct which used buffer layers of unseeded gas to prevent coating of the propellant duct walls by the seed, as in the nuclear light bulb engine. Separate tests were conducted with a reflecting outer wall in the simulated propellant duct. These tests indicated that the reflecting wall can be protected by an unseeded buffer layer. Also, it appears promising as a means for reducing radiation losses when a significant amount

of reradiation occurs in the direction of the wall. Tests of a divergent simulated propellant duct indicated that this type of duct might help overcome the effects of reduction in seed density due to expansion as the flow is heated.

Moreover, using the present d-c arc equipment with improved reflecting walls and with tungsten seeds instead of carbon, it should be possible to attain substantially higher bulk exit temperatures.

REFERENCES

1. McLafferty, G. H.: Investigation of Gaseous Nuclear Rocket Technology -- Summary Technical Report. United Aircraft Research Laboratories Report H-910093-46, prepared under Contract NASw-847, November 1969.

2. McLafferty, G. H.: Survey of Advanced Concepts in Nuclear Propulsion. Journal of Spacecraft and Rockets, Vol. 5, No. 10, October 1968.

3. McLafferty, G. H. and H. E. Bauer: Studies of Specific Nuclear Light Bulb and Open-Cycle Vortex Stabilized Gaseous Nuclear Rocket Engines. United Aircraft Research Laboratories Report F-910093-37, prepared under Contract NASw-847, September 1967. Also issued as NASA CR-1030.

4. Krascella, N. L.: Theoretical Investigation of the Absorption and Scattering Characteristics of Small Particles. United Aircraft Research Laboratories Report C-910092-1, prepared under Contract NASw-847, September 1964. Also issued as NASA CR-210.

5. Krascella, N. L.: Theoretical Investigation of the Absorptive Properties of Small Particles and Heavy-Atom Gases. United Aircraft Research Laboratories Report E-910092-7, prepared under Contract NASw-847, September 1965.

6. Marteney, P. J., N. L. Krascella, and W. G. Burwell: Experimental Refractive Indices and Theoretical Small-Particle Spectral Properties of Selected Metals. United Aircraft Research Laboratories Report D-910092-6, prepared under Contract NASw-847, September 1965.

7. Marteney, P. J. and N. L. Krascella: Theoretical and Experimental Investigations of Spectral Opacities of Mixtures of Hydrogen and Diatomic Gases. Air Force Systems Command Report RTD-TDR-63-1102, prepared by United Aircraft Research Laboratories under Contract AF 04(611)-8189, November 1963.

8. Krascella, N. L.: Tables of the Composition, Opacity, and Thermodynamic Properties of Hydrogen at High Temperatures. United Aircraft Research Laboratories Report B-910168-1, prepared under Contract NAS3-3382, September 1963. Also issued as NASA SP-3005.

9. Lanzo, C. D. and R. G. Ragsdale: Experimental Determination of Spectral and Total Transmissivities of Clouds of Small Particles. NASA Technical Note D-1405, September 1962.

REFERENCES (Concluded)

10. Lanzo, C. D. and R. G. Ragsdale: Heat Transfer to a Seeded Flowing Gas from an Arc Enclosed by a Quartz Tube. NASA Technical Memorandum X-52005, June 1964.

11. Marteney, P. J.: Experimental Investigation of the Opacity of Small Particles. United Aircraft Research Laboratories Report C-911092-2, prepared under Contract NASw-847, September 1964. Also issued as NASA CR-211.

12. Williams, J. R., J. R. Clement, A. S. Shenoy, and W. L. Partain: The Attenuation of Radiant Energy in Hot Seeded Hydrogen - An Experimental Study Related to the Gaseous Core Nuclear Rocket. Quarterly Status Report No. 2, NASA Research Grant NGR-11002-068, prepared by Georgia Institute of Technology, February 1969.

13. Mie, G.: Annalen der Physik, Vol. 30, 1919.

14. Klein, J. F. and W. C. Roman: Results of Experiments to Simulate Radiant Heating of Propellant in a Nuclear Light Bulb Engine Using a D-C Arc Radiant Energy Source. United Aircraft Research Laboratories Report J-910900-1, prepared under Contract SNPC-70, September 1970. Also issued as NASA CR-111099.

15. Roman, W. C., J. F. Klein, and P. G. Vogt: Experimental Investigation to Simulate the Thermal Environment, Transparent Walls and Propellant Heating in a Nuclear Light Bulb Engine. United Aircraft Research Laboratories Report H-910091-19, prepared under Contract NASw-847, September 1969.

16. Stull, D. R., et al.: JANAF Thermochemical Tables. The Dow Chemical Company, Midland, Michigan, 1964.

LIST OF SYMBOLS

A^F_C	View factor from d-c arc to calorimeter adaptor, dimensionless
P^F_C	View factor between simulated propellant and calorimeter adaptor, dimensionless
I	Transmitted intensity, kw/cm^2
I_A	Arc current, a
I_o	Incident intensity, kw/cm^2
P_T	Total arc power, kw
q_{INC}	Incident radiant flux, kw/cm^2
Q_{ABS}	Radiation absorbed by propellant stream, kw
Q_{CAL}	Power measured by calorimeter, kw
Q_{GAS}	Power in simulated propellant, kw
Q_{INC}	Radiation incident on simulated propellant test section, kw
Q_R	Arc power radiated in 12.7-cm (5.0-in.) test section, kw
Q_{RC}	Reradiation from simulated propellant to calorimeter, kw
Q_{RD}	Direct radiation entering calorimeter, kw
Q_{RR}	Total reradiation from simulated propellant, kw
t	Time, sec or min
T_E	Bulk exit temperature, deg K or R
T_{TC}	Local thermocouple temperature, deg K or R
V	Arc voltage, v
ΔT_w	Water cooling temperature rise, deg K or R
η_T	Fraction of radiation transmitted, dimensionless

APPENDIX A

DESCRIPTION OF D-C ARC SYSTEM

Electrical Components

A block diagram of the primary electrical components of the d-c arc system is shown in Fig. 28. The arc power is supplied by two shunt-wound General Electric motor-generator sets rated at 250 kw each. The motor-generators may be connected for either series or parallel operation; for these tests, they were connected in parallel. The d-c power output is varied using a remote-controlled rheostat. This permits the motor-generator field voltage to be preset prior to arc initiation. A more detailed schematic diagram of the electrical circuit is shown in Fig. 29. Included are the circuitry for the motor-generator sets, the d-c arc monitoring and control instruments, and the d-c arc starter system.

The operating range for which d-c arc stability can be attained (with its inherent nonlinear dependence between voltage and current) is restricted by configuration, circuit and flow considerations. The arc may also exhibit large variations in static voltage-current characteristics, depending on environmental conditions. From electrical circuit considerations, the arc circuit is stable provided $R_B + dV_A/dI_A > 0$, where R_B is ballast resistance, V_A is arc voltage, and I_A is arc current. To satisfy this stability criterion, ballast resistors are included in the d-c arc power supply circuit (Fig. 29). A distinct advantage of using motor-generator power supplies is the elimination of undesirable power supply ripple inherent in all moving-coil-transformer or saturable-reactor type power supplies.

D-C Arc Configuration

Electrodes

The d-c arc configuration consists of a vortex-stabilized arc enclosed within an uncooled fused silica tube (see Fig. 3). The nominal dimensions of the fused silica tube are 4.0-cm (1.57-in.) ID by 4.3-cm (1.69-in.) OD. The arc is established between a pin type cathode and a hollow cylindrical anode.

The cathode is a 0.64-cm (0.25-in.)-dia, hemispherically-tipped, 2.0-percent-thoriated tungsten rod. The cathode is recessed and silver soldered into a water-cooled copper well. The vertical location of the cathode can be varied to optimize the location, size, operating temperature and constriction of the cathode attachment spot. Experiments have indicated that the cathode operating temperature plays a role in achieving stable, uncontaminated, long-lifetime operation, particularly at high power levels. The cathode water-cooling flow rate, which influences the cathode temperature, can also be varied.

The cylindrical water-cooled copper anode (Fig. 3) contains a 1.27-cm (0.5-in.)-dia hole, with rounded corners, on its centerline. A water-cooled magnetic field coil is wound around the outer circumference of the anode. The magnet coil is powered by a separate power supply. Interaction between the magnetic field generated by the coil and the arc current in the anode attachment region (JXB Force) causes the arc anode attachment spot(s) to rotate rapidly. By magnetically driving the anode spot(s) at high speeds (approximately 2000 rev/sec) over the anode surface, the very high heat load in the anode spot region is spread over a significantly larger area. This permits the high-velocity cooling water which flows meridionally within the anode coolant passage to remove heat more effectively. This magnetically augmented, water-cooled anode is capable of operation at currents up to 3000 a for several hundred tests (about 0.5-sec per test). At currents up to approximately 1500 a, the useful life is several hours.

Vortex Injectors

The arc column is stabilized by a vortex flow which is introduced into the plenum surrounding the cathode assembly (Fig. 3). The vortex generator injection assembly has four equally spaced vertical stainless steel tubes through which argon gas flows. Each of these tubes has four 0.038-cm (0.015-in.)-dia holes, spaced 0.29 cm (0.118 in.) apart. In addition to desirable arc column characteristics, the argon provides a nonoxidizing environment which minimizes erosion of the tungsten cathode. The angle of vortex injection can be varied from full radial (resulting in a coaxial flow parallel to discharge axis) to full tangential (resulting in a vortex flow) during arc operation by a variable-speed servo-motor drive and gear assembly. This permits establishing a satisfactory vortex geometry for a particular power level and vortex tube length-to-diameter ratio. The best operating condition is when the discharge axis is colinear with the axis of the fused silica tube surrounding the discharge. The vortex generator section is connected to the lower end of the inner fused silica tube through a convergent nozzle section. Argon weight flow rates up to 13.6 g/sec (0.03 lb/sec) were used in the vortex generator.

Gas and Water Cooling Systems

The gas and water cooling systems are shown schematically in Fig. 30. A centrifugal-type water pump, rated at 180 psig and 150 gpm, supplied the water-cooling for the anode, cathode, mirror assembly and mirrored propellant duct insert. A reciprocating-type water pump rated at 450 psig and 20 gpm supplied the water-cooling for the calorimeter and magnetic field coil. The water-coolant lines were connected from the individual pump manifolds to the various elements of the test equipment by high pressure, electrically nonconducting, flexible nylon hoses. The water-coolant flow rate to each element was controlled by means of separate valves. The low pressure return lines were connected to rotameters to permit determination of the coolant flow rate through each element. After flowing through the rotameters, all coolant flows

were connected to a common water exhaust manifold and drain. The temperature of the water entering the water-flow system was monitored by a thermocouple located at the inlet manifold. The temperature of the water leaving each element was monitored by separate thermocouples located close to the exhaust of each element. Copper/constantan thermocouples were used to measure all water temperatures.

Argon for the d-c arc vortex generator and the simulated propellant stream was provided from separate high pressure supplies. The d-c arc vortex generator argon supply consisted of two argon bottles (245 scf each) manifolded together. The argon supply for the simulated propellant flows consisted of eleven argon bottles (245 scf each) manifolded together. The argon flow rates were monitored using rotameters. The d-c arc heater vent was connected to a 1500-cfm axial fan which was located directly above the test section. Figure 11 is a photograph of the test configuration. Illustrated are the major arc components, the water-cooling and gas connections, the propellant duct, and the exhaust vent. The vortex control system is shown in the lower right-hand corner of Fig. 11.

The test stand (see Fig. 11) allows easy removal and attachment of the various d-c arc and propellant heating components. Vertical adjustments can be made to permit location of the 12.7-cm (5-in.)-long test section in different positions relative to the diagnostic equipment located outside the test chamber (e.g., the radiometer and cameras).

Arc Starting and Control Systems

Starting Systems

The arc was initiated by employing a secondary tungsten-tipped stainless steel anode (0.64-cm (0.25-in.)-dia rod, 76.84-cm (30.25-in.)-long) which initially made contact with the cathode tip, and was then rapidly withdrawn upward through the primary anode. In this way, the arc was drawn vertically upward until it reached the level of the primary anode (see Fig. 29). The time for the secondary anode to withdraw through the primary anode was about 0.05 sec. Arc transfer from the secondary anode to the primary anode was accomplished as the secondary anode continued upward to its fully retracted position. The starting system was actuated by a two-way pneumatic cylinder. The starting sequence was synchronized such that withdrawal of the secondary anode lagged the main arc power initiation by approximately 0.4 sec. This fully established the arc prior to rapidly drawing apart the electrodes. During the starting sequence, an air-cooled ballast resistor was used to limit the arc current to approximately 50 a. The current-limiting technique was used to reduce contamination of the test-section walls due to tungsten sputtering caused by a sudden high-current arc, or the contamination which would be given off had an exploding wire starting technique been employed. After the arc transfers from the secondary anode

to the primary anode, less ballast resistance is present in the arc circuit (see Fig. 29). The circuitry for the starter system is shown on the right side of Fig. 29. This shows the relationship between the secondary anode and current limiting ballast, and the anode and the d-c arc ballast.

Because of the current limiting technique used during starting, the d-c arc makes a transition from a low current arc to a high current arc when the arc transfers from the secondary anode to the magnetically augmented anode. The low current arc and the high current arc operating phases require different vortex argon flow rates. For this reason, the vortex argon must be increased during the starting sequence.

Control System

Test times for high power operation of the d-c arc were limited to about 0.5 sec due to cooling and power supply requirements. This short test time required the very rapid sequencing of events which in the past had been performed manually. For this reason, a timing control system was installed to automatically perform rapid sequencing of events required to control the d-c arc operation. The control system automatically sequences the following events after pressing the start control to initiate arc power:

(1) the time delay between pressing the starting control and withdrawal of secondary anode,

(2) the time delay between pressing the starting control and the initiation of the secondary vortex argon for the high current arc mode, and

(3) the time delay between withdrawal of the secondary anode and termination of the arc power.

All three time delays can be varied independently through the use of separate time delay relays: the starter withdrawal time delay and the secondary argon time delay can be varied from 0 to 1.0 sec, and the time delay to termination of arc power can be varied from 0 to 100 sec. In addition to operation in the automatic sequencing mode, the control system can be operated in the manual mode in which all the control functions can be performed manually as in previous d-c arc systems (Refs. 14 and 15).

As shown in Fig. 31, the control console incorporates, in addition to the d-c timing controls, the starter rod indexing control, anode magnet power control, water-coolant controls, arc vortex angle controls, arc argon control, strip-chart recorders, and simulated propellant gas control.

Incorporated into the control circuitry are various safety interlocks which prevent starting of the arc unless all the water-coolant flows, the anode magnet coil, and the arc vortex argon are turned on prior to initiation of the arc power. This is an important self-checking feature since arc initiation without any one of these items could result in damage, particularly at high arc power conditions. The system allows for each of the interlock features to be overridden if it is desired.

The control system can be operated in the "timing" or "run" mode. The "timing" mode allows the timing relationships to be adjusted and checked without initiating arc power. The "run" mode is the normal arc operating mode. This automatic control system has proved to be an important asset for the d-c arc operation with the simulated propellant heating tests.

Summary of Modifications to the D-C Arc System

The d-c arc system incorporates several major changes from configurations used in the previous simulated propellant heating experiments (Refs. 14 and 15). The objective in making the changes was to increase the radiant flux incident on the simulated propellant, thereby increasing the obtainable simulated propellant bulk exit temperature.

The following are the major changes to the basic configuration:

(1) The former water-cooled fused-silica tube enclosing the arc (see Fig. 3 of Ref. 15) was replaced by an uncooled fused silica tube. The water cooling was responsible for absorbing about 30 percent of the arc radiation. Therefore, its removal is a direct step towards increasing the radiation from the arc to the simulated propellant. However, removal of the water-cooling also dictates that the arc tests be limited to short times (about 0.5 sec). The inside diameter of the fused silica tube enclosing the d-c arc was increased from 3.2 cm (1.26 in.) to 4.0 cm (1.57 in.) to allow for high current operation.

(2) The arc length was decreased from 26.04 cm (10.25 in.) to 17.78 cm (7.0 in.) by removing the arc locator. For the same total arc power, this increased the amount of radiation in the 5-in. simulated propellant heating test length because the power per unit length was increased.

(3) The position of the cathode in the d-c arc vortex inlet was changed to improve the vortex stabilizing effect at the cathode. An effective vortex at the cathode is particularly important for stable, high current, d-c arc operation. One constraint on the position of the cathode with respect to the vortex inlet is that the cathode must be positioned to

minimize possible melting of the porous foam used in the inlet to the simulated propellant heating test section. For the configuration discussed in Ref. 14, the desire to satisfy this constraint and simultaneously maximize the radiant heat flux required that the cathode be placed outside the region of strongest vortex effect. Also, the cathode water-cooling well was modified to prevent possible water leaks through the silver solder joint caused by the high cathode temperature at high currents.

(4) The motor-generators were changed from series to parallel operation. This was done to provide high current (up to 3000 a) d-c arc operation.

(5) The power for the anode magnet coil current was changed from series connection with the d-c arc current to a separate power supply. This was done so that the anode magnetic field could be fully established prior to d-c ignition. It is desirable to have the anode magnetic field fully established to minimize possible anode erosion and anode spot sticking during high-power starting.

(6) The method for starting the arc was changed to allow high power conditions to be reached rapidly within the 0.5-sec test time. In previous tests (Refs. 14 and 15), the arc was established between the cathode and primary anode at a moderate power; then the motor-generator field voltage was increased, using the rheostat control to obtain high power. The response of the field voltage to the rheostat control is too slow to use this method for the present test configuration. Now the field voltage is pre-set at its high power level and a higher ballast resistance is used in the secondary anode circuit. This decreases the anode life somewhat because of the high-power arc transfer from the secondary anode to the primary anode.

(7) The pneumatics of the d-c arc secondary anode withdrawal were modified to increase the speed of the starter withdrawal. After the modifications, the starter rod withdraws in about 0.05 sec. Rapid secondary anode withdrawal is desirable for high-power starting to minimize secondary anode erosion.

(8) An automatic control system to sequence the starting and arc control functions which were previously performed manually was installed. The need for this system was dictated by the desire for short tests, with high-power starting conditions.

APPENDIX B

CALORIMETER CORRECTIONS

The primary objective of the simulated propellant heating tests was to obtain high simulated propellant bulk exit temperatures by absorption of thermal radiation. There are several difficulties associated with determining the bulk or local temperature of the high-temperature, low-velocity, seeded simulated propellant. These difficulties are aggravated by direct and indirect effects of the intense radiation from the d-c arc on the measurements, and by the short test times.

A diagnostic technique was developed by which the time-averaged bulk exit temperature could be determined. This technique was cased on calorimetric measurement of energy added to the simulated propellant, an estimate of the simulated propellant weight flow rate, and measurement of the test time.

The calorimeter must be thermally isolated from its surroundings. Tests were conducted which indicated that the calorimeter was effectively isolated from erroneous heat exchange except for direct radiation from the d-c arc passing obliquely through the test section to the calorimeter adaptor (see Fig. 13). There were two methods by which direct radiation could be minimized: (1) by not exposing the calorimeter adaptor to radiation and (2) by blocking the radiation from entering the calorimeter. The first method would have required positioning the calorimeter adaptor about 5.0 cm (2.0 in.) beyond the end of the test section. This would result in a low calorimeter measurement because the hot simulated propellant would probably cool rapidly by reradiation in this distance; the amount of cooling would be difficult to estimate. The second method was more straightforward to apply because the opacity of the simulated propellant naturally blocks the radiation from direct entry into the calorimeter adaptor. If the carbon seed opacity is sufficiently high, the simulated propellant will absorb most of the radiation from the d-c arc before it reaches the calorimeter. To compensate for the decrease in seed density due to expansion by heating, the initial simulated propellant opacity must be very high.

Since the velocity and temperature distributions within the simulated propellant flow are not known, the exact blocking effect of the simulated propellant is not known. It is expected that, for low transmission conditions, the simulated propellant will be hottest in the front (close to the arc) and relatively cold in the rear of the simulated propellant duct. The hottest portions of the flow will expand and, therefore, the opacity in this portion of the flow will be lower than the opacity in the lower-temperature portions. As a result, the simulated propellant in the rear of the flow is more effective in blocking the radiation than the simulated propellant in the front of the flow. Also, the view factor from the arc to the calorimeter adaptor is highest at the rear of the adaptor, and is effectively zero at the front of the adaptor.

Measurements of the transmission through the seed were made in the middle of the test section. Fractional transmissions as low as 0.0005 were obtained. Moreover, the radiation path length through the simulated propellant from the d-c arc to the radiometer is clearly shorter than the oblique path from the d-c arc to the calorimeter adaptor. The combined effects of the longer oblique path length, reduced opacity in the front portion of the flow, and higher view factor from the arc to the rear of the calorimeter cannot be precisely evaluated without knowledge of the temperature, opacity, radiation, and flux distributions in the simulated propellant.

For the purpose of estimating the effect of direct radiation on the calorimeter measurements, the transmission measured at the axial midstation was taken as representative of the transmission to the calorimeter. The direct radiation entering the calorimeter was assumed to be

$$Q_{RD} = \eta_T \, {}_AF_C \, Q_{INC} \qquad (1)$$

where η_T is the simulated propellant transmission, ${}_AF_C$ is the fraction of the radiation incident on the test section that reaches the calorimeter if the seed is transparent, and Q_{INC} is the radiation incident on the test section from the d-c arc. A value of 0.073 for ${}_AF_C$ was obtained from measurements of the energy absorbed by the calorimeter for tests without seeds flowing.

The effect of radiation reaching the calorimeter due to reradiation from the hot simulated propellant was also estimated. Equation (2) expresses the total reradiation, Q_{RR}, as the difference between the heat absorbed, Q_{ABS}, and the heat in the simulated propellant, Q_{GAS}, as it enters the calorimeter:

$$Q_{RR} = Q_{ABS} - Q_{GAS} \qquad (2)$$

The heat reradiated that reaches the calorimeter, Q_{RC}, can be expressed as

$$Q_{RC} = {}_PF_C \, Q_{RR} \qquad (3)$$

where ${}_PF_C$ is the view factor between the simulated propellant and the calorimeter. An estimated value of ${}_PF_C = 0.02$ was used in the data correction.

The heat reradiated that reaches the calorimeter can be expressed as

$$Q_{RC} = (1 - \eta_T)\ {}_pF_C\ Q_{INC} - {}_pF_C\ Q_{GAS} \tag{4}$$

by combining Eqs. (2), (3), and the definition of Q_{ABS}.

The heat absorbed by the calorimeter can be expressed as

$$Q_{CAL} = Q_{GAS} + Q_{RD} + Q_{RC} \tag{5}$$

or

$$Q_{CAL} = Q_{GAS} + \eta_T\ {}_AF_C\ Q_{INC} + (1 - \eta_T)\ {}_pF_C\ Q_{INC} - {}_pF_C\ Q_{GAS} \tag{6}$$

Solving for the ratio of Q_{GAS}/Q_{CAL},

$$\left(\frac{Q_{GAS}}{Q_{CAL}}\right) = \left(\frac{1}{1 - {}_pF_C}\right)\left[1 - \left[\eta_T\ {}_AF_C + (1 - \eta_T)\ {}_pF_C\right]\right]\left(\frac{Q_{INC}}{Q_{CAL}}\right) \tag{7}$$

All the quantities on the right side of Eq. (7) were measured in the experiments except ${}_pF_C$, which was estimated. From Eq. (7), the calorimeter measurements can be corrected for the estimated effect of radiation by multiplying Q_{CAL} by (Q_{GAS}/Q_{CAL}), to give Q_{GAS}. The effects of this correction on the data are indicated in Tables I and II.

TABLE I

SIMULATED PROPELLANT HEATING DATA WITHOUT ORIFICE FOR SEED DEAGGLOMERATION

Incident Radiation Q_{INC}-kw	Fraction Of Radiation Transmitted η_T	Absorbed Radiation Q_{ABS}-kw	Calorimeter Power Q_{CAL}-kw	Calorimeter Power Correction Factor K	Power In Gas Q_{GAS}-kw	Bulk Exit Temperature T_E-K	Local Thermocouple Temperature T_{TC}-K
			Non-Reflecting Walls				
34.0560	.0005	34.0390	6.0980	.9025	5.5032	3861	
13.5300	.0040	13.4759	2.8840	.9206	2.6550	2324	
11.3520	.0070	11.2725	2.7180	.9310	2.5303	2230	
13.5300	.0090	13.4082	2.9820	.9227	2.7514	2375	
30.4040	.0110	30.0696	5.3910	.8981	4.8417	3694	
17.7300	.0140	17.4818	3.2290	.9005	2.9077	2478	
34.0560	.0150	33.5452	5.7960	.8917	5.1683	3789	
11.3520	.0180	11.1477	2.5980	.9242	2.4011	2145	
23.0160	.0190	22.5787	3.9750	.8923	3.5471	2916	
7.1520	.0200	7.0090	1.6400	.9239	1.5152	1532	922.2
7.1520	.0200	7.0090	1.6300	.9233	1.5050	1532	
9.7980	.0200	9.6020	2.1280	.9185	1.9546	1828	
26.4380	.0220	25.3564	4.8730	.8996	4.3837	3464	
13.6860	.0250	13.3439	2.7860	.9103	2.5361	2225	1672.2
23.0160	.0270	22.3946	3.8990	.8873	3.4596	2858	
30.4040	.0280	29.5527	5.8670	.9034	5.3001	3805	
34.0560	.0300	33.0343	5.7040	.8848	5.0470	3750	
30.4040	.0330	29.4007	5.1230	.8847	4.5322	3555	
11.3520	.0360	10.9433	2.3680	.9102	2.1553	1972	
8.5560	.0480	8.1453	2.1090	.9246	1.9500	1825	
18.0400	.0670	16.8313	3.7670	.9023	3.3990	2781	
30.4040	.0730	28.1845	5.8280	.8900	5.1870	3778	
9.7980	.0800	9.0142	1.9000	.8886	1.6902	1656	977.7
9.7980	.0900	8.9162	1.9640	.8912	1.7503	1697	922.2
13.5300	.0960	12.2311	2.9720	.9011	2.6781	2318	
8.5560	.0970	7.7261	1.8910	.9016	1.7049	1663	
34.0560	.1000	30.6504	6.0000	.8702	5.2214	3792	
34.0560	.1000	33.7154	5.2370	.8796	4.6066	3519	
8.5560	.1060	7.6491	1.8340	.8956	1.6426	1630	977.7
32.8930	.1200	28.9458	6.1450	.8731	5.3652	3819	
23.0160	.1230	20.1850	3.4300	.8345	2.8622	2430	
13.6860	.1380	11.7973	2.5920	.8705	2.2551	2039	
33.8250	.1380	29.1571	5.8860	.8567	5.0423	3700	
26.4380	.1430	22.6574	5.1400	.8725	4.4849	3521	
26.4380	.1430	22.6574	4.3870	.8470	3.7159	3003	
4.3240	.1470	4.1149	1.2110	.9052	1.0962	1222	588.8

(Continued)

TABLE I (Continued)

Incident Radiation Q_{INC}-kw	Fraction Of Radiation Transmitted η_T	Absorbed Radiation Q_{ABS}-kw	Calorimeter Power Q_{CAL}-kw	Calorimeter Power Correction Factor K	Power In Gas Q_{GAS}-kw	Bulk Exit Temperature T_E-K	Local Thermocouple Temperature T_{TC}-K
13.6860	.1750	11.2909	1.6440	.7663	1.2598	1491	769.4
17.7300	.1810	14.5209	2.7290	.8202	2.2383	2017	1394.4
4.8240	.1870	3.9219	1.2280	.8984	1.1032	1231	866.6
13.6860	.1940	11.0309	2.5870	.8538	2.2089	1993	1033.3
13.6860	.2000	10.9488	2.3030	.8313	1.9144	1795	1338.3
18.6620	.2380	14.2204	2.6410	.7810	2.0625	1891	1060
13.6860	.2440	10.3466	2.1050	.7981	1.6800	1641	
11.3950	.2680	8.3411	2.0780	.8260	1.7164	1653	
8.5540	.2720	6.2273	1.2980	.7851	1.0191	1159	866.6
13.6860	.3310	9.1559	1.8690	.7357	1.3751	1417	
8.5540	.3380	5.6627	1.4430	.7879	1.1369	1242	866.6
28.1490	.3570	18.0998	3.0540	.6490	1.9821	1839	700.0
18.6620	.3810	11.5518	2.3080	.6843	1.5794	1570	533.3
11.3530	.4640	6.0852	2.1020	.7721	1.6231	1591	
28.1490	.5330	13.1456	3.8460	.6566	2.5253	2217	
23.0170	.5420	10.5418	2.8910	.6208	1.7946	1725	
13.6860	.5620	5.9945	1.6760	.6017	1.0085	1159	
			Reflecting Walls				
33.5900	.0510	31.8769	4.8860	.8564	4.1844	3277	
27.9900	.0950	25.3309	3.7620	.8253	3.1048	2564	
33.5900	.1020	30.1638	4.8430	.8360	4.0487	3168	
34.5300	.1090	30.7662	4.2650	.8020	3.4203	2765	
33.5900	.1780	27.6110	5.0780	.8176	4.1518	3242	
18.0400	.2100	14.2516	3.2860	.8428	2.7695	2341	
18.0400	.2200	14.0712	3.2440	.8375	2.7169	2309	
18.0400	.3000	12.6280	2.7090	.7727	2.0932	1896	

TABLE II

SIMULATED PROPELLANT HEATING DATA WITH ORIFICE FOR SEED DEAGGLOMERATION

Incident Radiation Q_{INC}-kw	Fraction of Radiation Transmitted η_T	Absorbed Radiation Q_{ABS}-kw	Calorimeter Power Q_{CAL}-kw	Calorimeter Power Correction Factor K	Power In Gas Q_{GAS}-kw	Bulk Exit Temperature T_E-K
			Non-Reflecting Walls			
2.0220	.3161	1.3828	.2757	.7412	.2043	616
2.0220	.3226	1.3697	.4001	.8265	.3307	796
1.8660	.3655	1.1840	.5868	.8914	.5231	1083
2.0220	.3677	1.2785	.3308	.7709	.2550	685
2.0220	.3677	1.2785	.4640	.8428	.3910	908
1.8660	.4000	1.1196	.6031	.8892	.5363	1097
3.9660	.4120	2.3320	1.5050	.9071	1.3651	2312
4.0430	.4250	2.3247	.4592	.6336	.2909	758
1.8660	.4276	1.0681	.4767	.8484	.4044	903
1.8660	.4276	1.0681	.6295	.8903	.5605	1139
5.0540	.4380	2.8403	.7946	.7368	.5854	1178
4.0430	.4550	2.2034	.5367	.6775	.3636	855
3.1100	.4860	1.5985	.6718	.8023	.5390	1121
5.0540	.5000	2.5270	.9536	.7666	.7310	1401
5.0540	.5000	2.5270	.8651	.7405	.6406	1262
5.0540	.5000	2.5270	.9413	.7633	.7185	1386
3.1100	.5090	1.5270	.7790	.8275	.6446	1260
5.0540	.5160	2.4461	.8146	.7178	.5847	1178
6.9980	.5200	3.3590	1.5250	.7958	1.2136	2112
3.1100	.5290	1.4648	.6235	.7738	.4825	1038
5.0540	.5600	2.2238	1.0513	.7748	.8145	1511
5.0540	.5600	2.2238	.8272	.7080	.5857	1178
4.9760	.5920	2.0302	.8268	.7024	.5807	1179
4.9740	.6180	1.9001	1.0010	.7510	.7518	1430
4.0440	.6200	1.5367	.5908	.6483	.3830	884
4.9740	.6210	1.8851	.9564	.7376	.7054	1363
4.0440	.6330	1.4841	.6681	.6872	.4591	994
8.3980	.6400	3.0233	1.8730	.7721	1.4462	2443
4.9740	.6500	1.7409	.8894	.7075	.6293	1249
4.0440	.6583	1.3818	.6303	.6585	.4151	925
4.9740	.6710	1.6364	.8265	.6769	.5595	1138
8.3980	.6730	2.7461	1.8250	.7575	1.3824	2345
4.0440	.6867	1.2670	.5146	.5650	.2907	758
5.9100	.7030	1.7553	1.2010	.7312	.8782	1613
5.9100	.7130	1.6962	1.4350	.7763	1.1140	2460
5.9100	.7230	1.6371	1.2010	.7260	.8719	1614
5.9100	.7330	1.5780	1.1890	.7203	.8565	1586

K-910900-B

NUCLEAR LIGHT BULB CONCEPT AND D-C ARC CONFIGURATION

SECTIONS SHOWN ARE AT AXIAL MID STATIONS OF ENGINE UNIT CAVITY AND ARC EXPERIMENT

(a) NUCLEAR LIGHT BULB

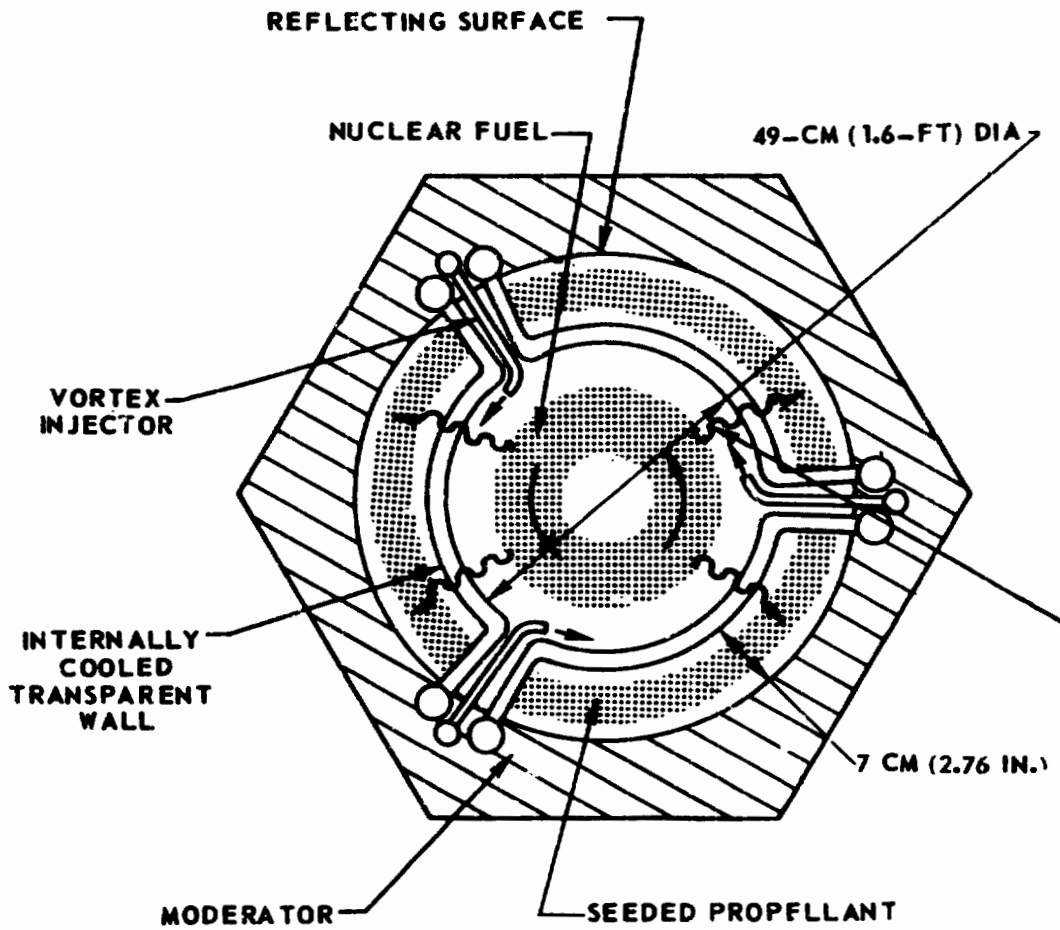

(b) D-C ARC CONFIGURATION

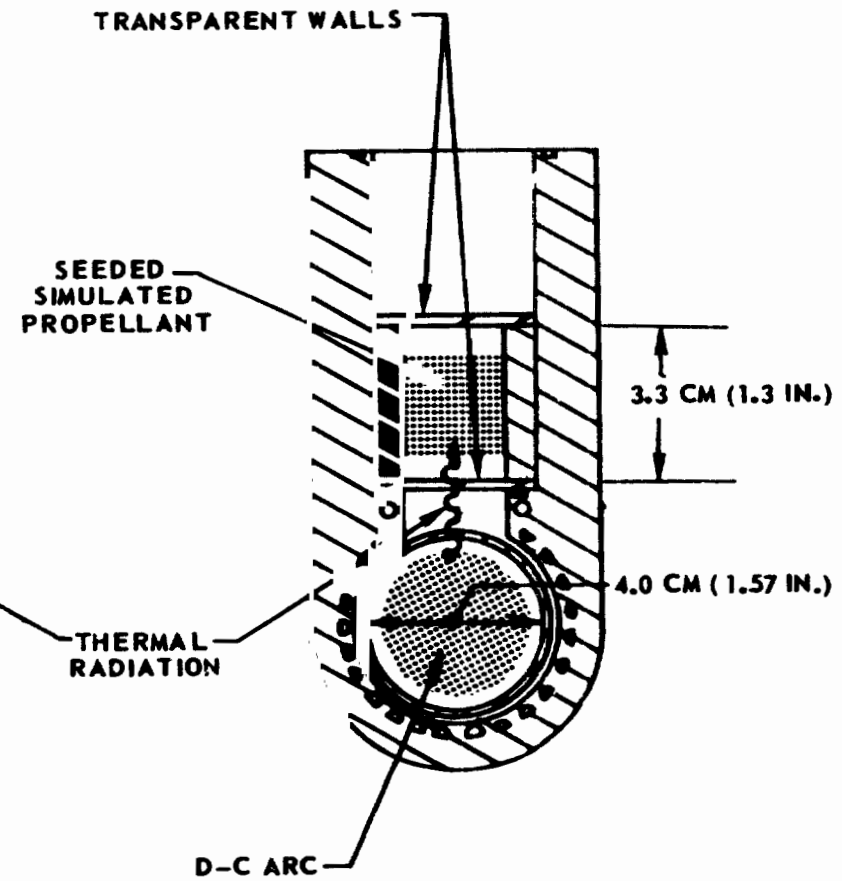

FIG. 1

DIMENSIONS OF UNIT CAVITY IN REFERENCE ENGINE

COMPLETE ENGINE IS COMPOSED OF A SEVEN-UNIT-CAVITY CLUSTER

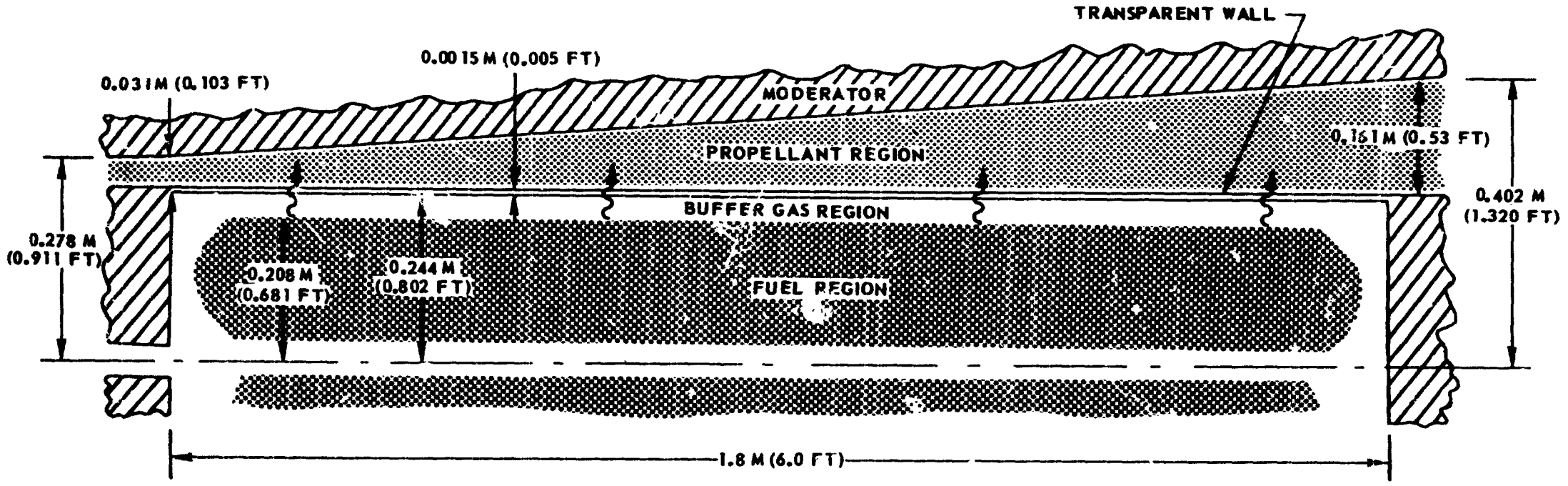

FIG. 2

SKETCH OF BASIC D-C ARC AND RADIOMETER OPTICAL SYSTEM

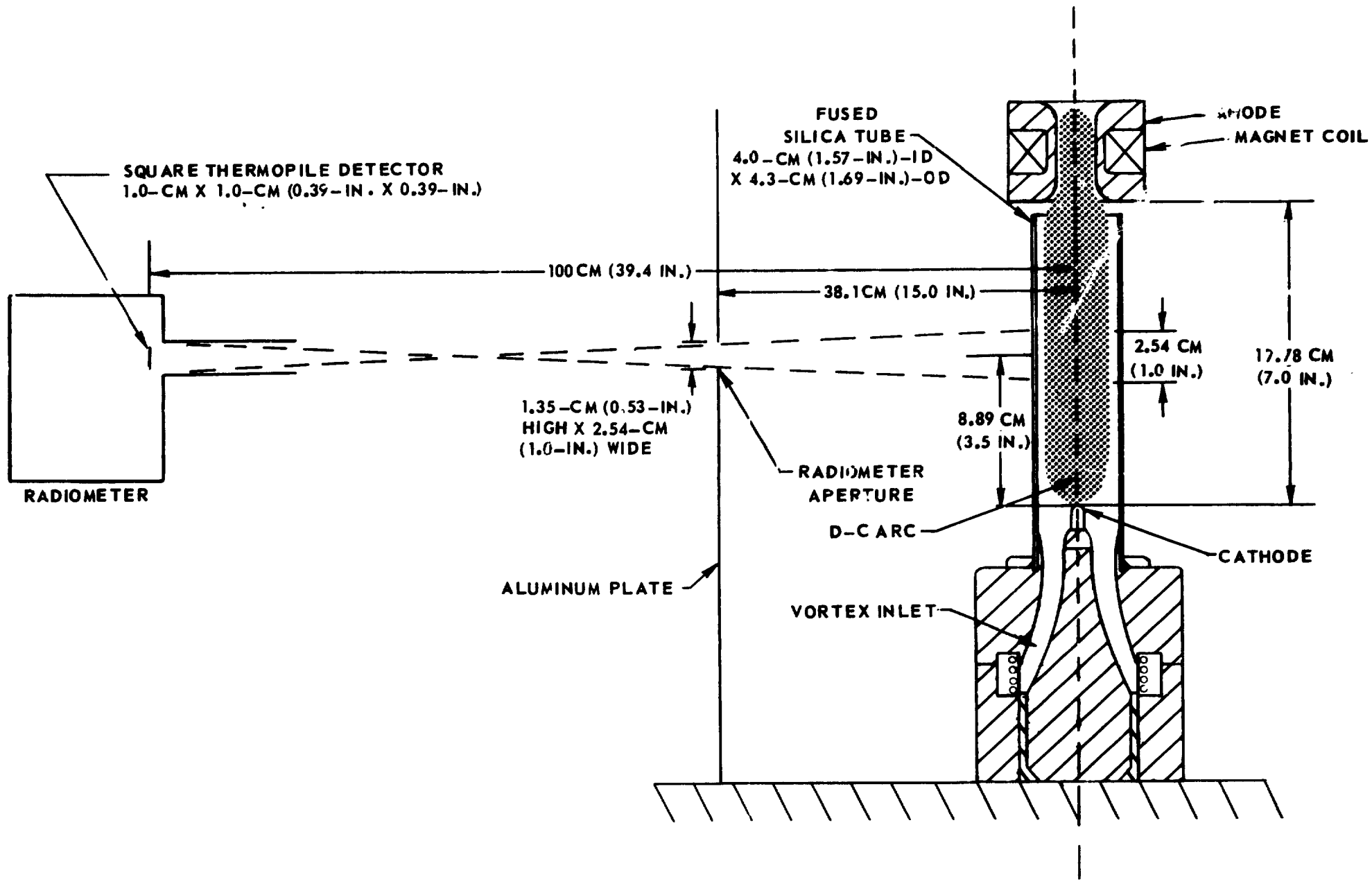

FIG. 3

FIG. 4

VARIATION OF POWER RADIATED FROM 12.7-CM TEST SECTION WITH TOTAL ARC POWER

SEE FIG. 3 FOR ARC CONFIGURATION
1 ATM PRESSURE ARGON ARC
17.78-CM (7.0-IN.) CATHODE TO ANODE DISTANCE
RADIATION EFFICIENCY PER UNIT LENGTH = 50 TO 80 PERCENT (SEE TEXT)

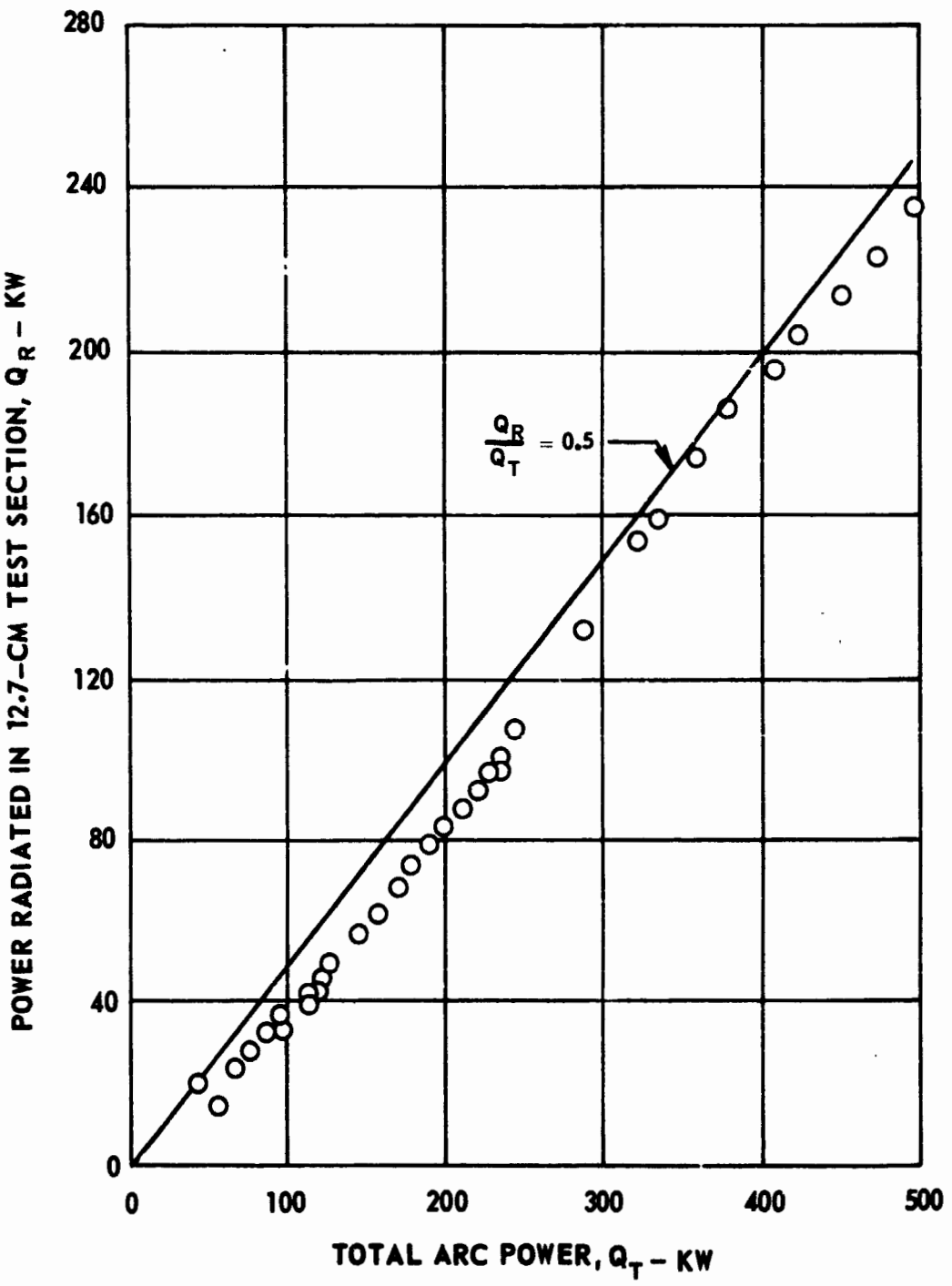

FIG. 5

ELECTRICAL OPERATING CHARACTERISTICS OF D-C ARC FOR PROPELLANT HEATING TESTS

SEE FIG. 3 FOR ARC CONFIGURATION

1 ATM PRESSURE ARGON ARC

17.78-CM (7.0-IN.) CATHODE TO ANODE

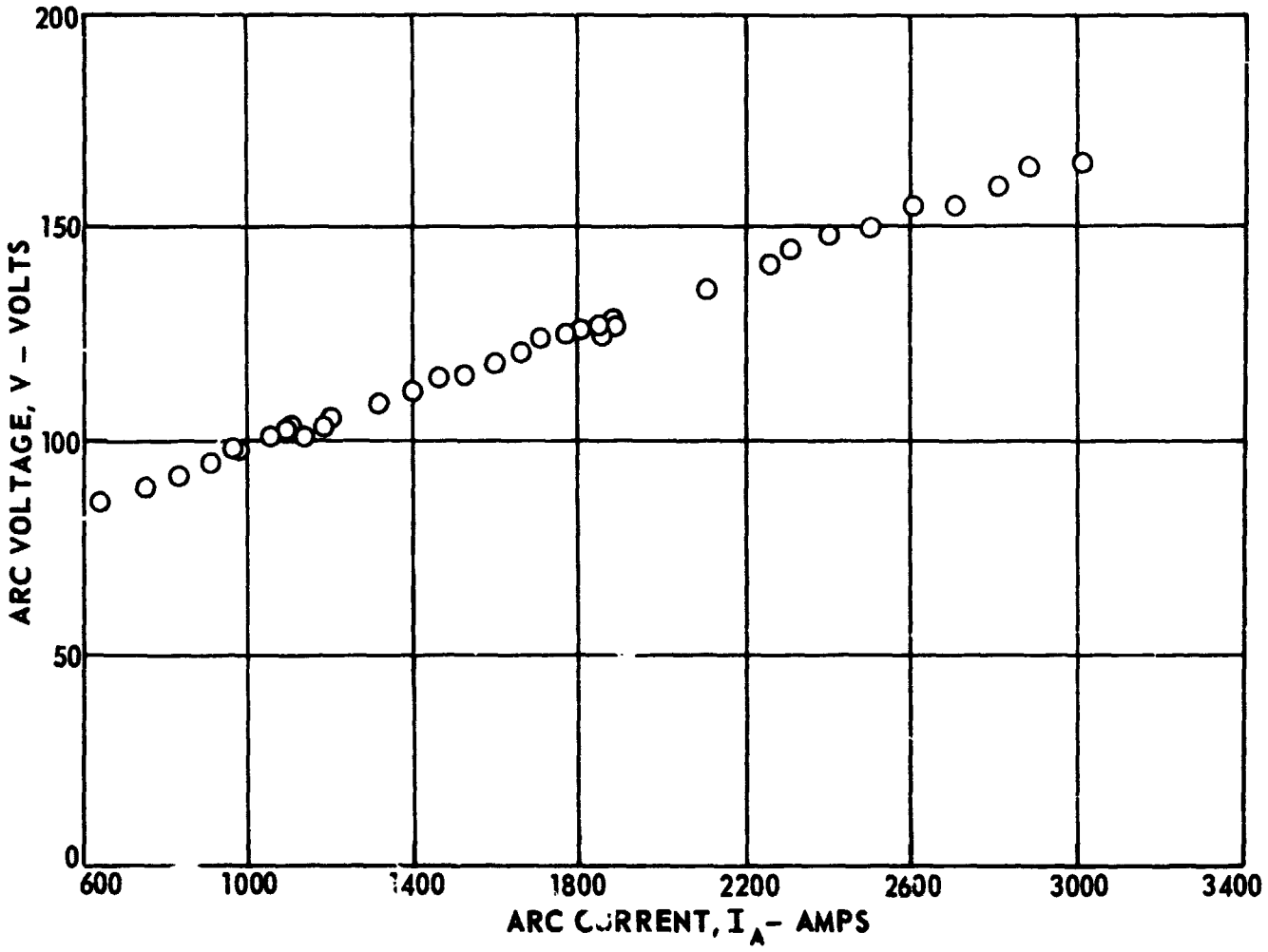

K-910900-8

FIG. 6

SCHEMATIC DIAGRAM OF SIMULATED PROPELLANT FLOW SYSTEM AND HIGH-PRESSURE SEED DISPERSAL SYSTEM

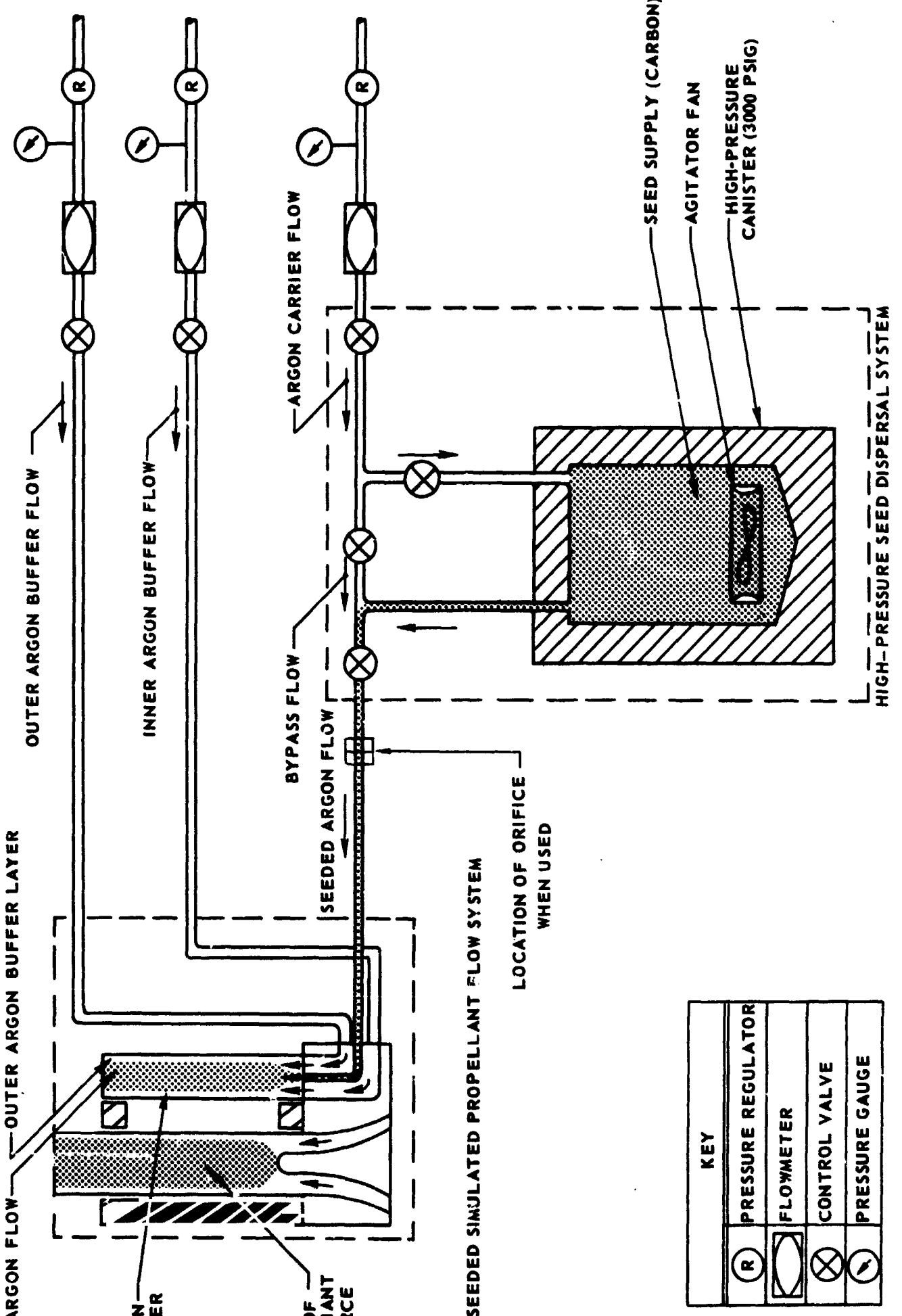

FIG. 7

SKETCH OF CROSS SECTION OF RECTANGULAR PROPELLANT DUCT MOCK-UP

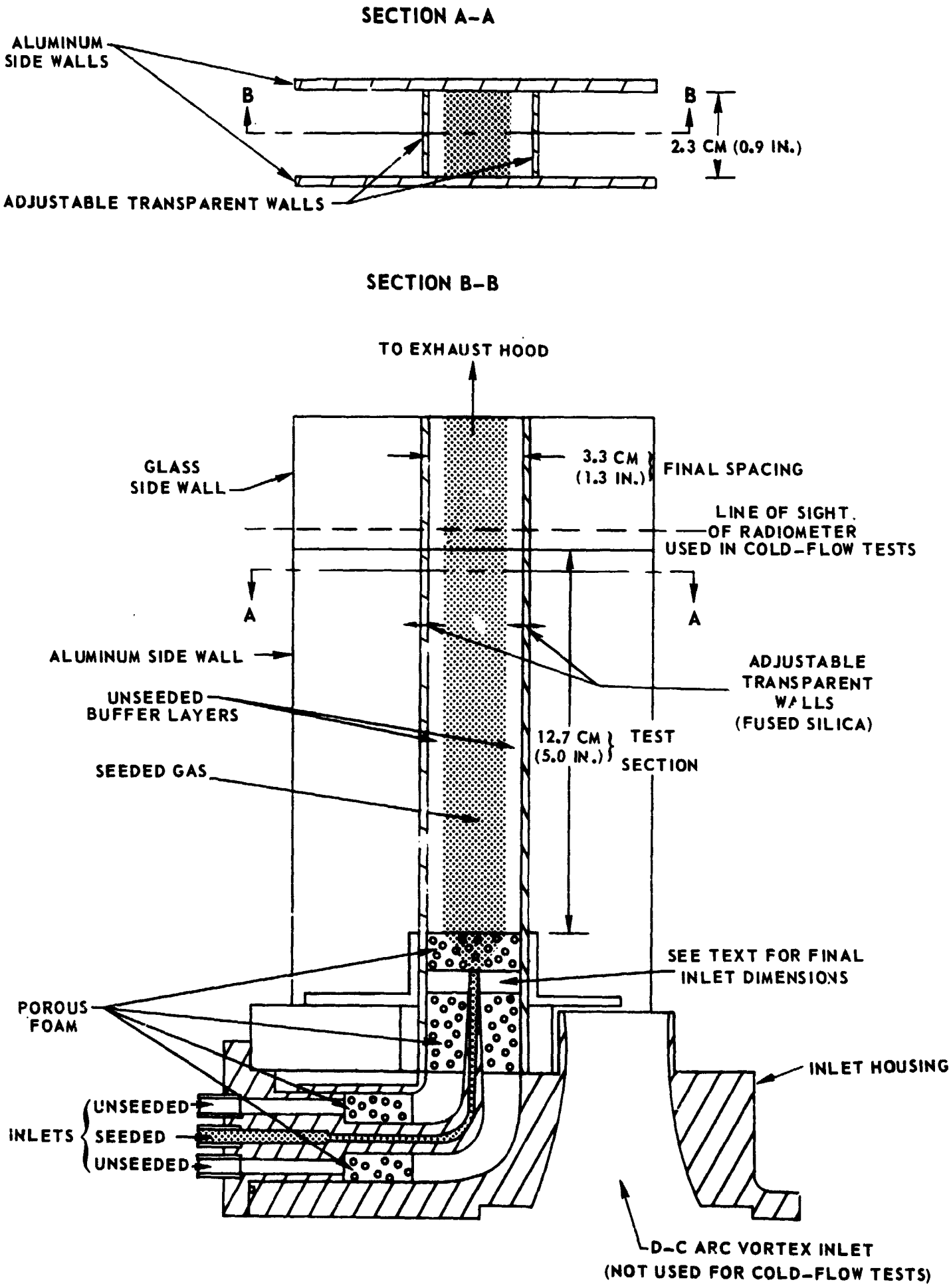

PHOTOGRAPHS OF RECTANGULAR PROPELLANT DUCT MOCK-UP FOR COLD-FLOW TESTS

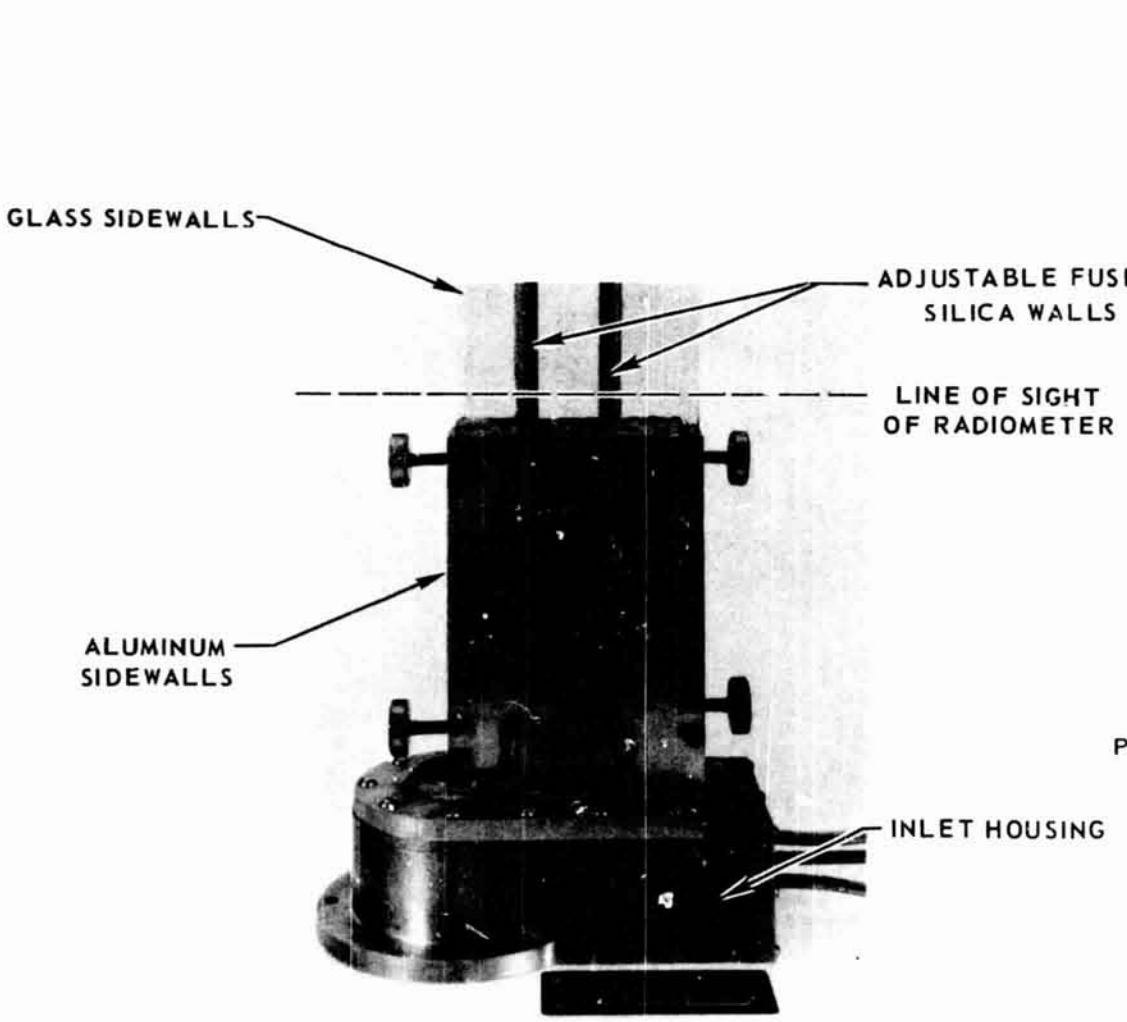

SIDE VIEW

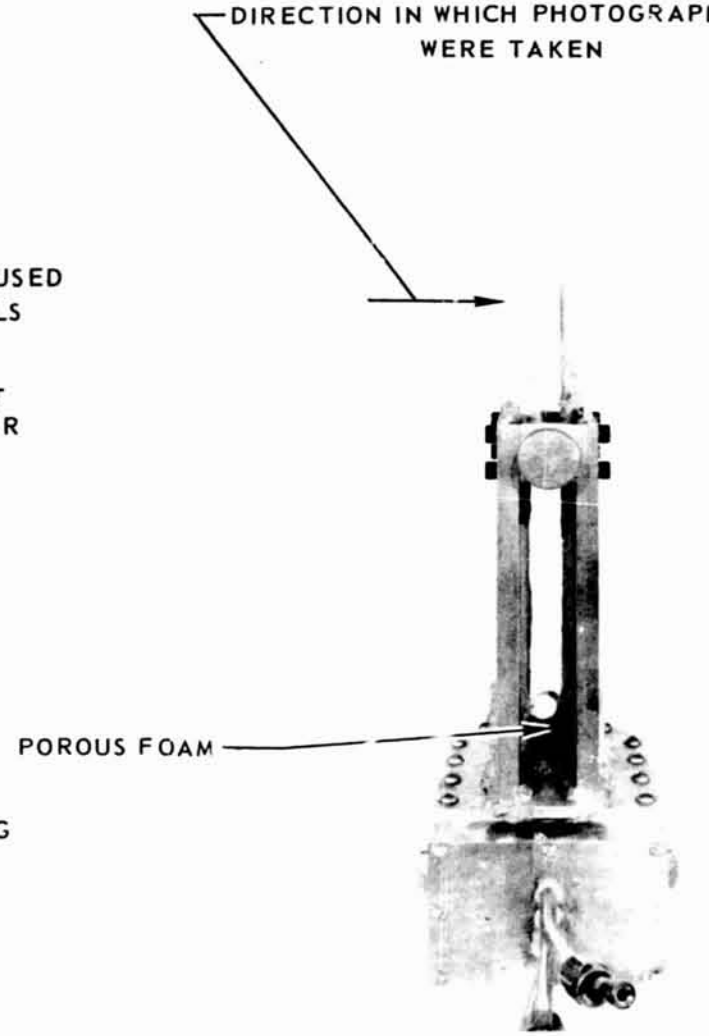

FRONT VIEW

FIG. 8

FIG. 9

PHOTOGRAPHS OF COLD FLOW TESTS

SEE TEXT FOR DISCUSSION

SEE FIG. 10 FOR CORRESPONDING TRANSMISSION MEASUREMENTS

SONIC ORIFICE USED TO DEAGGLOMERATE SEEDS
TOTAL ARGON WEIGHT FLOW RATE = 1.09 G/SEC (0.0024 LB/SEC)
ESTIMATED CARBON SEED WEIGHT FLOW RATE = 0.05 G/SEC (0.00012 LB/SEC)

(a) TEST CONFIGURATION

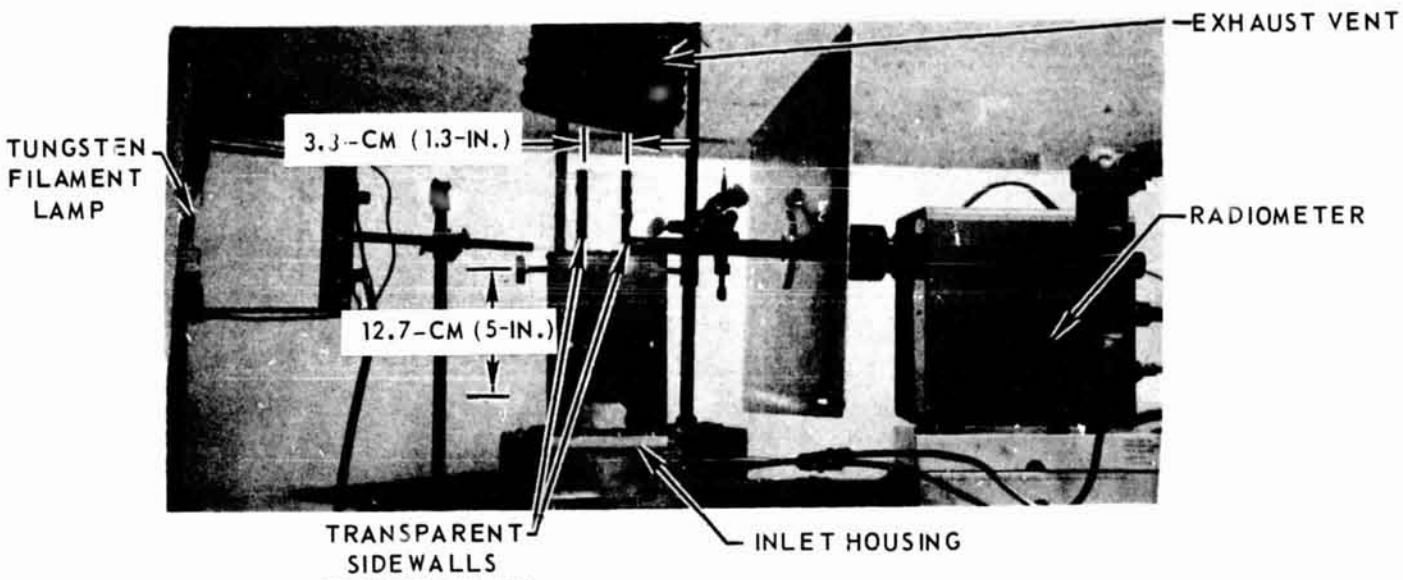

(b)

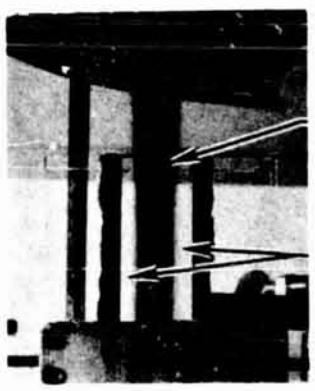

TIME -MIN. = 1.4
SEED TRANSMISSION = 0.013

(c)

TIME -MIN. = 3.4
WALL TRANSMISSION = 0.993

(d)

TIME -MIN. = 6.6
SEED TRANSMISSION = 0.0

(e)

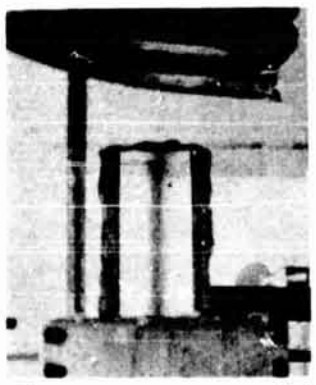

TIME -MIN. = 8.4
WALL TRANSMISSION = 0.99

(f)

TIME -MIN. = 13.4
SEED TRANSMISSION = 0.282

(g)

TIME -MIN. = 32.4
WALL TRANSMISSION = 0.772

NOTE*: COATING ON THE WALLS WHICH WERE NOT PROTECTED BY UNSEEDED BUFFER LAYERS

TRANSMISSION MEASUREMENTS OF THE PROPELLANT DUCT WALLS AND SEEDED GAS FLOW

SONIC ORIFICE USED TO DEAGGLOMERATE SEEDS

SEE FIG. 7 FOR TEST CONFIGURATION AND FIG. 9 FOR FLOW CONDITIONS

① WALL TRANSMISSION MEASUREMENT TAKEN AT THIS TIME

◯ CORRESPONDING PHOTOGRAPH IN FIG. 9 TAKEN AT THIS TIME

—— THROUGH TEST SECTION WITHOUT SEEDS FLOWING

---AVERAGE VALUE WITH SEEDS FLOWING

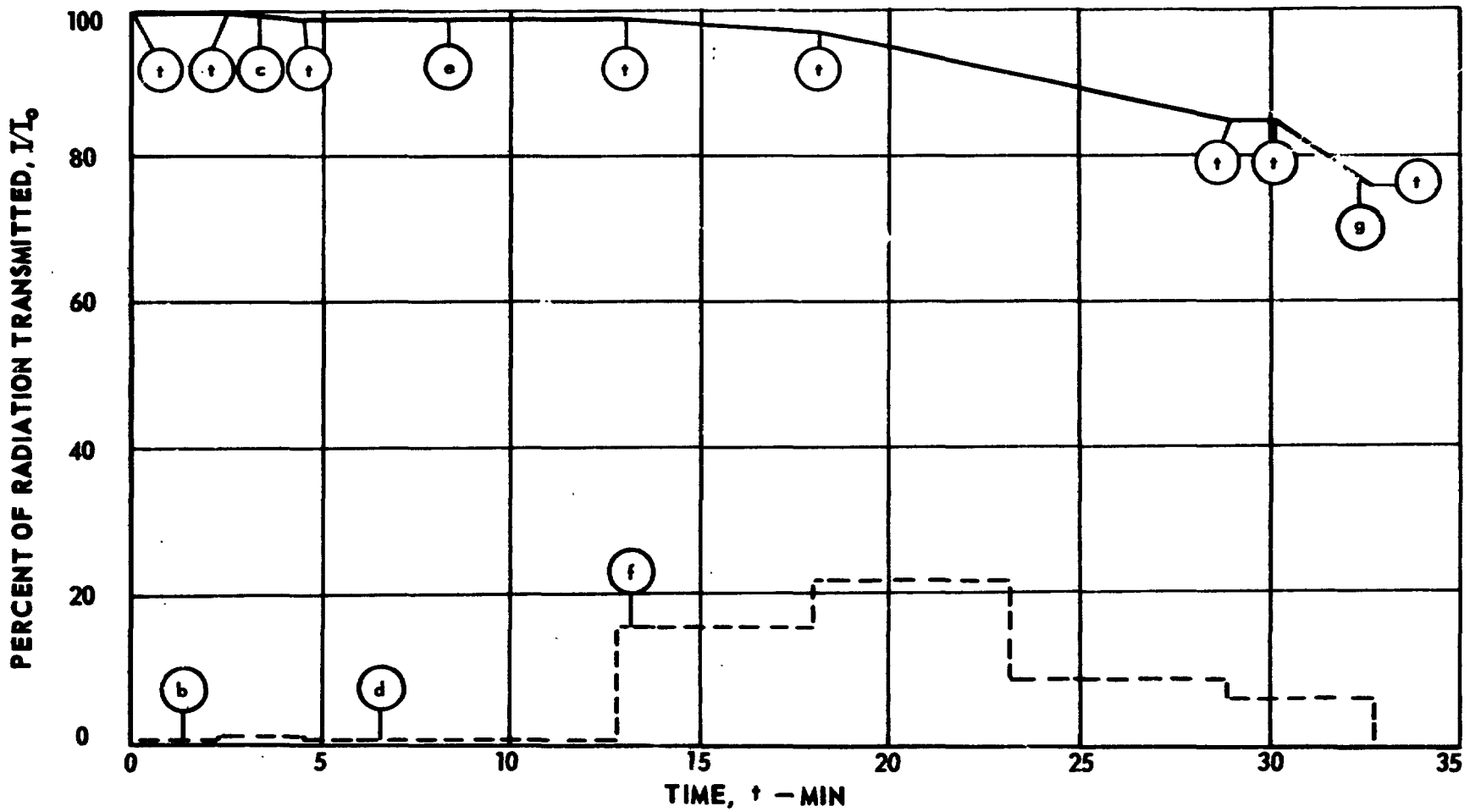

FIG. 10

FIG. 11

PHOTOGRAPH OF D-C ARC PROPELLANT HEATING CONFIGURATION

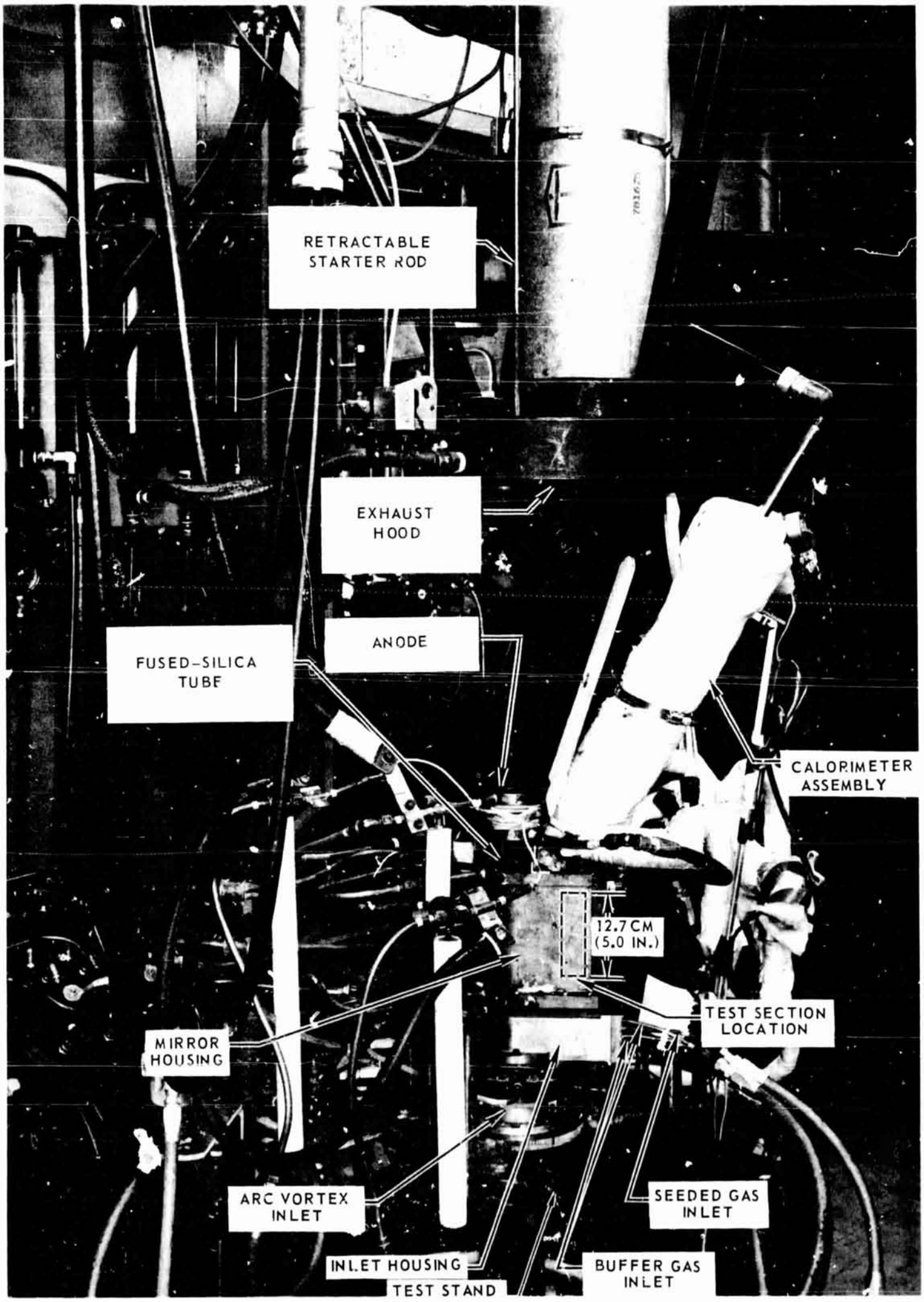

RL-71-168-A

FIG. 12

SKETCH OF LOWER PORTION OF PROPELLANT HEATING CONFIGURATION FOR TESTS WITH NON-REFLECTING PROPELLANT DUCT WALLS

SEE FIG. 13 FOR UPPER PORTION DETAILS

REFLECTING SURFACES MARKED (m)

SECTION A-A

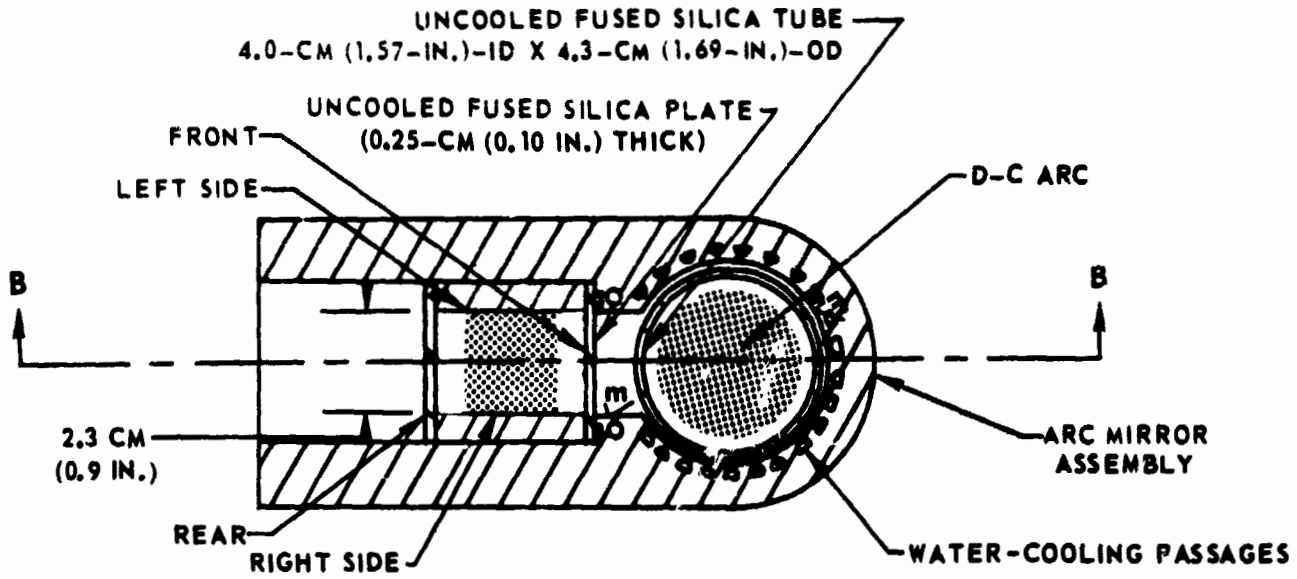

SECTION B-B

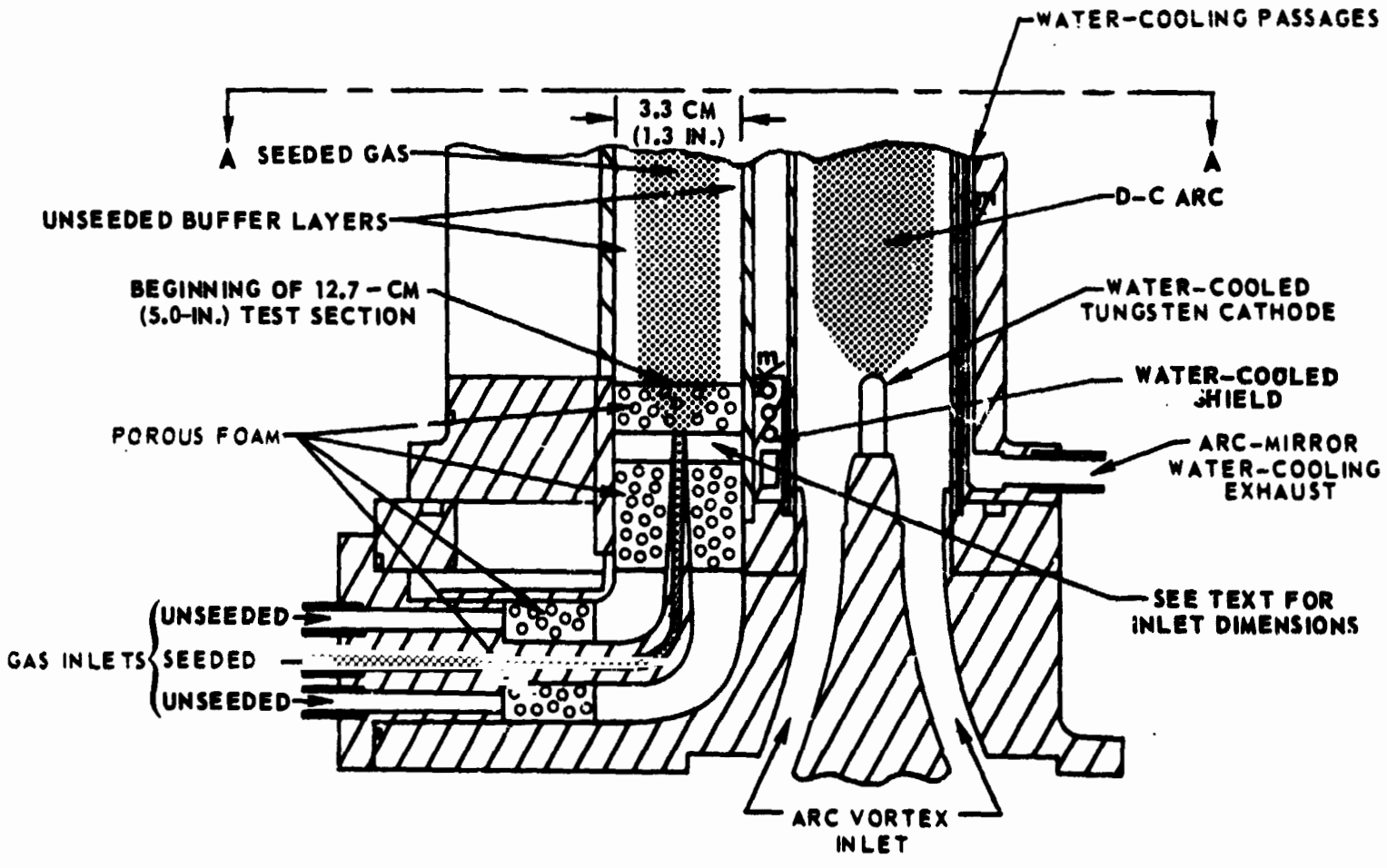

SKETCH OF UPPER PORTION OF PROPELLANT HEATING CONFIGURATION FOR TESTS WITH NON-REFLECTING PROPELLANT DUCT WALLS

SEE FIG. 12 FOR LOWER PORTION DETAILS

REFLECTING SURFACES MARKED ✓

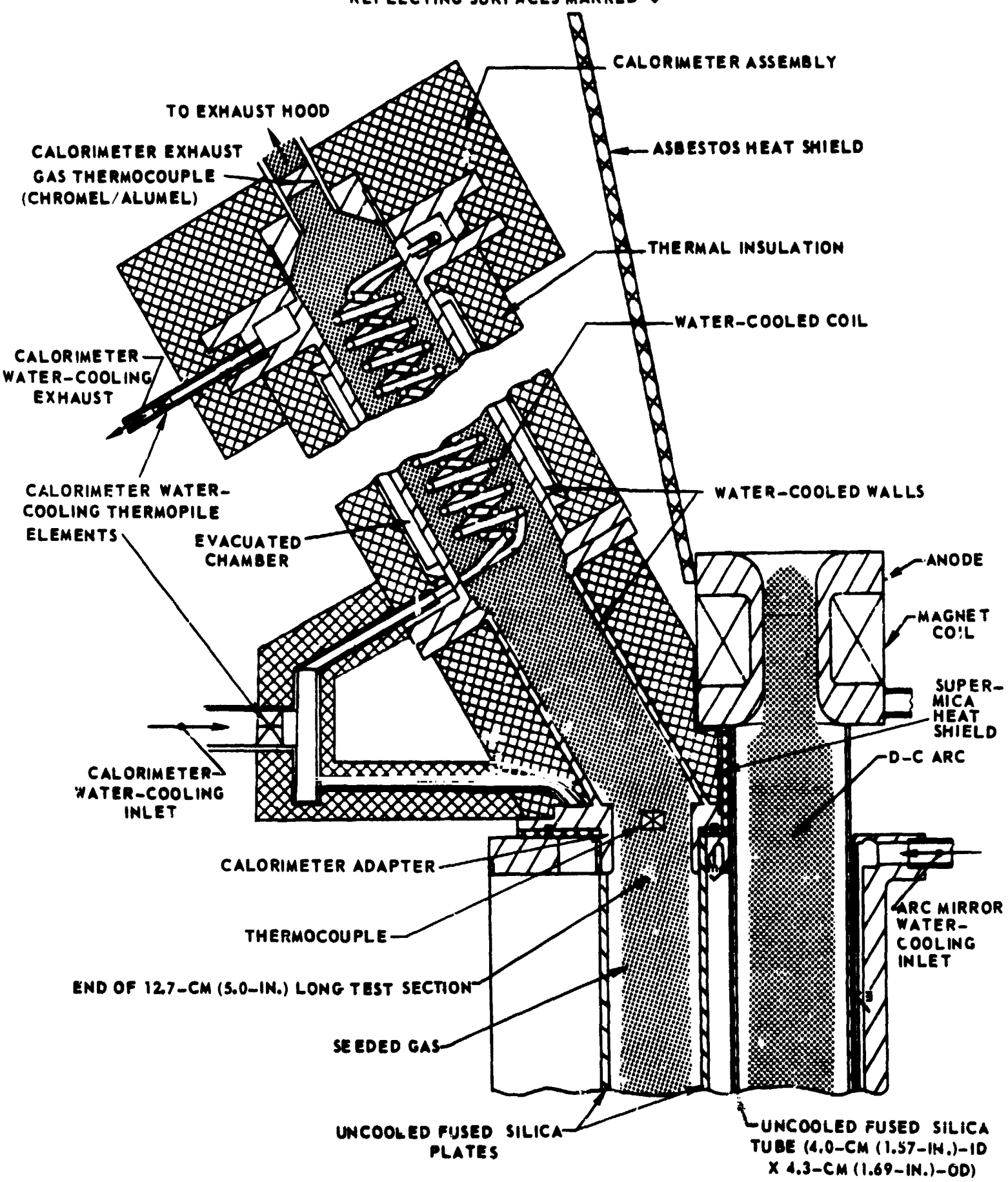

FIG. 14

EXAMPLE OF CALORIMETER WATER-COOLING TEMPERATURE RISE TRACE

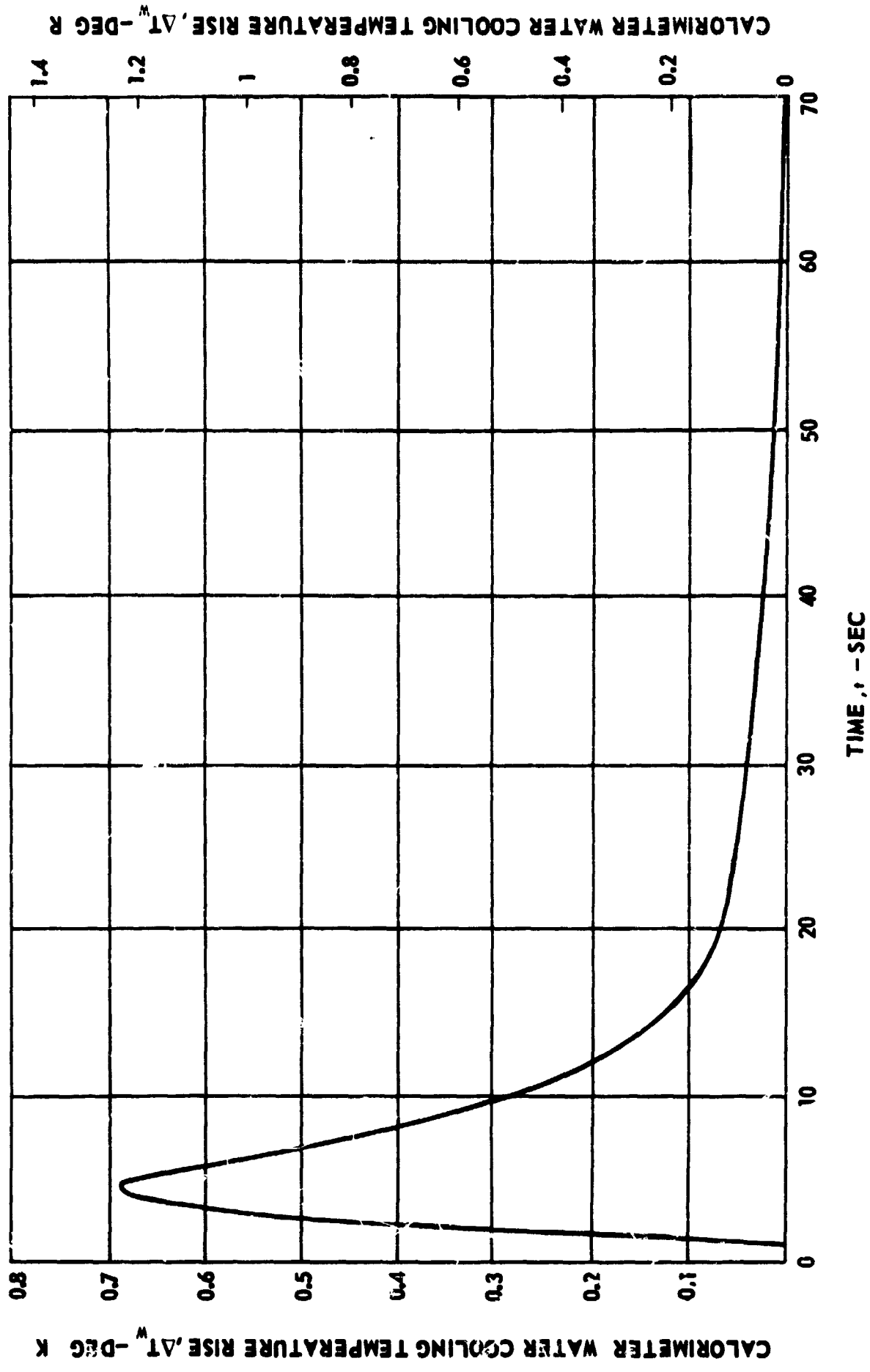

FIG. 15

SKETCH OF D-C ARC CONFIGURATION FOR COPPER SLUG RADIATION MEASUREMENTS

SEE FIG. 3 FOR ARC CONFIGURATION DIMENSIONS

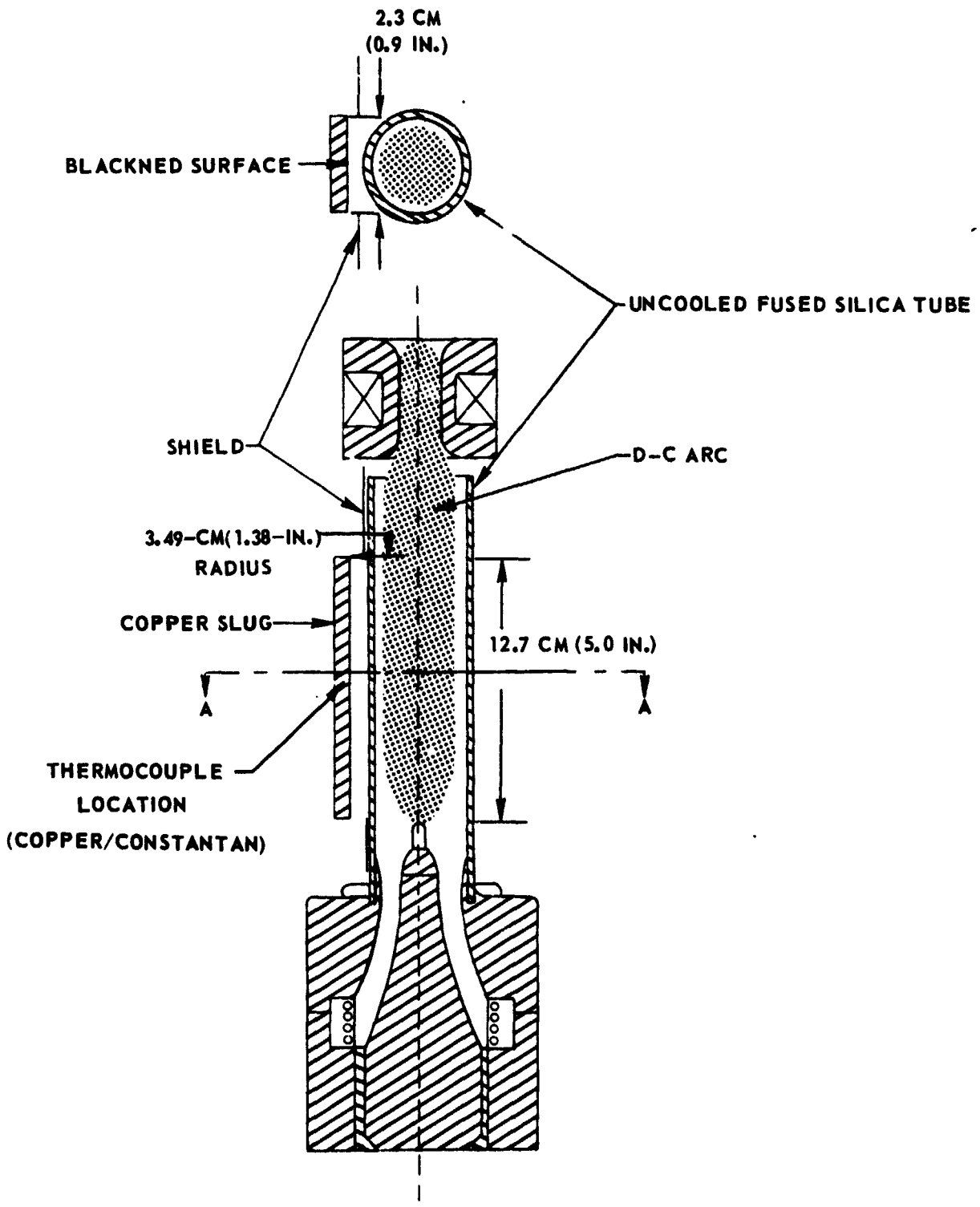

FIG. 16

EFFECT OF MIRROR ASSEMBLY ON RADIANT FLUX INCIDENT ON TEST SECTION

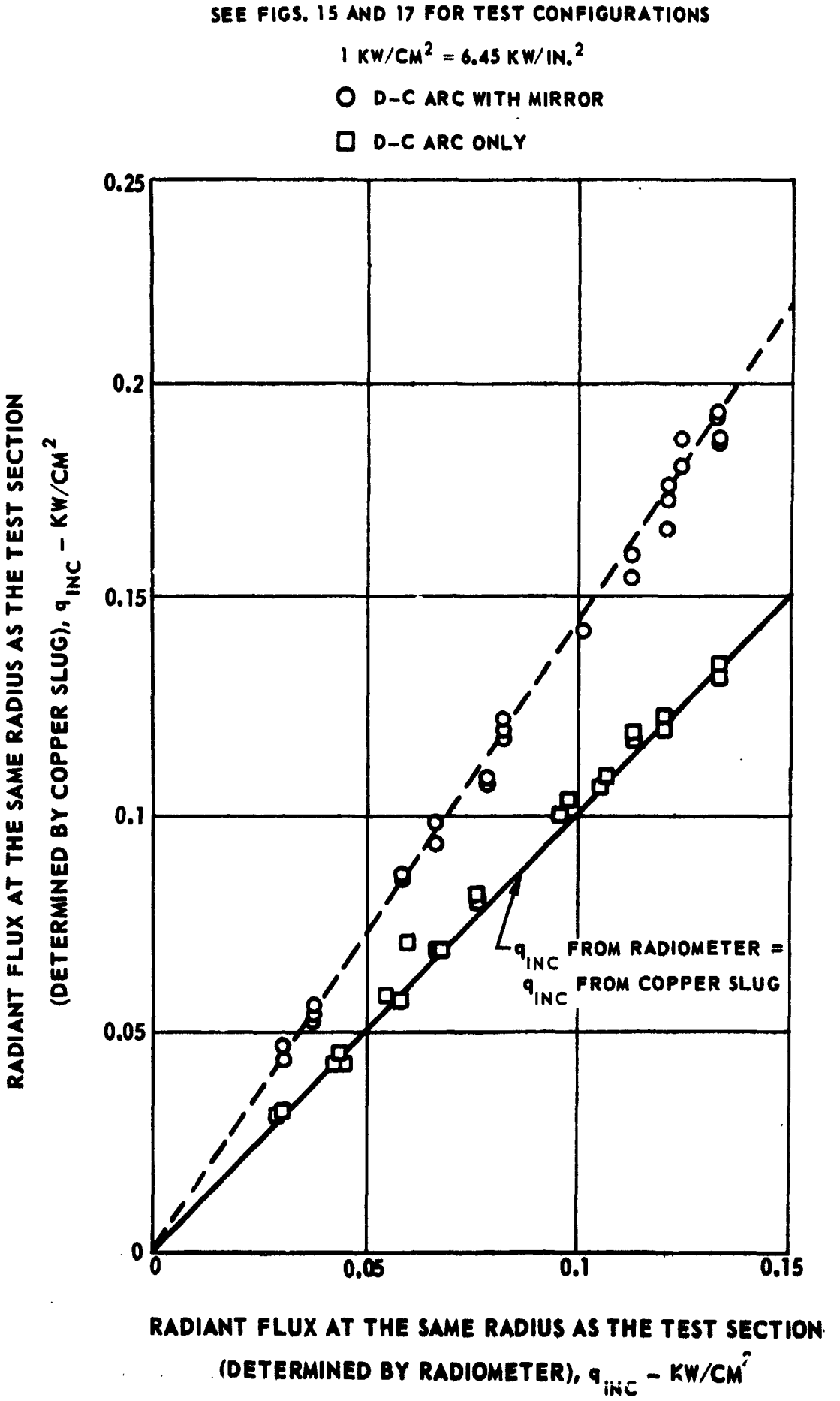

K-9 10900-B

FIG. 17

SKETCH OF MIRROR CONFIGURATION FOR COPPER SLUG RADIATION MEASUREMENTS

REFLECTING SURFACES MARKED (m)

SECTION A-A

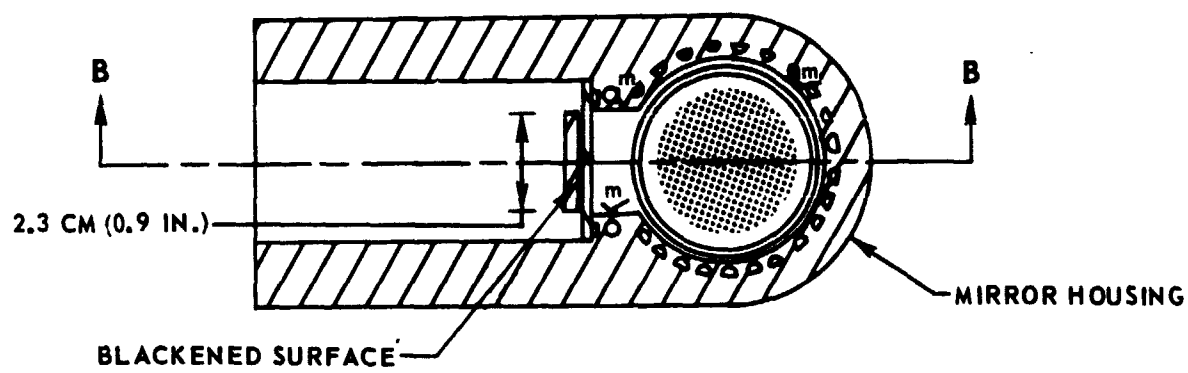

SECTION B-B

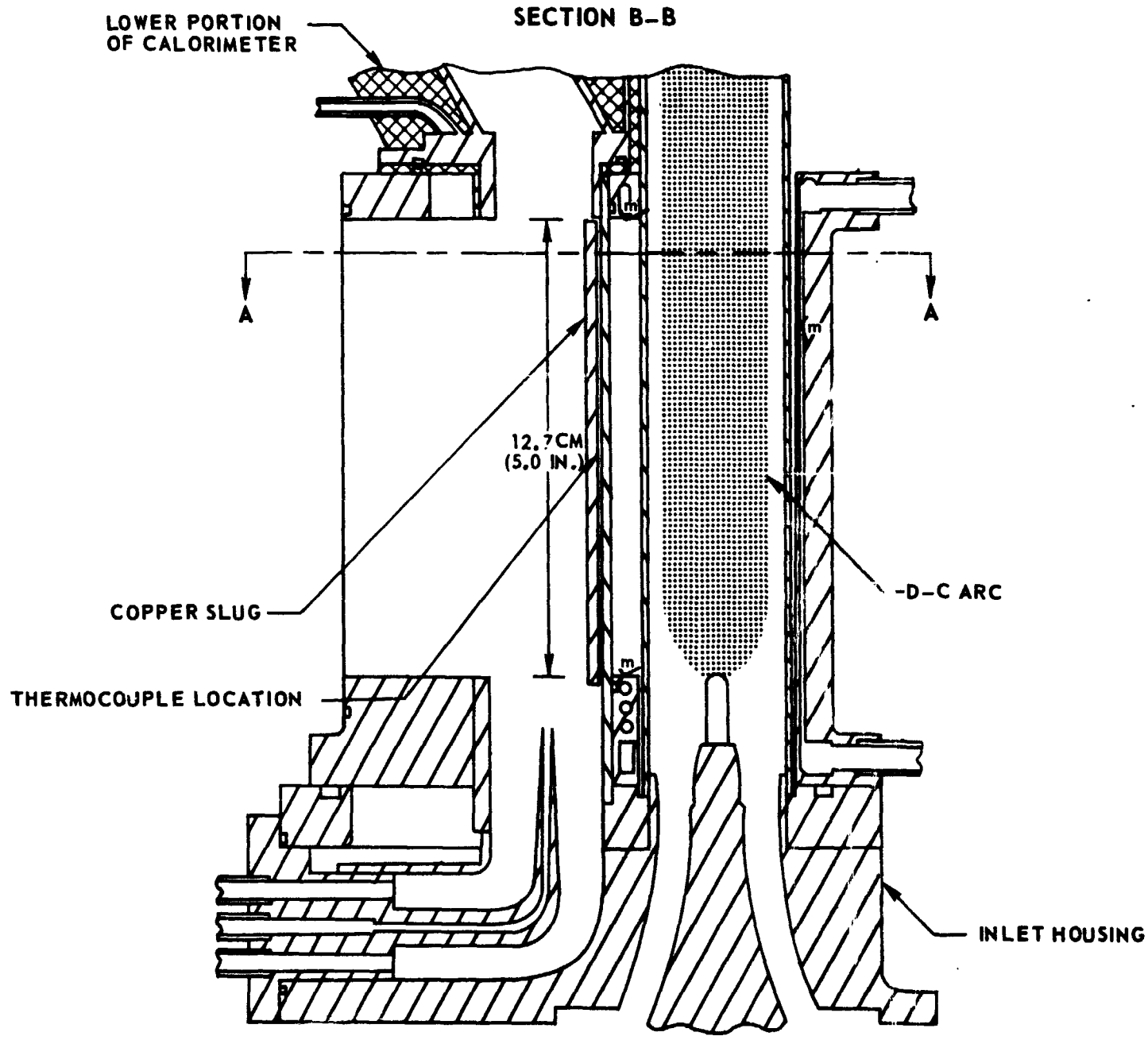

FIG. 18

VARIATION OF BULK EXIT TEMPERATURE WITH RADIATION INCIDENT ON TEST SECTION FOR TESTS WITHOUT ORIFICE FOR SEED DEAGGLOMERATION

NON-REFLECTING AND NON-DIVERGENT PROPELLANT DUCT WALLS

SEE FIGS 12 AND 13 FOR TEST CONFIGURATION

SEE TABLE I FOR FURTHER DETAILS OF DATA

ARGON WEIGHT FLOW RATE = 1.09 G/SEC(0.0024 LB/SEC)

SIMULATED PROPELLANT FLOW RATE = 1.53 G/SEC (0.00336 LB/SEC)

$$\eta_T = \frac{\text{RADIATION TRANSMITTED THROUGH SEED}}{\text{RADIATION INCIDENT ON SEED}}$$

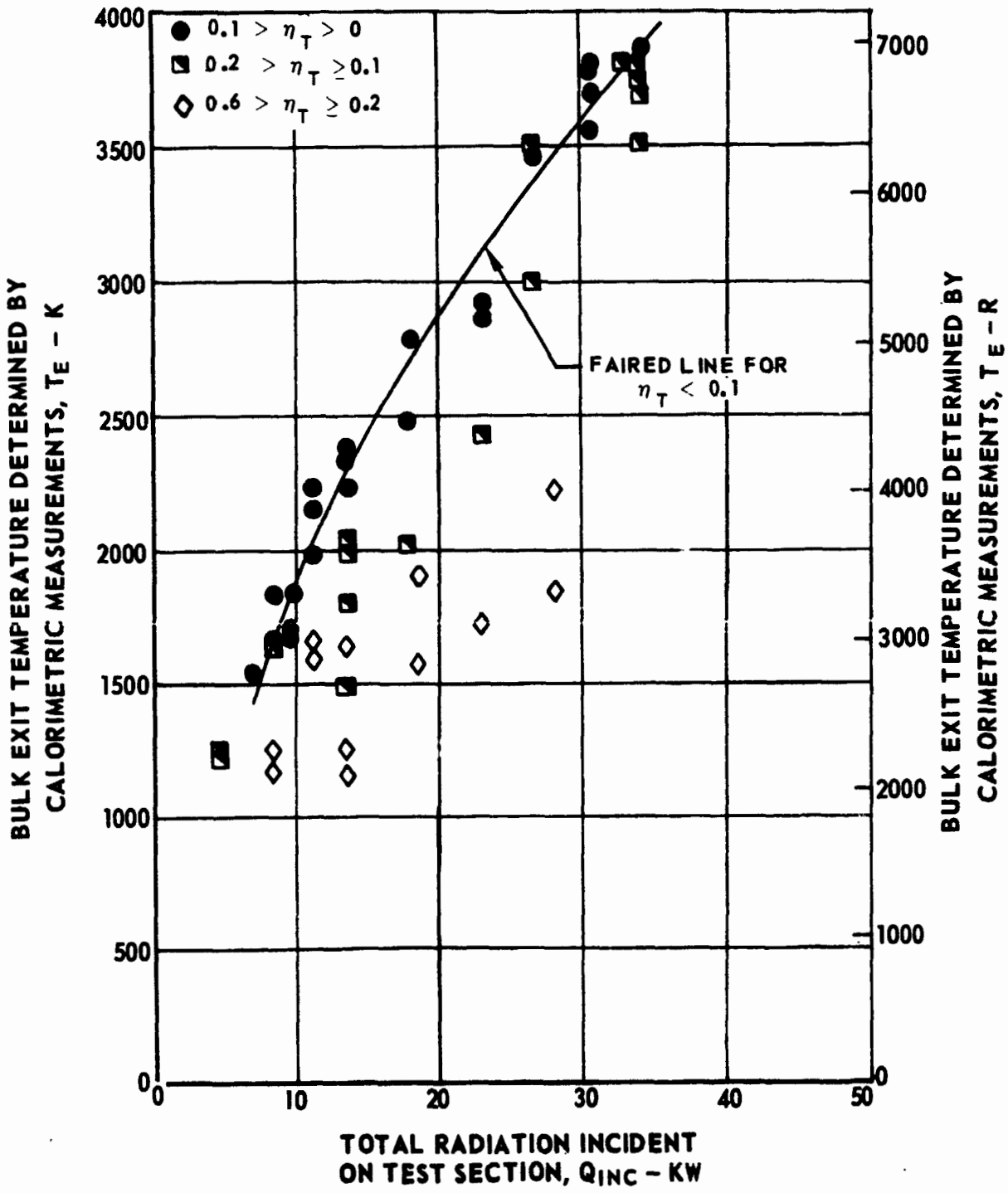

FIG. 19

VARIATION OF BULK EXIT TEMPERATURE WITH RADIATION ABSORBED BY PROPELLANT FOR TESTS WITHOUT ORIFICE FOR SEED DEAGGLOMERATION

NON-REFLECTING AND NON-DIVERGENT PROPELLANT DUCT WALLS

SEE FIGS. 12 AND 13 FOR TEST CONFIGURATION

SEE TABLE I FOR FURTHER DETAILS OF DATA

ARGON WEIGHT FLOW RATE = 1.09 G/SEC (0.0024 LB/SEC)

SIMULATED PROPELLANT FLOW RATE = 1.53 G/SEC (0.00336 LB/SEC)

$$\eta_T = \frac{\text{RADIATION TRANSMITTED THROUGH SEEDS}}{\text{RADIATION INCIDENT ON SEEDS}}$$

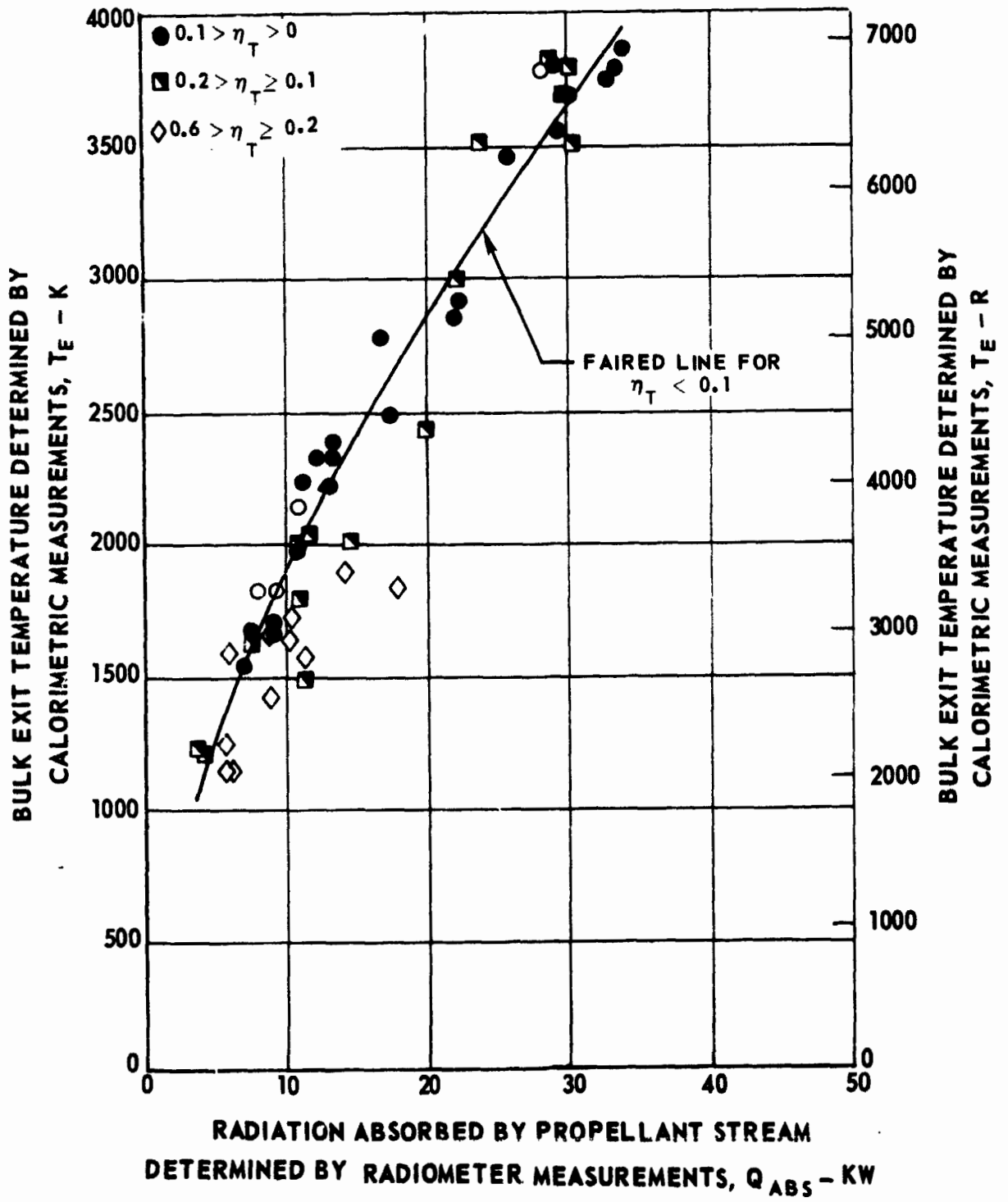

FIG. 20

CALCULATED VARIATION OF BULK EXIT TEMPERATURE WITH POWER DEPOSITED IN GAS FOR DIFFERENT SEED WEIGHT FLOW FRACTIONS

m_S = CARBON SEED WEIGHT FLOW RATE (VARIED)

m_A = ARGON WEIGHT FLOW RATE, 1.09 G/SEC (0.0024 LB/SEC) (CONSTANT)

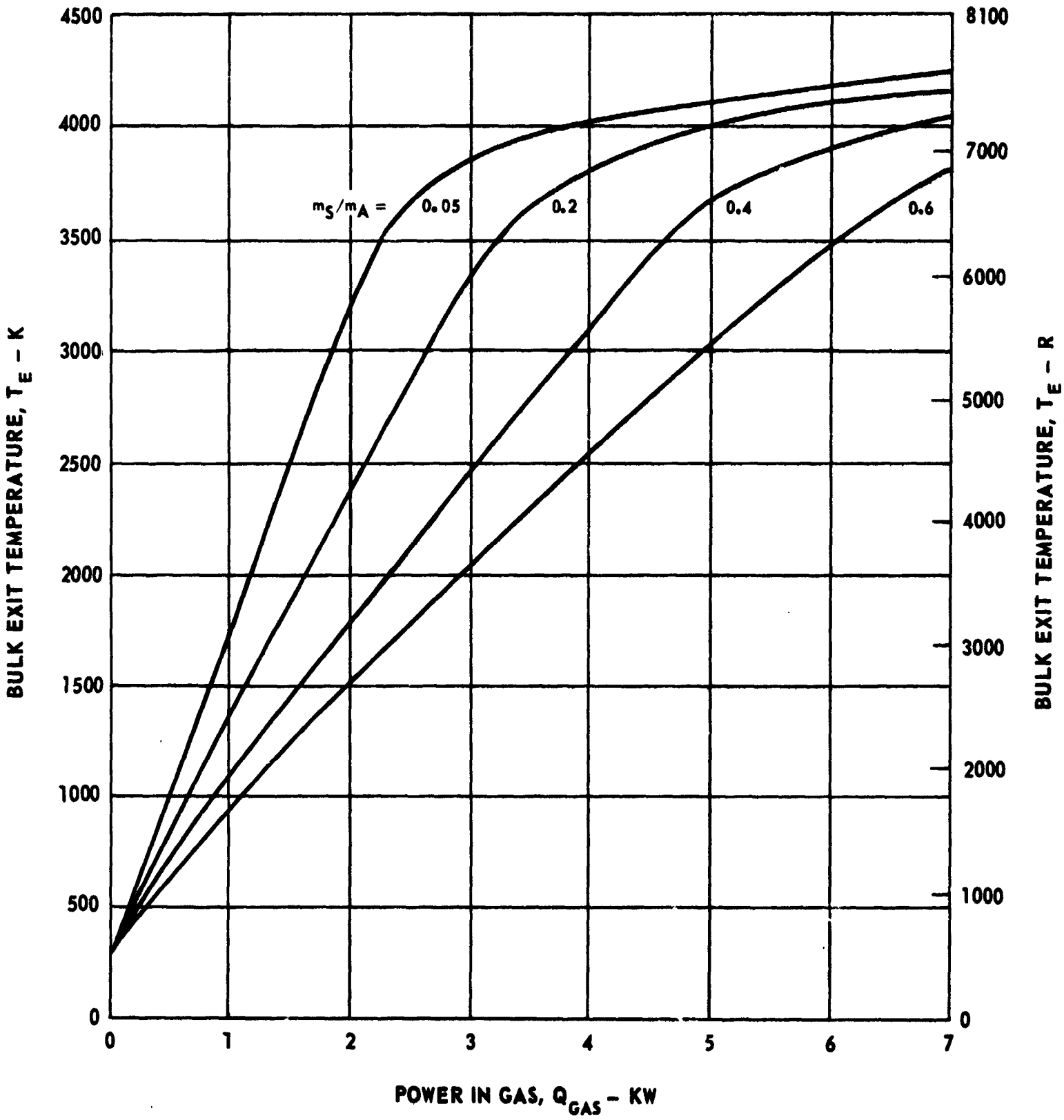

FIG. 21

LOCAL SIMULATED PROPELLANT TEMPERATURE COMPARED WITH BULK EXIT TEMPERATURE

WITHOUT ORIFICE FOR SEED DEAGGLOMERATION

NON-REFLECTING AND NON-DIVERGENT PROPELLANT DUCT WALLS

SEE FIGS. 12 AND 13 FOR TEST CONFIGURATIONS

POSITION OF THERMOCOUPLE SHOWN ON FIG. 13

FACTORS AFFECTING TEMPERATURE MEASURED USING THERMOCOUPLE

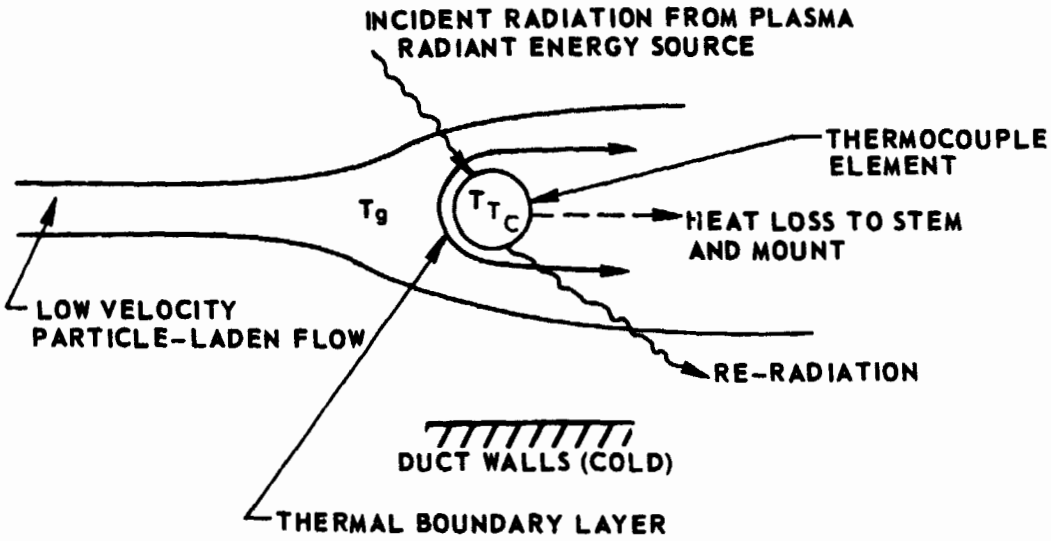

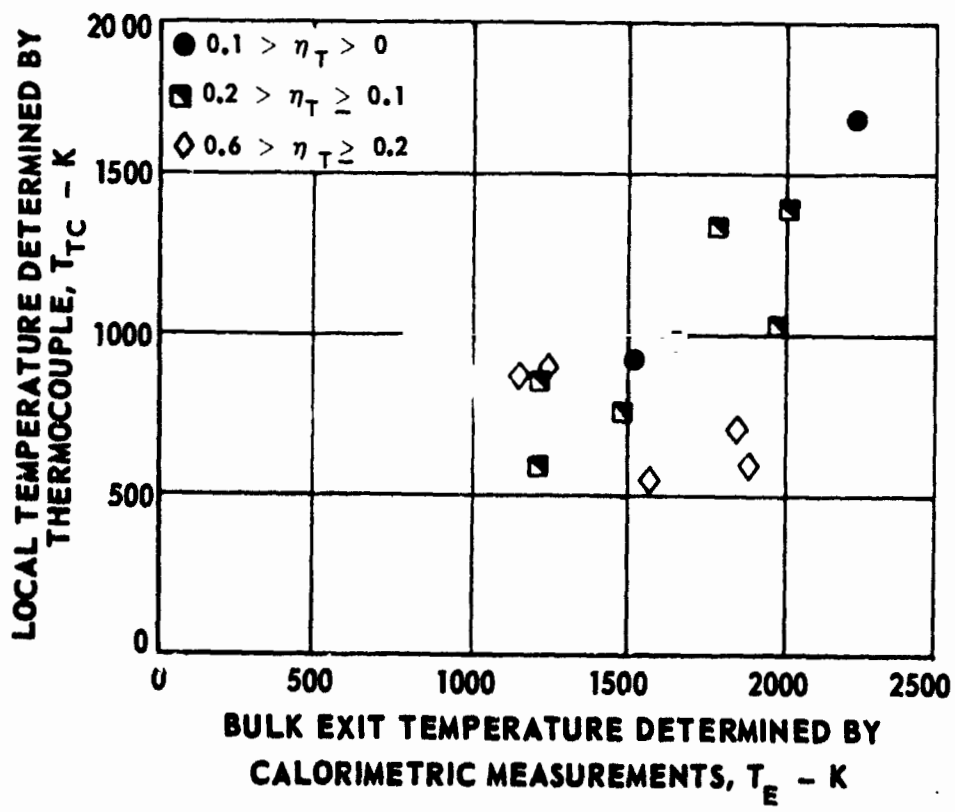

FIG. 22

VARIATION OF BULK EXIT TEMPERATURE WITH RADIATION ABSORBED BY PROPELLANT FOR TESTS WITH ORIFICE FOR SEED DEAGGLOMERATION

NON-REFLECTING AND NON-DIVERGENT PROPELLANT DUCT WALLS

SEE FIGS 12 AND 13 FOR TEST CONFIGURATION

SEE TABLE II FOR FURTHER DETAILS OF DATA

ARGON WEIGHT FLOW RATE = 1.09 G/SEC (0.0024 LB/SEC)

ESTIMATED CARBON SEED WEIGHT FLOW RATE = 0.05 G/SEC (0.00012 LB/SEC)

$$\eta_T = \frac{\text{RADIATION TRANSMITTED THROUGH SEEDS}}{\text{RADIATION INCIDENT ON SEEDS}}$$

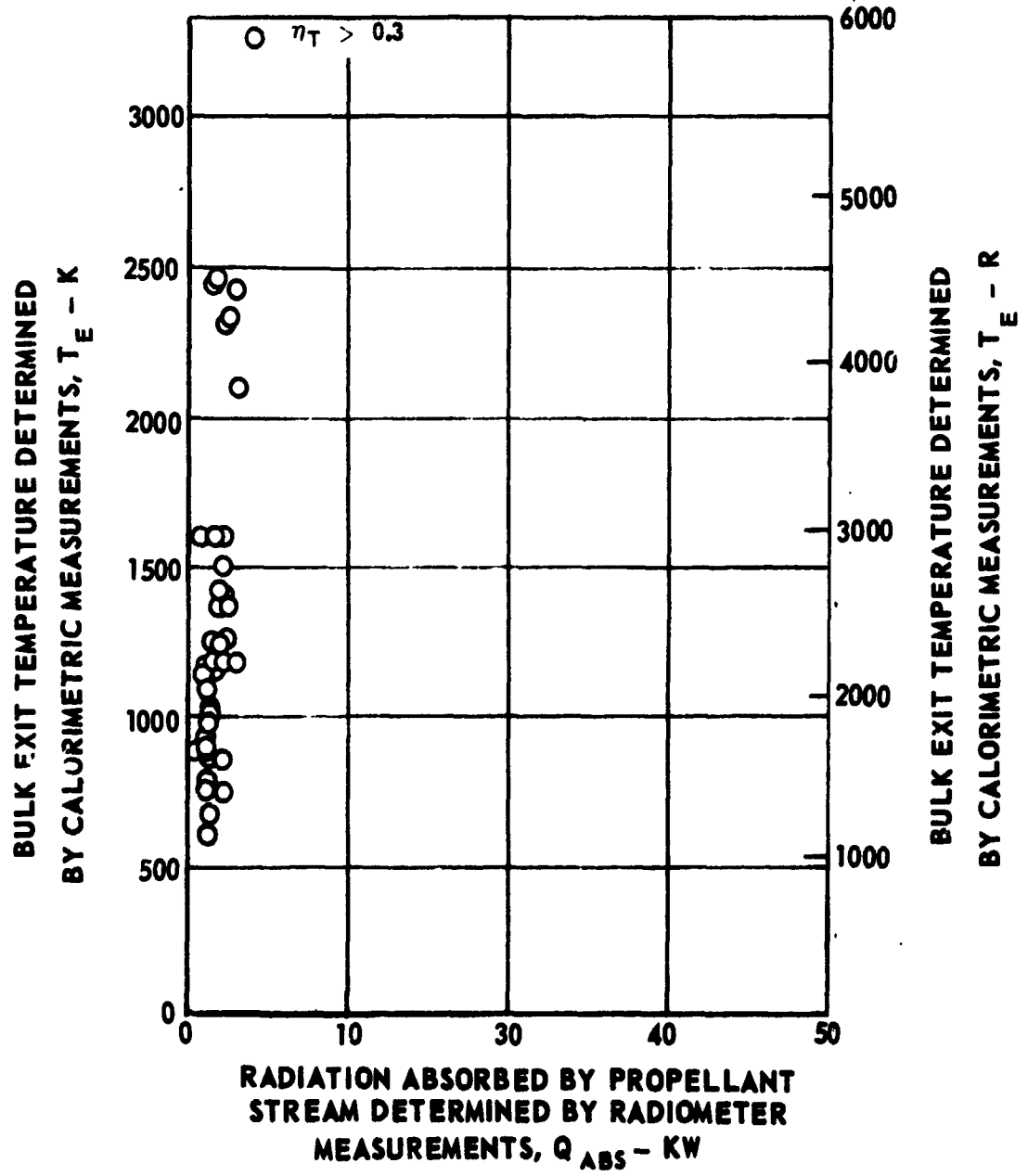

K-910900-8

FIG. 23

SKETCH OF LOWER PORTION OF PROPELLANT HEATING CONFIGURATION FOR TESTS WITH REFLECTING PROPELLANT DUCT WALLS

SEE FIG. 24 FOR UPPER PORTION DETAILS
REFLECTING SURFACES MARKED m

SECTION A–A

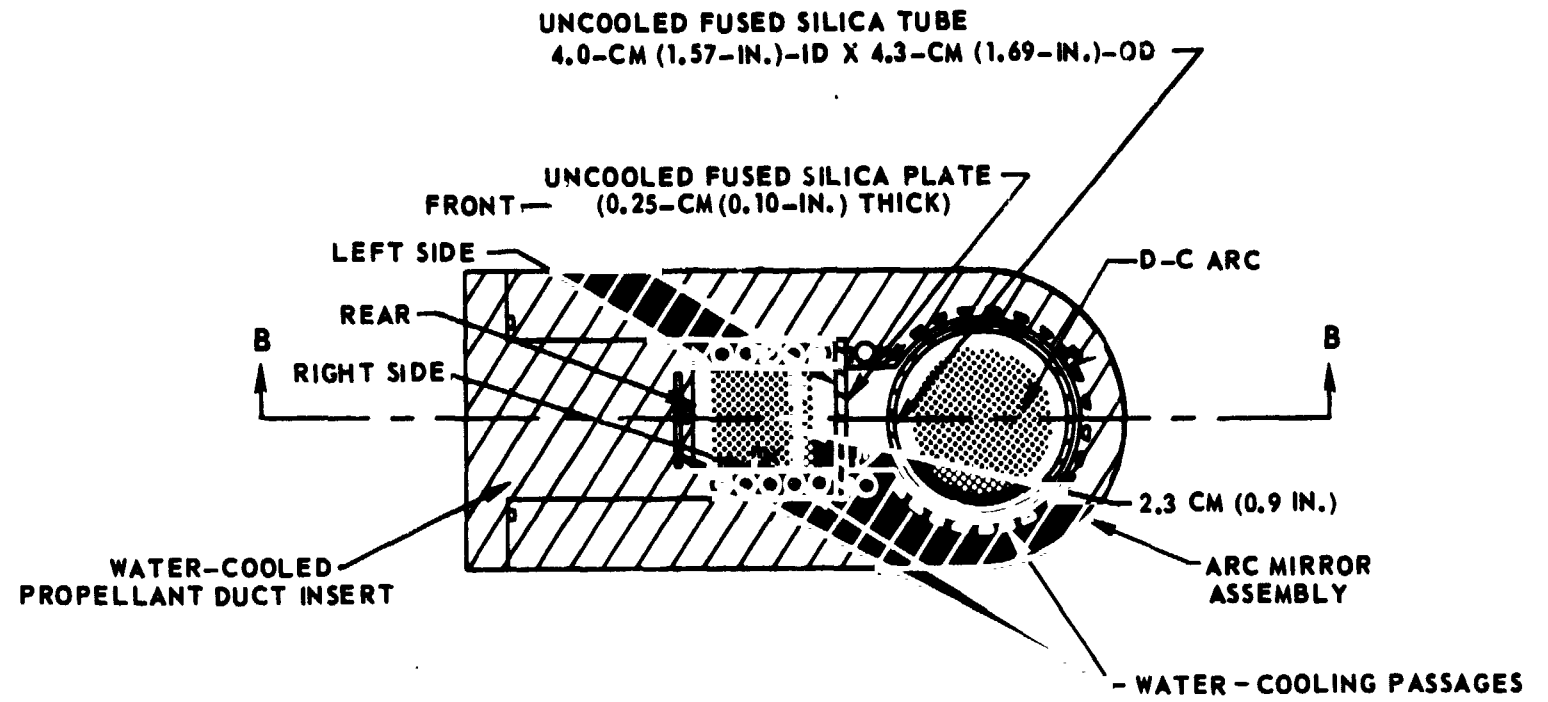

SECTION B–B

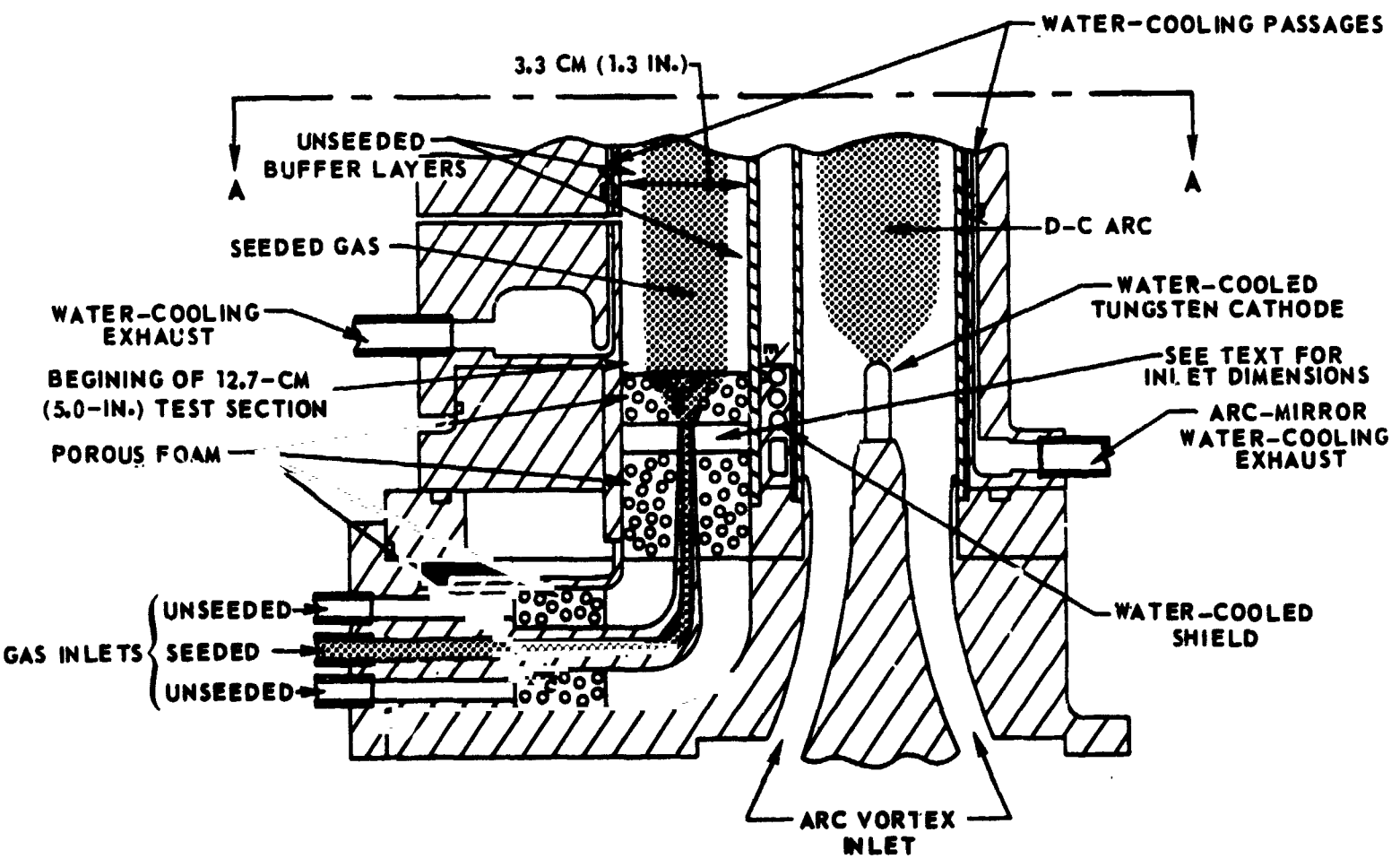

FIG. 24

SKETCH OF UPPER PORTION OF PROPELLANT HEATING CONFIGURATION FOR TESTS WITH REFLECTING PROPELLANT DUCT WALLS

SEE FIG. 23 FOR LOWER PORTION DETAILS

REFLECTING SURFACES MARKED m

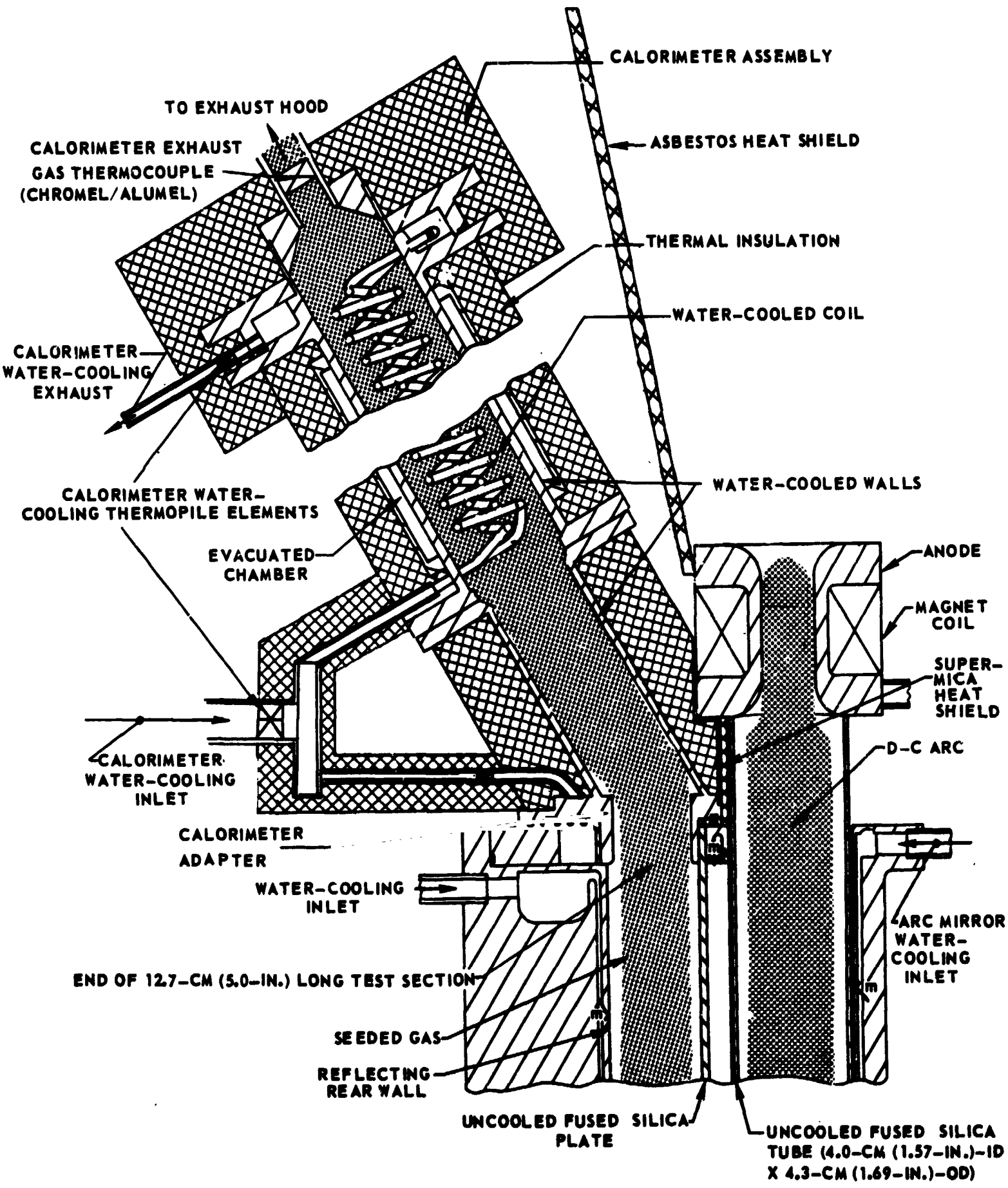

VARIATION OF BULK EXIT TEMPERATURE WITH RADIATION INCIDENT ON TEST SECTION FOR TESTS WITH REFLECTING PROPELLANT DUCT WALLS

WITHOUT ORIFICE FOR SEED DEAGGLOMERATION

NON-DIVERGENT PROPELLANT DUCT WALLS

SEE FIGS. 23 AND 24 FOR TEST CONFIGURATION

SEE TABLE I FOR FURTHER DETAILS OF DATA

ARGON WEIGHT FLOW RATE = 1.09 G/SEC (0.0024 LB/SEC)

SIMULATED PROPELLANT FLOW RATE = 1.53 G/SEC (0.00336 LB/SEC)

$$\eta_T = \frac{\text{RADIATION TRANSMITTED THROUGH SEEDS}}{\text{RADIATION INCIDENT ON SEEDS}}$$

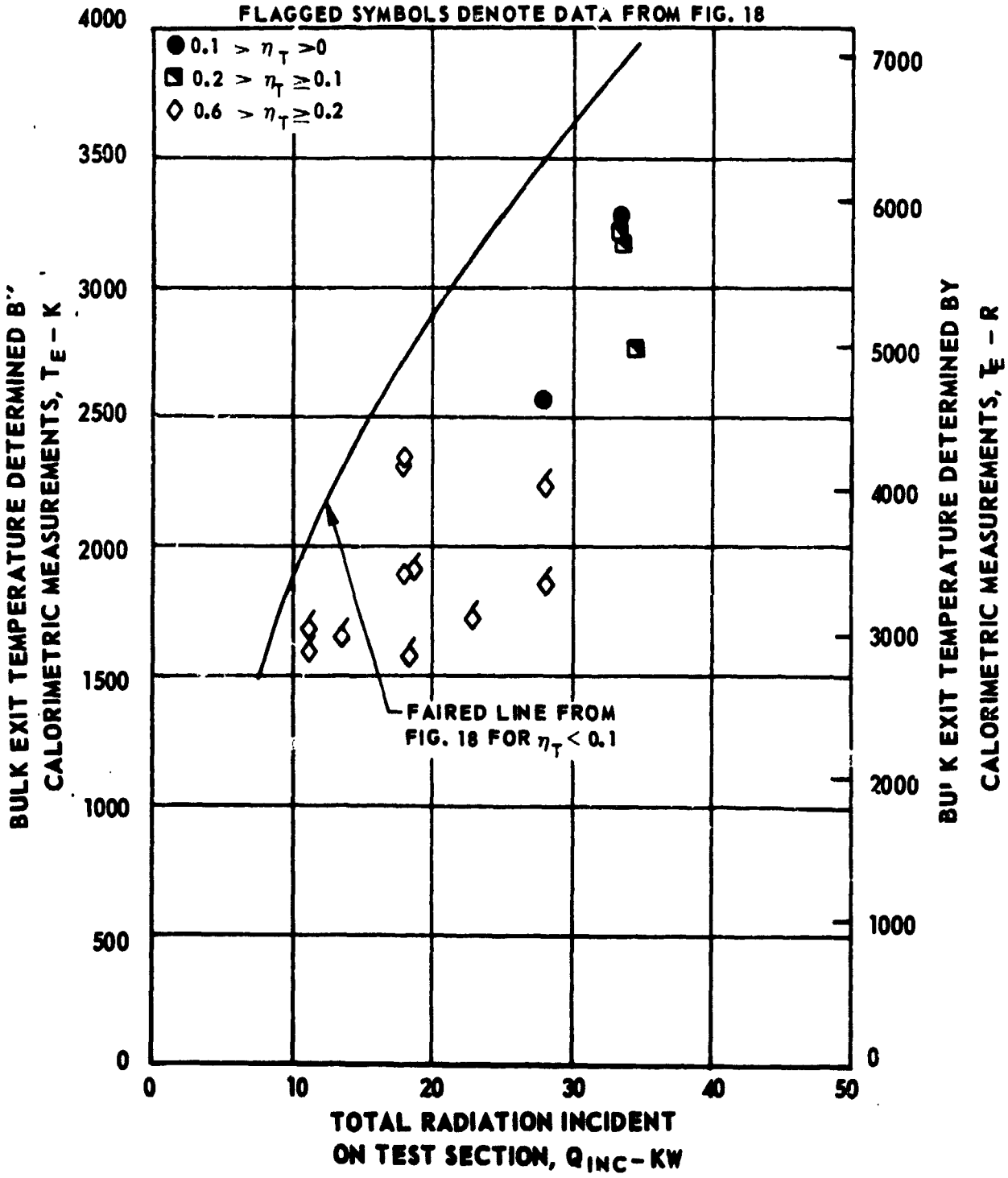

FIG. 26

VARIATION OF BULK EXIT TEMPERATURE WITH RADIATION ABSORBED BY PROPELLANT FOR TESTS WITH REFLECTING PROPELLANT DUCT WALLS

WITHOUT ORIFICE FOR SEED DEAGGLOMERATION

NON-DIVERGENT PROPELLANT DUCT WALLS

SEE FIGS. 23 AND 24 FOR TEST CONFIGURATION

SEE TABLE I FOR FURTHER DETAILS OF DATA

ARGON WEIGHT FLOW RATE = 1.09 G/SEC (0.0024 LB/SEC)

SIMULATED PROPELLANT FLOW RATE = 1.53 G/SEC (0.00336 LB/SEC)

$$\eta_T = \frac{\text{RADIATION TRANSMITTED THROUGH SEEDS}}{\text{RADIATION INCIDENT ON SEEDS}}$$

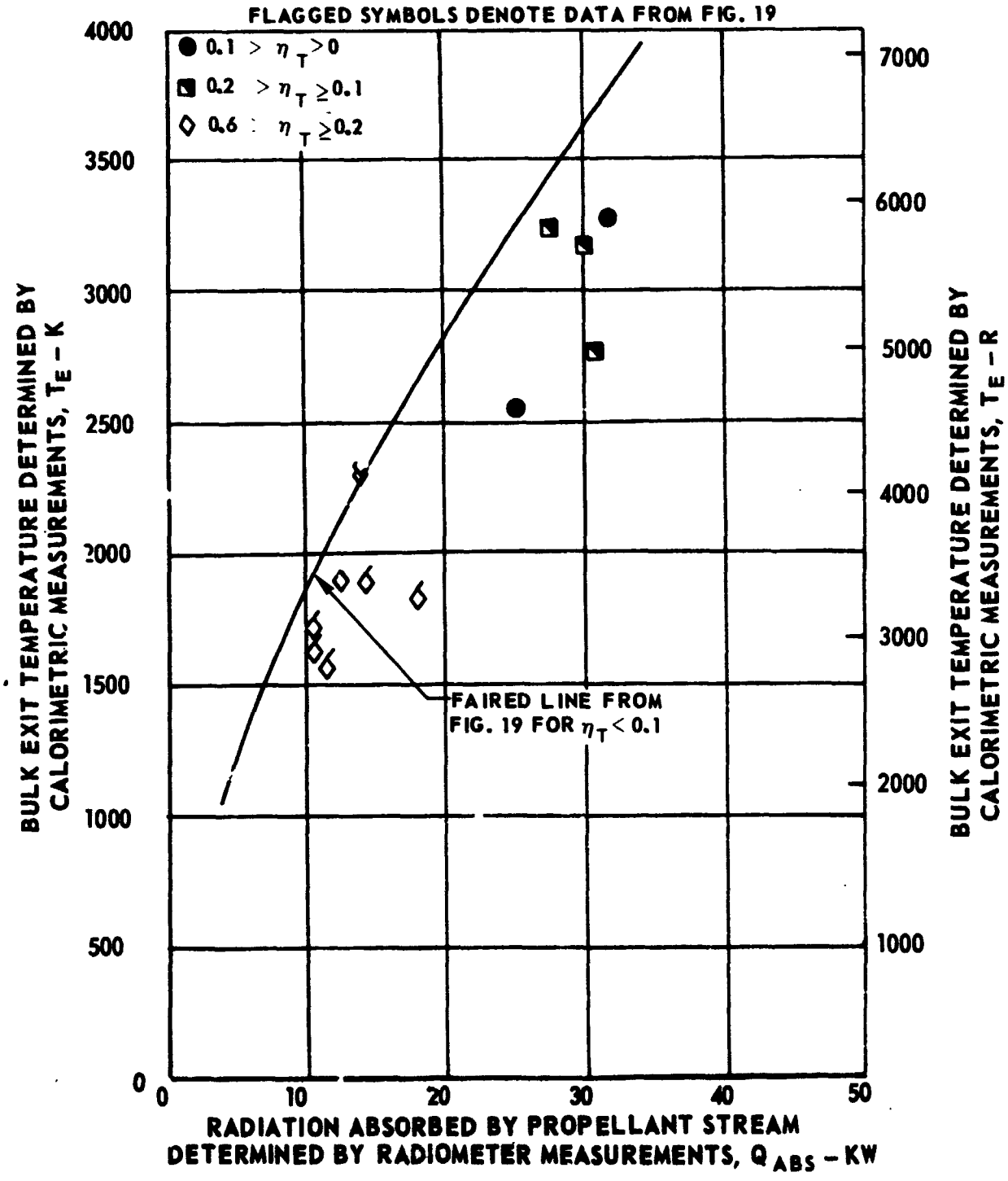

FIG. 27

SKETCH OF PROPELLANT HEATING CONFIGURATION FOR TESTS WITH DIVERGENT DUCT

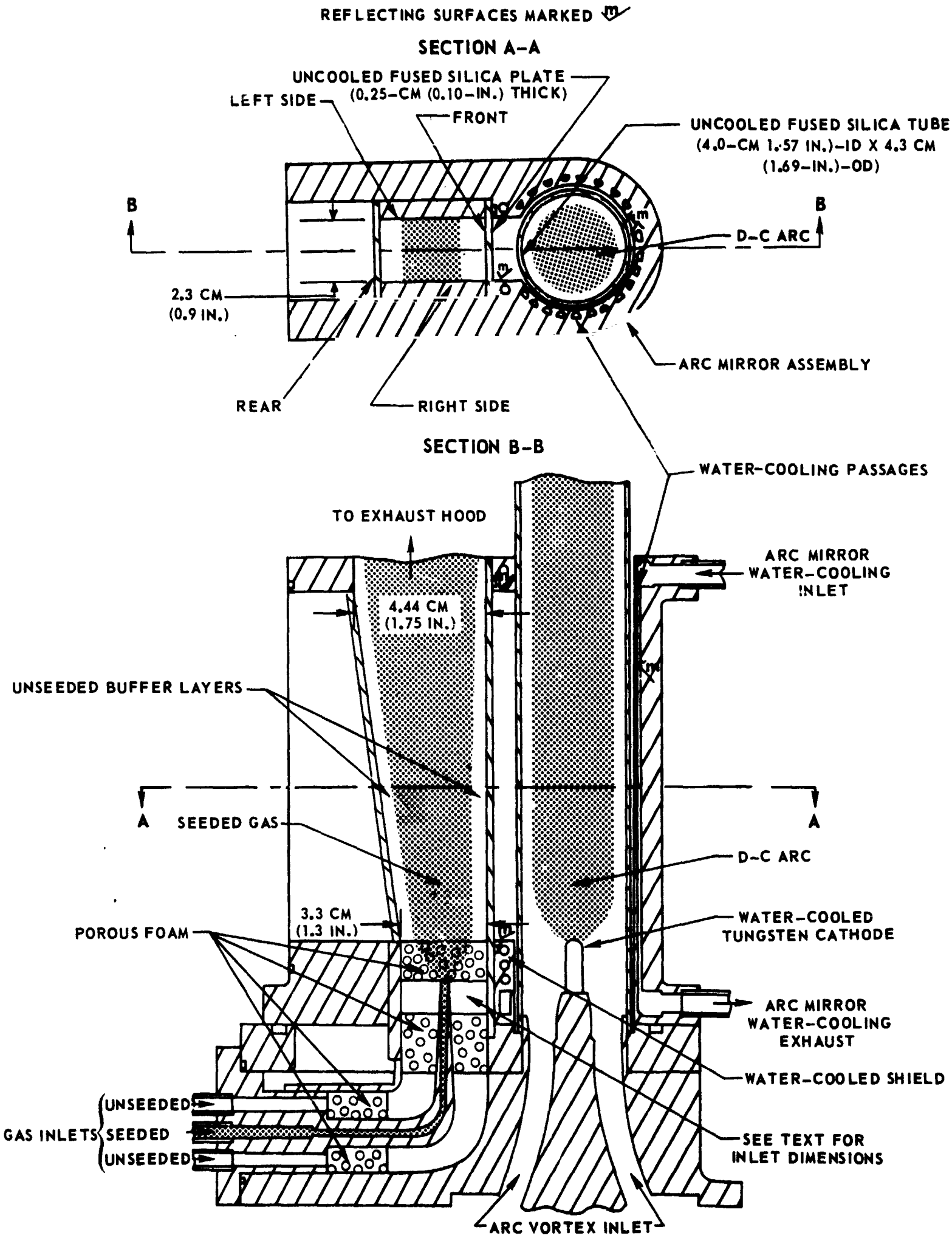

K-910900-8

FIG. 28

BLOCK DIAGRAM OF ELECTRICAL COMPONENTS OF D-C ARC HEATER

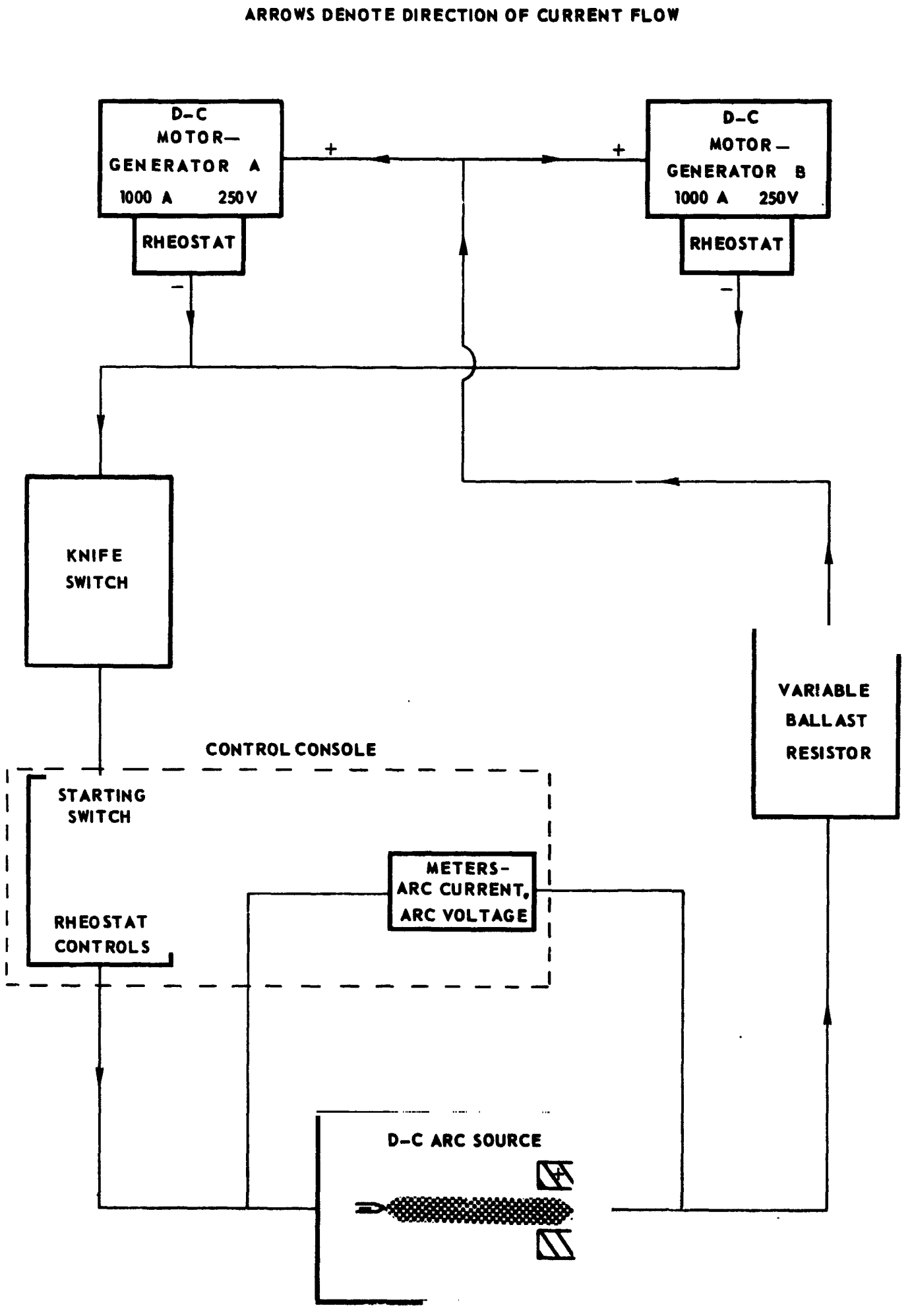

SCHEMATIC DIAGRAM OF D-C ARC HEATER ELECTRICAL CIRCUIT

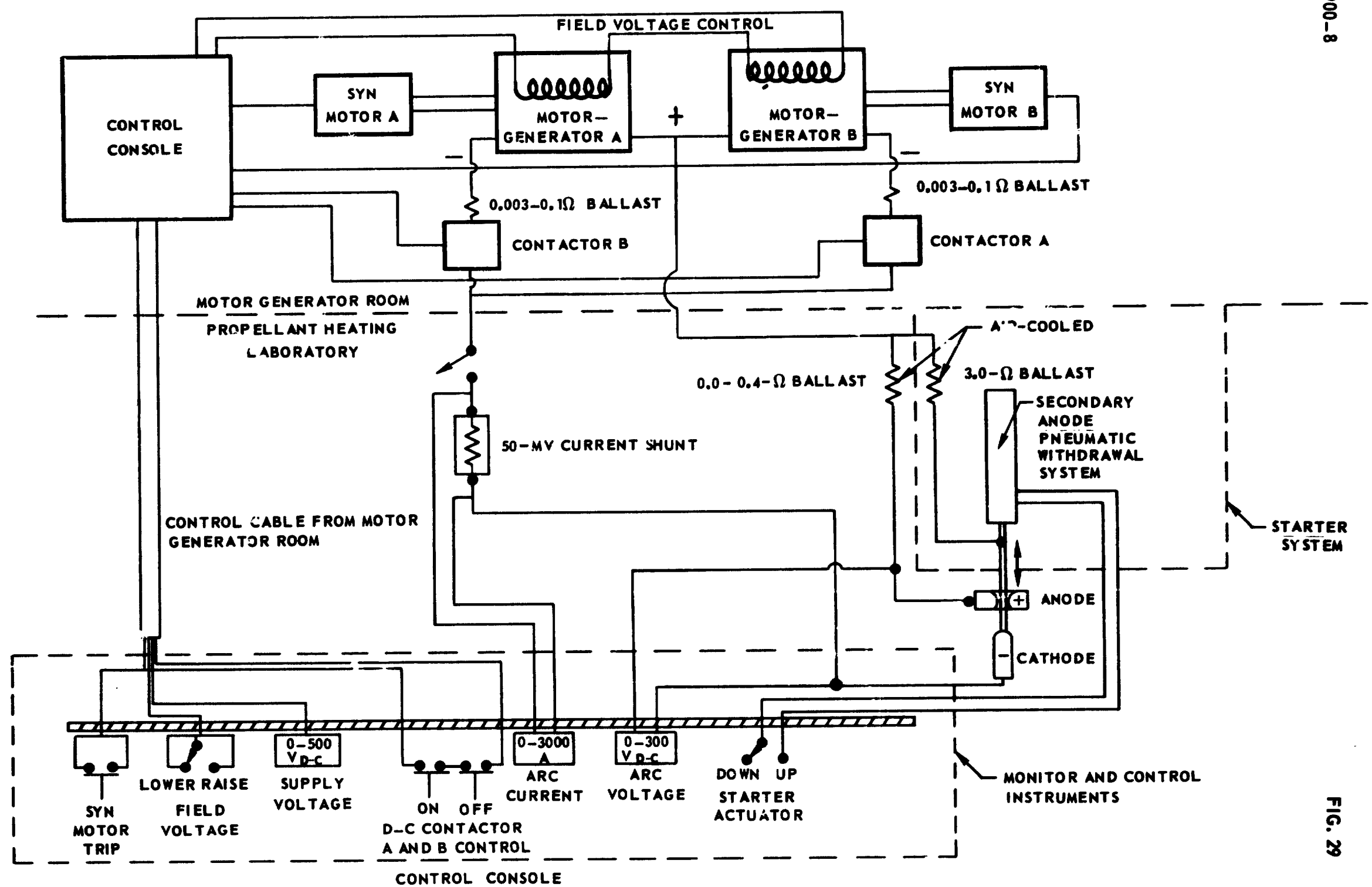

K-910900-8

FIG. 29

SCHEMATIC DIAGRAM OF D-C ARC HEATER GAS AND WATER FLOW SYSTEMS

ARROWS DENOTE DIRECTION OF FLOW

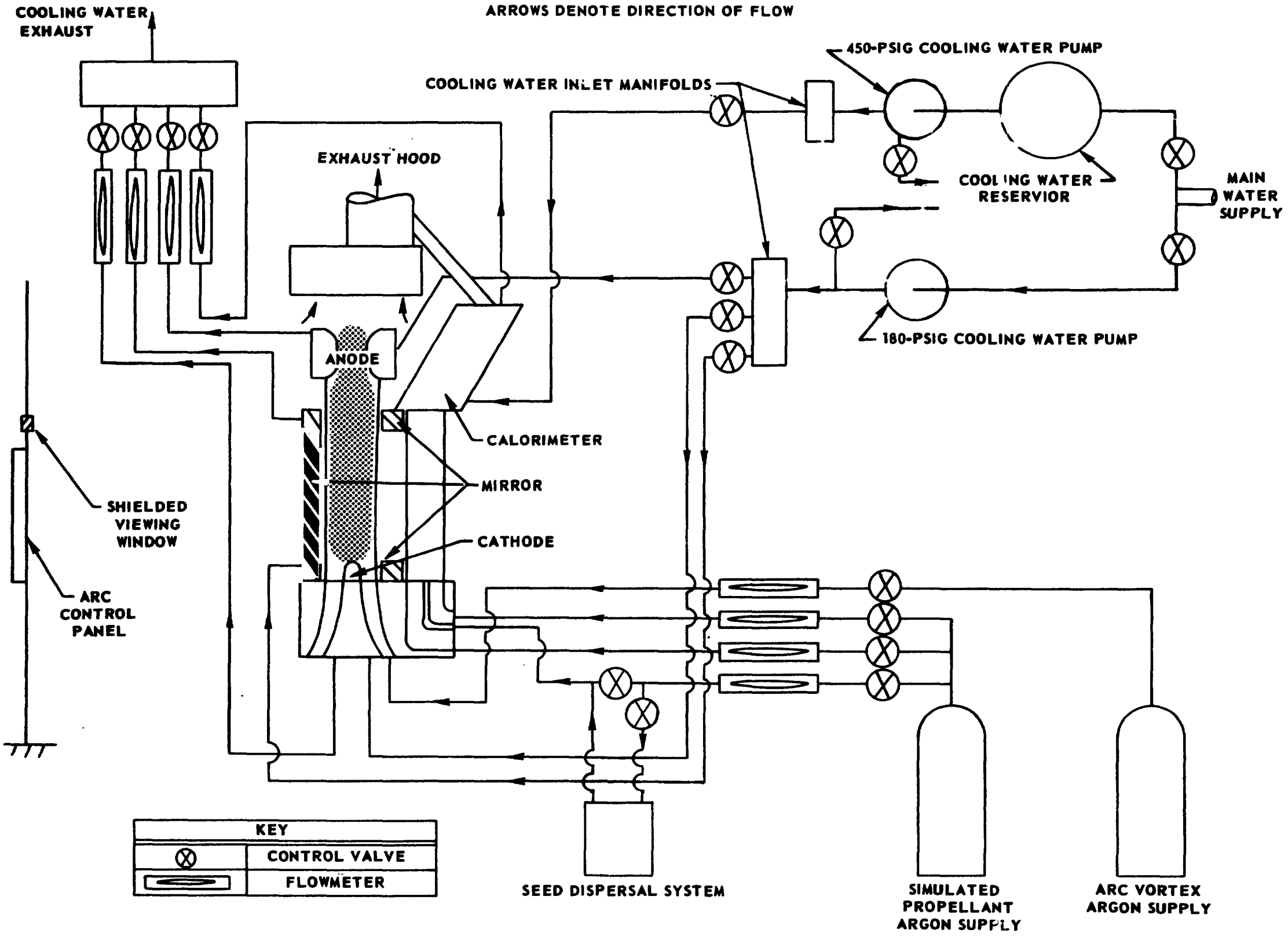

FIG. 30

K-910900-8

FIG. 31

PHOTOGRAPH OF PROPELLANT HEATING CONTROL CONSOLE